## 5.1 Introduction

Liquid crystals have unique characteristics: their order is lower than crystalline solid but higher than liquid. Due to their scientific and technological value, liquid crystals are becoming a fascinating field of research. Azo dyes are the most important synthetic dyes, accounting for more than 60% of all commercial dyes, and have been extensively studied [1]. The advantage of the introduction of an azo linkage (-N=N-) into the LC compound is that the -N = N- bond has unique characteristics of cis-trans isomerization in the presence of ultraviolet light [2–8]. A more stable (trans) E configuration is converted to Z (cis) configuration on UV absorption (~ 365 nm). The reverse conversion, Z configuration (cis) to E configuration (trans) can be achieved, either by illuminating it with ~ 450 nm light or keeping it in the dark, known as thermal back relaxation [2, 9, 10]. The azobenzene derivatives have certain application potential in the field of the optoelectronic field, such as dynamic holography [11, 12], optical computing, pattern recognition, LC dopant [13], optical data storage devices [14, 15], photo chromic switches[16, 17], and molecular logic gates [18]. The design of a liquid crystal compound containing azomethine an additional functional group in its molecular structure is particularly attractive [19]. The introduction of the azomethine linking group into the mesogenic structure increases the length of the molecular, molecular core polarizability and the stability of the mesophase [20]. Schiff bases derived from substituting salicylaldehyds called salicylaldimine derivatives are well recognized as liquid crystals because azomethine bonds are readily formed and stabilized by intramolecular hydrogen bonds [21, 22]. The intramolecular association in salicylaldimine derivatives causes a shielding effect due to the –OH group is less effective in broadening the molecule. Intramolecular hydrogen bonding may increase the rigidity of the molecule while significantly improving the chemical stability of the highly reactive unsubstituted Schiff base [22, 23].

Consequently, the combination of azo and azomethine linking groups in the mesogenic core can provide mesophase and multifunctional materials with enhanced properties. These linking groups connect the two central aromatic units and extend the conjugation into longer molecules, thereby improving polarization anisotropy. Research papers are available on azo-azomethine liquid crystal compounds [19, 24-30].

M.-M. Iftime et al. [19] reported mesomorphic behavior and optical properties of azo-azomethine derivatives from 4-butyloxybenzldehyde with p-chloro, p-methyl, o-methyl azobenzene moieties **(Figure 1).** They found that p-chloro, p-methyl derivatives exhibited enantiotropic SmA and nematic phase while for o-methyl derivative unsolved texture was observed at room temperature.

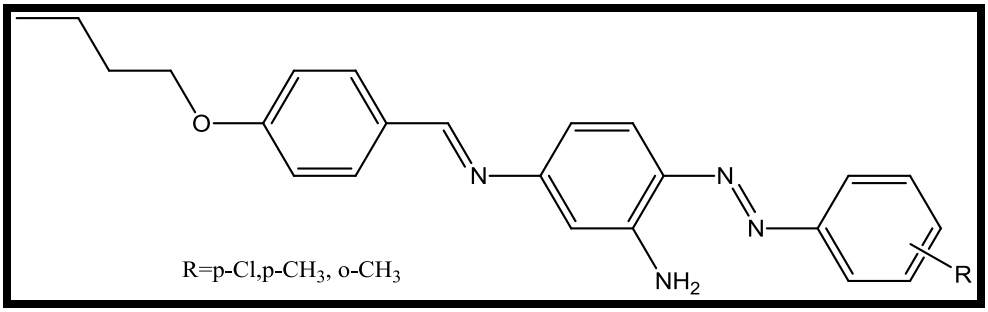


**Figure 1**. 4-butyloxybenzldehyde with p-chloro, p-methyl, o-methyl azobenzene moieties

Liquid crystalline properties of series 5-((4-hexadecyloxyphenyl) azo)-N-(4-n-alkoxy phenyl) salicylaldimine with different alkoxy chain length studied by Abbasi AR et al. [24] **(Figure 2).** Longer chain length *n*-hexadecyloxy derivative has an enatiotropic SmA phase, while *n*-octyloxy and *n*-dodecyloxy exhibit monotropic SmA phase. Based on the findings, they conclude that the stability of the phase is controlled by the alkoxy chain length.

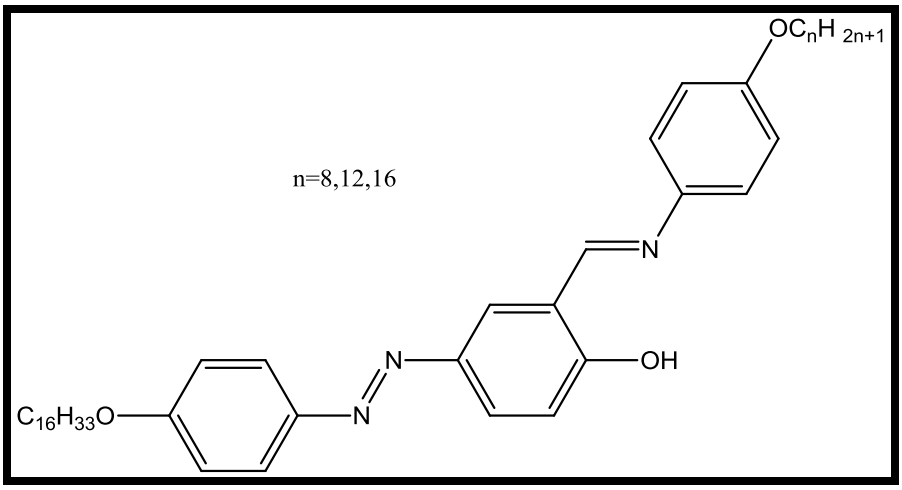


**Figure 2.** 5-((4-hexadecyloxyphenyl) azo)-N-(4-n-alkoxyphenyl) salicylaldimine series

N. H. S. Ahmed and G. R. Saad [25] reported two homologous series based on azo-azomethine derivatives to study the influence of replacing the terminal phenyl ring with 3-pyridyl and inversion of imine linkage on the liquid crystalline properties **(Figure 3).** They found that replacing of the phenyl group with a 3-pyridyl and inversion of the imine linkage have significant effect on the N and SmA mesophases and increased the thermal stability of the mesophase.

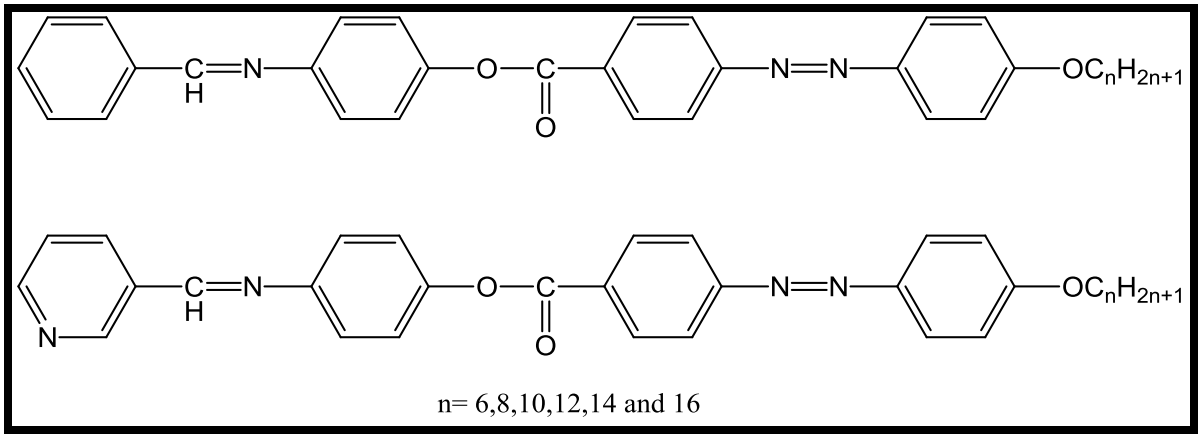


**Figure 3.** Homologous series based on azo-azomethine derivatives

L. Hamryszak et al. [27] studied mesomorphic behavior of symmetrical and unsymmetrical azo-azomethine derivatives with fluorinated alkyl chain **(Figure 4).** The SmX

and SmA phases are shown by unsymmetrical derivative while SmX1, SmX2, SmA and N phases are shown by symmetrical derivative.

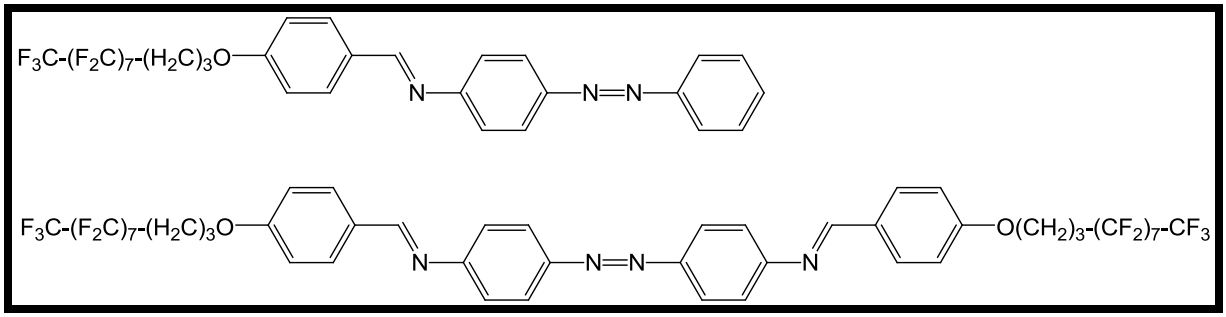


**Figure 4.** Symmetrical and unsymmetrical azo-azomethine derivatives with fluorinated alkyl chain

A. Iwan et al. [28] reported liquid crystalline properties of azo-azomethine derived from 4-biphenyl carboxaldehyde. The compound showed smectic X2 and N phases **(Figure 5).**

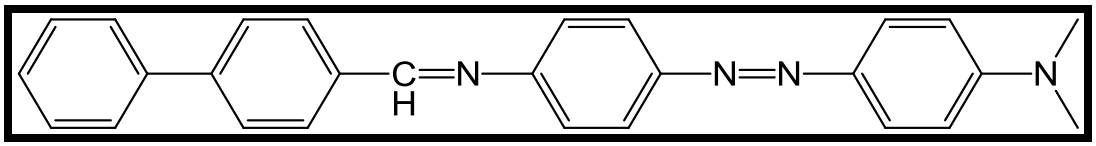


**Figure 5**. Azo-azomethine derived from 4-biphenyl carboxaldehyde

Terminal substituents play an important role in the behavior of liquid crystal. Long alkoxy chains provide flexibility to the rigid core structure, which tends to have a lower melting point [31]. It is also responsible for stabilizing the orientation of the molecules required for the formation of the liquid crystalline phase. Studying the correlation between molecular structure and mesomorphic behavior is an interesting field of liquid crystal research [32–36]. In the present study, we report the synthesis, characterization,

photoisomerization, DFT calculation, and mesomorphic behavior of new liquid crystalline materials with three phenyl rings linked through–N=N–and –C=N– central bridges as rigid core and the rest of the molecular part –OH, $–CH_3$, $–NH_2$ as lateral substitution and –OR as a terminal end group. Consequently, the objective of this study is to understand and establish the effect of molecular flexibility on the properties of liquid crystals. In addition, we used the DFT / B3LYP 631 + G (d, p) basis set to evaluate the molecular geometry, stability, frontier molecular orbital energy (FMO), dipole moment, and molecular electrostatic mapping of the compounds**.**

## 5.2. Experimental

### 5.2.1. Material

All reagents were purchased from commercial sources and used as received. 2,4 dihydroxybenzaldehyde from TCI; alkyl bromides from SRL and Spectrochem; 1,3 phenylenediamine and 2,4 dimethyl aniline from SRL. Column chromatographic separations were performed using silica gel (60–120 mesh). The purity of the synthesized compounds was checked by using Silica Gel TLC Plate from Merck.

### 5.2.2. Characterization

The $^{1}H$ NMR spectra and $^{13}C$ NMR spectra were recorded on an AV 400MHz Bruker FT-NMR spectrometer in $CDCl_3$ solution with tetramethylsilane (TMS) as an internal standard. IR spectra were recorded on Bruker spectrometer as KBr pellets. TG-DTA measurements were carried out on a SII EXSTAR6000TG-DTA instrument. The Experiments were performed in $N_2$ at a heating rate of 10 $^{o}C\ min^{-1}$ in the temperature range 30–550 $^{o}C$ using an aluminum pan. The transition temperatures and enthalpies were investigated by differential scanning calorimeter (DSC) using a PerkinElmer Thermal Analyzer with heating and cooling rate 10 $^{o}C\ min^{-1}$. The Leica DM 2500P polarizing optical microscope (POM) provided with a Linkam heating stage was used to study thermal behavior and optical texture of different compounds. The photoisomerization study was carried out by UV-Vis spectroscopy. The measurements were conducted for 2.5 x $10^{-5}$ M solution of compound **G7** in chloroform. Both process the isomerization and the relaxations were evaluated. The mercury lamp with a filter (365 nm) was used to irradiate the materials for photoisomerization studies. The solvent was of spectrophotometric grade and was obtained from spectrochem. UV-Vis spectra were recorded after different irradiation times for excitation and different intervals after the irradiation was switched off for relaxation studies. Electronic spectra of the compounds in

DCM were recorded on a Perkin-Elmer Lambda 35 spectrophotometer using a quartz cuvette. All the optical analyses were performed at room temperature. The characterization of DFT material has been done by the following methods. Calculation type: OPT+FREQ; Calculation Method: RB3LYP; Basis Set: 6-31+G(d,p); Charge : 0 ; Spin: Singlet; Solvation : none.

## 5.3. Synthesis

### 5.3.1. Synthesis of 2-hydroxy-4-*n*-alkoxybenzaldehyde

2-Hydroxy- 4-*n*-alkoxy benzaldehye were prepared by following the method described in chapter 2, section 2.3.1.

### 5.3.2. Synthesis of (E)-4-((2,4-dimethylphenyl)diazenyl) benzene-1,3-diamine[37]

At a temperature of 0-5°C, concentrated hydrochloric acid (5.4 ml) and 20 ml of water were added to 20 mmol of 2, 4-dimethylaniline to prepare a salt solution. Then a solution of 20 mmol sodium nitrite in 3.0 ml water was added drop wise to the cooled salt solution, and the mixture was stirred at 0-5°C for 15 minutes. Then 20 ml of 1, 3 phenylenediamine in 16 ml of methanol was slowly poured into the solution. The reaction mixture was stirred in an ice bath for 30 minutes and neutralized to pH 5-6 with sodium acetate. After the temperature rose to 20°C, the mixture was stirred for 1 hour. The product was filtered off, washed with water, and recrystallised from ethanol.

Red brownish solid; Yield: 82%; $^{1}$H NMR (400 MHz, $CDCl_3$, TMS) $\delta_H$ 7.70 (d, Ar**H**, 1H, *J*=8.8 Hz), 7.59 (d, Ar**H**, 1H, *J*=8.4 Hz), 7.12 (s, Ar**H**, 1H), 7.08 (d, Ar**H**, 1H, *J*=8.0 Hz), 6.27 (s, N**H**$_2$, 2H), 6.20 (dd, Ar**H**, 1H, *J*=8.8 Hz, *J*=2.4 Hz), 5.93 (d, Ar**H**, 1H, *J*=2.4 Hz), 3.97 (s, N**H**$_2$, 2H), 2.58 (s, -C**H**$_3$, 3H), 2.38 (s, -C**H**$_3$, 3H). $^{13}$CNMR (100MHz, $CDCl_3$, TMS) $\delta_C$ 149.9, 149.3, 144.0, 138.6, 135.2, 132.4, 131.9, 131.5, 127.3, 114.9, 106.0, 99.7, 21.3, 18.1; IR ($\upsilon_{max}$, cm$^{-1}$, KBr: 3419, 3358 ($\upsilon NH_2$), 3259, 3218 ($\upsilon NH_2$), 3002, 2962, 2919 ($\upsilon$ aliphatic C-H), 1631 ($\upsilon$N=N), 1572, 1546 ($\upsilon$ aromatic C=C).

### 5.3.3. Synthesis of 2-((E)-((3-amino-4-((E)-(2,4-dimethylphenyl) diazenyl)phenyl) imino)methyl)-5-alkoxyphenol.

In a minimum amount of absolute ethanol, dissolve 5 mmol 4-*n*- alkox-2-hydroxybenzaldehyde, 5 mmol (E)-4-((2, 4-dimethylphenyl) diazenyl) benzene-1, 3-diamine and a few drops of glacial acetic acid. The reaction mixture was refluxed for 4 hours, and a reddish crystalline compound was obtained after cooling. The product was filtered, washed with cold ethanol, and dried in a vacuum.

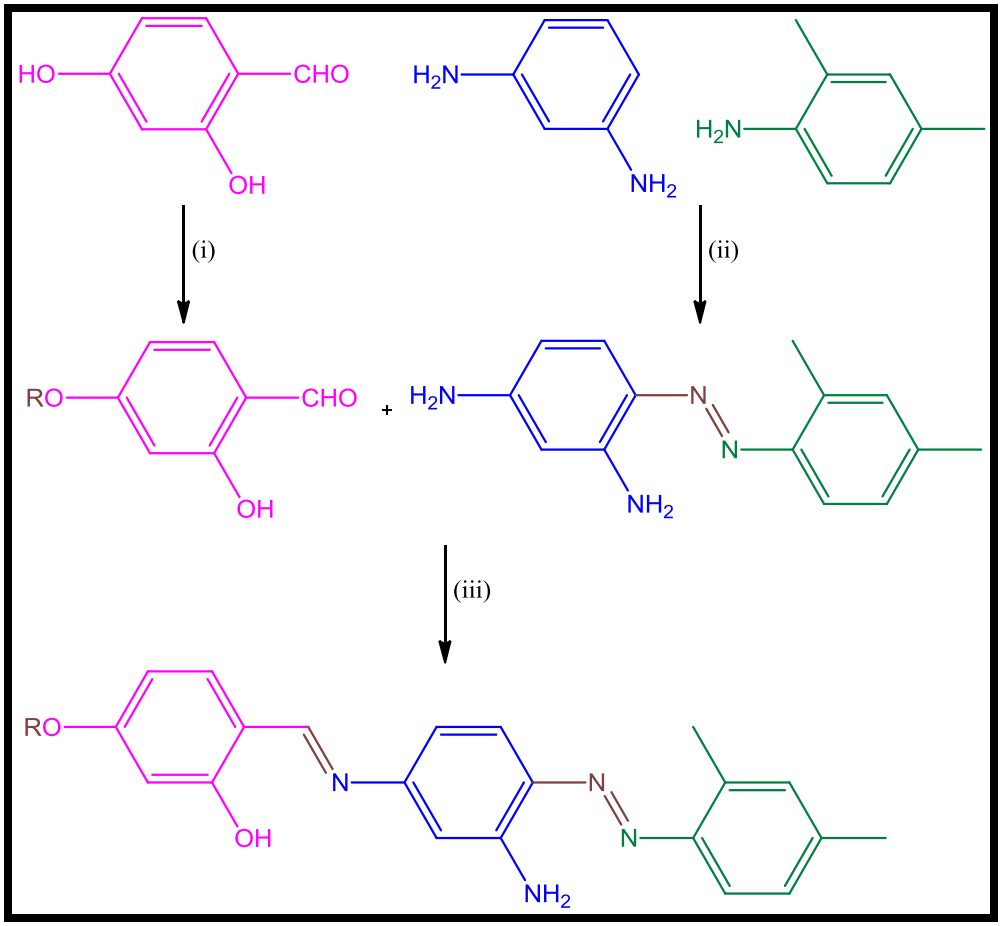


Where R= $C_nH_{2n+1}$ and n= 2 to 8, 10, 12, 14, 16, 18.

i) RBr, $KHCO_3$, KI, dry acetone, reflux 24 hr.

ii) 0-5 $^oC$ ,HCl + $NaNO_2$,$H_2O$, $CH_3COONa$

iii) Few drops of glacial acetic acid, absolute ethanol, reflux 4 hr

**Scheme 1.** Synthetic protocol of series G

**2-((E)-((3-amino-4-((E)-(2,4-dimethylphenyl)diazenyl)phenyl)imino)methyl)-5-ethoxy phenol (G2)**

Red brownish solid; Yield: 67%; $^{1}$H NMR (400 MHz, $CDCl_3$, TMS) $\delta_H$ 13.78 (s, ArO**H**, 1H),8.57 (s, -C**H**N-, 1H),7.90 (d, Ar**H**, 1H, *J*=8.4 Hz), 7.63 (d, Ar**H**, 1H, *J*=8.4 Hz), 7.30-7.27 (m, Ar**H**, 1H), 7.16 (s, Ar**H**, 1H), 7.10 (d, Ar**H**, 1H, *J*=8.8 Hz), 6.77 (dd, Ar**H**, 1H, *J*=8.4 Hz, *J*=2.0 Hz), 6.63 (d, Ar**H**, 1H, *J*=2.0 Hz),6.51-6.49 (m, Ar**H**, 2H), 6.17 (s, N**H$_2$**, 2H), 4.12-4.07 (t, -OC**H$_2$**$CH_2$-, 2H), 2.63 (s, -C**H$_3$**, 3H), 2.40 (s, -C**H$_3$**, 3H), 1.48-1.44 (t, -$CH_2$C**H$_3$**, 3H); $^{13}$CNMR (100MHz, $CDCl_3$, TMS) $\delta_C$ 164.5, 163.7, 161.6, 150.7, 149.1, 143.2, 140.2, 136.5, 136.2, 133.8, 131.7, 130.3, 127.4, 115.0, 112.9, 110.3, 109.0, 107.9, 101.5, 63.8, 21.4, 18.1, 14.7 IR ($\upsilon_{max}$, $cm^{-1}$, KBr): 3397 3272 ($\upsilon NH_2$) 2975, 2922, 2875 (υ aliphatic C-H), 1601 (υC=N), 1564 (υ aromatic C=C), 1517,1456 (υN=N), 1179, 1139 (υ PhO).

**2-((E)-((3-amino-4-((E)-(2,4-dimethylphenyl)diazenyl)phenyl)imino)methyl)-5-propoxy phenol (G3)**

Red brownish solid; Yield: 68%; $^{1}$H NMR (400 MHz, $CDCl_3$, TMS) $\delta_H$ 13.76 (s, ArO**H**, 1H), 8.58 (s, -C**H**N-, 1H), 7.90 (d, Ar**H**, 1H, *J*=8.4 Hz), 7.63 (d, Ar**H**, 1H, *J*=8.4 Hz), 7.30-7.28 (m, Ar**H**, 1H), 7.16 (s, Ar**H**, 1H), 7.10 (d, Ar**H**, 1H, *J*=8.0 Hz), 6.77 (dd, Ar**H**, 1H, *J*=8.8 Hz, *J*=2.0 Hz), 6.64 (d, Ar**H**, 1H, *J*=2.0 Hz),6.53-6.50 (m, Ar**H**, 2H), 6.17 (s, N**H$_2$**, 2H), 4.00-3.97 (t, -OC**H$_2$**$CH_2$-, 2H), 2.64 (s, -C**H$_3$**, 3H), 2.40 (s, -C**H$_3$**, 3H), 1.90-1.81 (m, -C**H$_2$**-, 2H), 1.09-1.05 (t, -$CH_2$C**H$_3$**, 3H); $^{13}$CNMR (100MHz, $CDCl_3$, TMS) $\delta_C$ 164.5, 164.0, 161.7, 150.8, 149.1, 143.2, 140.2, 136.5, 136.2, 133.8, 131.7, 130.3, 127.4, 115.0, 112.9, 110.3, 109.0, 107.9, 101.6, 69.7, 22.4, 21.4, 18.1, 10.5 IR ($\upsilon_{max}$, $cm^{-1}$, KBr): 3419, 3272 ($\upsilon NH_2$), 3013, 2964, 2936, 2876 (υ aliphatic C-H), 1600 (υC=N), 1566 (υ aromatic C=C), 1513,1460 (υN=N), 1184, 1138 (υ PhO$CH_2$-).

**2-((E)-((3-amino-4-((E)-(2,4-dimethylphenyl)diazenyl)phenyl)imino)methyl)-5-butoxy phenol (G4)**

Red brownish solid; Yield: 65%; $^{1}$H NMR (400 MHz, $CDCl_3$, TMS) $\delta_H$ 13.74 (s, ArO**H**, 1H),8.58 (s, -C**H**N-, 1H),7.90 (d, Ar**H**, 1H, *J*=8.4 Hz), 7.63 (d, Ar**H**, 1H, *J*=8.4 Hz), 7.30-7.28 (m, Ar**H**, 1H), 7.16 (s, Ar**H**, 1H), 7.10 (d, Ar**H**, 1H, *J*=8.4 Hz), 6.77 (dd, Ar**H**, 1H, *J*=8.8 Hz, *J*=2.4 Hz), 6.64 (d, Ar**H**, 1H, *J*=2.0 Hz),6.52-6.50(m, Ar**H**, 2H), 6.15 (s, N**H$_2$**, 2H), 4.05-4.02 (t, -OC**H$_2$**$CH_2$-, 2H), 2.64 (s, -C**H$_3$**, 3H), 2.40 (s, -C**H$_3$**, 3H), 1.84-1.52 (m, -C**H$_2$**-, 4H), 0.91-0.88 (t, -$CH_2$C**H$_3$**, 3H); $^{13}$CNMR (100MHz, $CDCl_3$, TMS) $\delta_C$ 164.5, 164.0, 161.7, 150.8, 149.1, 143.2, 140.2, 136.5, 136.2, 133.7, 131.7, 130.3, 127.4, 115.0, 112.8, 110.3, 109.0, 107.9, 101.5, 68.0, 31.1, 21.4, 19.22, 18.1, 13.7 IR ($\upsilon_{max}$, $cm^{-1}$, KBr): 3420, 3274 ($\upsilon NH_2$), 2965, 2938, 2873 (υ aliphatic C-H), 1597 (υC=N), 1566 (υ aromatic C=C), 1513, 1458 (υN=N), 1184, 1139 (υ Ph$OCH_2$-).

**2-((E)-((3-amino-4-((E)-(2,4-dimethylphenyl)diazenyl)phenyl)imino)methyl)-5-pentyloxy phenol(G5)**

Red brownish solid; Yield: 64%; $^{1}$H NMR (400 MHz, $CDCl_3$, TMS) $\delta_H$ 13.74 (s, ArO**H**, 1H),8.58 (s, -C**H**N-, 1H),7.90 (d, Ar**H**, 1H, *J*=8.4 Hz), 7.63 (d, Ar**H**, 1H, *J*=8.4 Hz), 7.30-7.28 (m, Ar**H**, 1H), 7.16 (s, Ar**H**, 1H), 7.10 (d, Ar**H**, 1H, *J*=8.4 Hz), 6.77 (dd, Ar**H**, 1H, *J*=8.8 Hz, *J*=2.4 Hz), 6.64 (d, Ar**H**, 1H, *J*=2.0 Hz),6.52-6.50(m, Ar**H**, 2H), 6.15 (s, N**H$_2$**, 2H), 4.03-4.02 (t, -OC**H$_2$**$CH_2$-, 2H), 2.64 (s, -C**H$_3$**, 3H), 2.40 (s, -C**H$_3$**, 3H), 1.87-1.45 (m, -C**H$_2$**-, 6H), 0.91-0.88 (t, -$CH_2$C**H$_3$**, 3H); $^{13}$CNMR (100MHz, $CDCl_3$, TMS) $\delta_C$ 164.5, 164.0, 161.6, 149.1, 143.2, 140.3, 138.6, 136.5, 136.1, 135.3, 133.7, 130.3, 127.4, 115.0, 114.9, 112.8, 110.2, 109.0, 108.8, 107.9, 106.0, 101.5, 101.0, 99.64, 68.6, 28.7, 28.2, 28.1, 22.4, 18.1, 14.1 IR ($\upsilon_{max}$, $cm^{-1}$, KBr): 3406, 3280 ($\upsilon NH_2$), 3013, 2952, 2931, 2860 (υ aliphatic C-H), 1606 (υC=N), 1562 (υ aromatic C=C), 1512, 1460 (υN=N), 1179, 1142 (υ Ph$OCH_2$-).

**2-((E)-((3-amino-4-((E)-(2,4-dimethylphenyl)diazenyl)phenyl)imino)methyl)-5-hexyloxy phenol (G6)**

Red brownish solid; Yield: 70%; $^{1}$H NMR (400 MHz, $CDCl_3$, TMS) $\delta_H$ 13.74 (s, ArO**H**, 1H),8.58 (s, -C**H**N-, 1H),7.90 (d, Ar**H**, 1H, *J*=8.4 Hz), 7.63 (d, Ar**H**, 1H, *J*=8.0 Hz), 7.30-7.28 (m, Ar**H**, 1H), 7.16 (s, Ar**H**, 1H), 7.10 (d, Ar**H**, 1H, *J*=8.4 Hz), 6.77 (dd, Ar**H**, 1H, *J*=8.8 Hz, *J*=2.0 Hz), 6.64 (d, Ar**H**, 1H, *J*=2.0 Hz),6.52-6.49(m, Ar**H**, 2H), 6.15 (s, N**H$_2$**, 2H), 4.04-4.01 (t, -OC**H$_2$**$CH_2$-, 2H), 2.64 (s, -C**H$_3$**, 3H), 2.40 (s, -C**H$_3$**, 3H), 1.87-1.37 (m, -C**H$_2$**-, 8H), 0.91-0.88 (t, -$CH_2$C**H$_3$**, 3H); $^{13}$CNMR (100MHz, $CDCl_3$, TMS) $\delta_C$ 164.5, 164.0, 161.6, 150.7, 149.1, 143.2, 140.2, 136.5, 136.2, 133.7, 131.7, 130.4, 127.4, 115.0, 112.8, 110.2, 108.9, 107.9, 101.7, 101.5, 68.3, 31.5, 29.04, 25.7, 22.6, 22.6, 21.4, 18.1, 14.1, IR ($\upsilon_{max}$, $cm^{-1}$, KBr): 3404, 3278 ($\upsilon NH_2$), 2949, 2921, 2855 (υ aliphatic C-H), 1607 (υC=N), 1563 (υ aromatic C=C), 1513, 1460 (υN=N), 1169, 1142 (υ $PhOCH_2$-), 1113.

**2-((E)-((3-amino-4-((E)-(2,4-dimethylphenyl)diazenyl)phenyl)imino)methyl)-5-heptyloxy phenol (G7)**

Red brownish solid; Yield: 68%; $^{1}$H NMR (400 MHz, $CDCl_3$, TMS) $\delta_H$ 13.75 (s, ArO**H**, 1H),8.57 (s, -C**H**N-, 1H),7.90 (d, Ar**H**, 1H, *J*=8.4 Hz), 7.63 (d, Ar**H**, 1H, *J*=8.4 Hz), 7.29-7.27 (m, Ar**H**, 1H), 7.16 (s, Ar**H**, 1H), 7.10 (d, Ar**H**, 1H, *J*=8.4 Hz), 6.77 (dd, Ar**H**, 1H, *J*=8.4 Hz, *J*=2.4 Hz), 6.63 (d, Ar**H**, 1H, *J*=2.0 Hz), 6.51-6.49 (m, Ar**H**, 2H), 6.15 (s, N**H$_2$**, 2H), 4.03-4.00 (t, -OC**H$_2$**$CH_2$-, 2H), 2.64 (s, -C**H$_3$**, 3H), 2.40 (s, -C**H$_3$**, 3H), 1.86-1.34 (m, -C**H$_2$**-, 10H), 0.94-0.91 (t, -$CH_2$C**H$_3$**, 3H); $^{13}$CNMR (100MHz, $CDCl_3$, TMS) $\delta_C$ 164.5, 164.0, 161.6, 150.8, 149.1, 143.2, 140.2, 136.5, 136.2, 133.7, 131.7, 130.3, 127.4, 115.0, 112.8, 110.3, 109.0, 107.9, 101.5, 68.3, 31.8, 29.1, 26.0, 22.6, 22.6, 21.4, 18.1, 14.1 IR ($\upsilon_{max}$, $cm^{-1}$, KBr): 3402, 3276 ($\upsilon NH_2$), 3012, 2921, 2852 (υ aliphatic C-H), 1608 (υC=N), 1566 (υ aromatic C=C), 1513, 1461 (υN=N), 1168, 1142 (υ $PhOCH_2$-).

**2-((E)-((3-amino-4-((E)-(2,4-dimethylphenyl)diazenyl)phenyl)imino)methyl)-5-octyloxy phenol (G8)**

Red brownish solid; Yield: 78%; $^{1}$H NMR (400 MHz, $CDCl_3$, TMS) $\delta_H$ 13.76 (s, ArO**H**, 1H),8.58 (s, -C**H**N-, 1H),7.90 (d, Ar**H**, 1H, *J*=8.4 Hz), 7.63 (d, Ar**H**, 1H, *J*=8.0 Hz), 7.30-7.28 (m, Ar**H**, 1H), 7.16 (s, Ar**H**, 1H), 7.10 (d, Ar**H**, 1H, *J*=8.4 Hz), 6.77 (dd, Ar**H**, 1H, *J*=8.4 Hz, *J*=2.4 Hz), 6.64 (d, Ar**H**, 1H, *J*=2.0 Hz),6.51-6.50(m, Ar**H**, 2H), 6.16 (s, N**H$_2$**, 2H), 4.03-4.00 (t, -OC**H$_2$**$CH_2$-, 2H), 2.64 (s, -C**H$_3$**, 3H), 2.40 (s, -C**H$_3$**, 3H), 1.84-1.31 (m, -C**H$_2$**-, 4H), 0.91-0.89 (t, -$CH_2$C**H$_3$**, 3H); $^{13}$CNMR (100MHz, $CDCl_3$, TMS) $\delta_C$ 164.5, 164.0, 161.6, 149.1, 143.2, 140.2, 136.5, 136.1, 133.7, 131.7, 130.4, 127.4, 115.0, 112.8, 110.2, 109.0, 108.0, 101.5, 68.3, 31.8, 29.4, 29.3, 29.1, 26.0, 22.7, 21.4, 18.1, 14.2 IR ($\upsilon_{max}$, cm$^{-1}$, KBr): 3403, 3278 ($\upsilon NH_2$) 2920, 2852 (υ aliphatic C-H), 1607 (υC=N), 1563 (υ aromatic C=C), 1513, 1461 (υN=N), 1168, 1143 (υ $PhOCH_2$-).

**2-((E)-((3-amino-4-((E)-(2,4-dimethylphenyl)diazenyl)phenyl)imino)methyl)-5-decyloxy phenol (G10)**

Red brownish solid; Yield: 72%; $^{1}$H NMR (400 MHz, $CDCl_3$, TMS) $\delta_H$ 13.74 (s, ArO**H**, 1H),8.58 (s, -C**H**N-, 1H),7.90 (d, Ar**H**, 1H, *J*=8.4 Hz), 7.63 (d, Ar**H**, 1H, *J*=8.0 Hz), 7.30-7.28 (m, Ar**H**, 1H), 7.16 (s, Ar**H**, 1H), 7.10 (d, Ar**H**, 1H, *J*=8.4 Hz), 6.77 (dd, Ar**H**, 1H, *J*=8.8 Hz, *J*=2.4 Hz), 6.64 (d, Ar**H**, 1H, *J*=2.0 Hz),6.52-6.49(m, Ar**H**, 2H), 6.15 (s, N**H$_2$**, 2H), 4.04-4.00 (t, -OC**H$_2$**$CH_2$-, 2H), 2.64 (s, -C**H$_3$**, 3H), 2.40 (s, -C**H$_3$**, 3H), 1.85-1.30 (m, -C**H$_2$**-, 16H), 0.92-0.89 (t, -$CH_2$C**H$_3$**, 3H). $^{13}$CNMR (100MHz, $CDCl_3$, TMS) $\delta_C$ 164.4, 163.9, 161.6, 136.4, 133.7, 131.7, 130.3, 127.3, 114.9, 110.2, 108.9, 107.9, 101.5, 68.31, 31.9, 29.5, 29.4, 29.3, 29.0, 26.0, 22.7, 21.3, 18.1, 14.1 IR ($\upsilon_{max}$, cm$^{-1}$, KBr): 3404, 3279 ($\upsilon NH_2$) 2921, 2852 (υ aliphatic C-H), 1609 (υC=N), 1564, 1462 (υ aromatic C=C), 1514 (υN=N), 1169, 1144 (υ $PhOCH_2$-).

**2-((E)-((3-amino-4-((E)-(2,4-dimethylphenyl)diazenyl)phenyl)imino)methyl)-5-do decyloxy phenol (G12)**

Red brownish solid; Yield: 73%; $^{1}$H NMR (400 MHz, $CDCl_3$, TMS) $\delta_H$ 13.76 (s, ArO**H**, 1H),8.58 (s, -C**H**N-, 1H),7.90 (d, Ar**H**, 1H, *J*=8.4 Hz), 7.63 (d, Ar**H**, 1H, *J*=8.4 Hz), 7.30-7.28 (m, Ar**H**, 1H), 7.16 (s, Ar**H**, 1H), 7.10 (d, Ar**H**, 1H, *J*=7.2 Hz), 6.77 (dd, Ar**H**, 1H, *J*=8.4 Hz, *J*=2.4 Hz), 6.64 (d, Ar**H**, 1H, *J*=2.0 Hz),6.52-6.51(m, Ar**H**, 2H), 6.16 (s, N**H$_2$**, 2H), 4.03-4.00 (t, -OC**H$_2$**$CH_2$-, 2H), 2.64 (s, -C**H$_3$**, 3H), 2.40 (s, -C**H$_3$**, 3H), 1.85-1.28 (m, -C**H$_2$**-, 20H), 0.92-0.88 (t, -$CH_2$C**H$_3$**, 3H). $^{13}$CNMR (100MHz, $CDCl_3$, TMS) $\delta_C$ 164.4, 163.9, 161.6,150.7, 149.1, 136.4, 136.1, 133.7, 131.7, 130.3, 127.3, 114.9, 112.8, 110.2, 108.9, 107.9, 101.5, 68.3, 31.9, 29.7, 29.6, 29.4, 29.0, 26.0, 22.7, 21.3, 18.0, 14.1; IR ($\upsilon_{max}$, $cm^{-1}$, KBr): 3404, 3279 ($\upsilon NH_2$) 2920, 2850 (υ aliphatic C-H), 1609 (υC=N), 1564 (υ aromatic C=C), 1514, 1462 (υN=N), 1169, 1144 (υ $PhOCH_2$-).

**2-((E)-((3-amino-4-((E)-(2,4-dimethylphenyl)diazenyl)phenyl)imino)methyl)-5-tetra decyloxy phenol (G14)**

Red brownish solid; Yield: 62%; $^{1}$H NMR (400 MHz, $CDCl_3$, TMS) $\delta_H$ 13.74 (s, ArO**H**, 1H),8.58 (s, -C**H**N-, 1H),7.90 (d, Ar**H**, 1H, *J*=8.4 Hz), 7.63 (d, Ar**H**, 1H, *J*=8.4 Hz), 7.30-7.28 (m, Ar**H**, 1H), 7.16 (s, Ar**H**, 1H), 7.10 (d, Ar**H**, 1H, *J*=8.4 Hz), 6.77 (dd, Ar**H**, 1H, *J*=8.4 Hz, *J*=2.4 Hz), 6.64 (d, Ar**H**, 1H, *J*=2.0 Hz),6.52-6.50(m, Ar**H**, 2H), 6.15 (s, N**H$_2$**, 2H), 4.03-4.00 (t, -OC**H$_2$**$CH_2$-, 2H), 2.64 (s, -C**H$_3$**, 3H), 2.40 (s, -C**H$_3$**, 3H), 1.85-1.29 (m, -C**H$_2$**-, 24H), 0.92-0.89 (t, -$CH_2$C**H$_3$**, 3H). $^{13}$CNMR (100MHz, $CDCl_3$, TMS) $\delta_C$ : 164.5, 164.0, 161.6, 149.1, 143.5, 136.3, 133.9, 130.2, 127.2, 114.9, 112.8, 110.2, 108.9, 107.9, 101.5, 68.3, 31.9, 29.7, 29.6, 29.3, 29.0, 26.0, 22.7, 18.0, 14.1; IR ($\upsilon_{max}$, $cm^{-1}$, KBr): 3402, 3278 ($\upsilon NH_2$) 2919, 2859 (υ aliphatic C-H), 1609 (υC=N), 1563, 1463 (υ aromatic C=C), 1513 (υN=N), 1169, 1144 (υ $PhOCH_2$-).

**2-((E)-((3-amino-4-((E)-(2,4-dimethylphenyl)diazenyl)phenyl)imino)methyl)-5-hexa decyloxy phenol (G16)**

Red brownish solid; Yield: 78%; $^{1}$H NMR (400 MHz, $CDCl_3$, TMS) $\delta_H$ 13.76 (s, ArO**H**, 1H),8.58 (s, -C**H**N-, 1H),7.90 (d, Ar**H**, 1H, *J*=8.4 Hz), 7.63 (d, Ar**H**, 1H, *J*=8.0 Hz), 7.30-7.28 (m, Ar**H**, 1H), 7.16 (s, Ar**H**, 1H), 7.10 (d, Ar**H**, 1H, *J*=8.0 Hz), 6.77 (dd, Ar**H**, 1H, *J*=8.4 Hz, *J*=1.6 Hz), 6.64 (d, Ar**H**, 1H, *J*=1.6 Hz),6.52-6.51(m, Ar**H**, 2H), 6.17 (s, N**H$_2$**, 2H), 4.04-4.00 (t, -OC**H$_2$**$CH_2$-, 2H), 2.64 (s, -C**H$_3$**, 3H), 2.40 (s, -C**H$_3$**, 3H), 1.84-1.28 (m, -C**H$_2$**-, 28H), 0.91-0.88 (t, -$CH_2$C**H$_3$**, 3H); $^{13}$CNMR (100MHz, $CDCl_3$, TMS) $\delta_C$ 164.5, 164.0, 161.6, 150.8, 149.1, 143.2, 140.2, 136.5, 136.2, 133.7, 131.7, 130.4, 127.4, 115.0, 112.8, 110.3, 109.0, 108.0, 107.9, 101.5, 68.3, 32.0, 29.7, 29.6, 29.5, 29.4, 29.0, 26.0, 22.7, 21.4, 18.1, 14.2 IR ($\upsilon_{max}$, cm$^{-1}$, KBr): 3402, 3278 ($\upsilon NH_2$), 3013, 2964, 2919, 2849 ($\upsilon$ aliphatic C-H), 1610 ($\upsilon$C=N), 1564 ($\upsilon$ aromatic C=C), 1514, 1462 ($\upsilon$N=N), 1170, 1144 ($\upsilon$ Ph$OCH_2$-).

**2-((E)-((3-amino-4-((E)-(2,4-dimethylphenyl)diazenyl)phenyl)imino)methyl)-5-octa decyloxy phenol (G18)**

Red brownish solid; Yield: 65%; $^{1}$H NMR (400 MHz, $CDCl_3$, TMS) $\delta_H$ 13.76 (s, ArO**H**, 1H),8.59 (s, -C**H**N-, 1H),7.90 (d, Ar**H**, 1H, *J*=8.4 Hz), 7.63 (d, Ar**H**, 1H, *J*=8.4 Hz), 7.30-7.28 (m, Ar**H**, 1H), 7.16 (s, Ar**H**, 1H), 7.10 (d, Ar**H**, 1H, *J*=8.0 Hz), 6.77 (dd, Ar**H**, 1H, *J*=8.4 Hz, *J*=2.0 Hz), 6.65 (d, Ar**H**, 1H, *J*=2.4 Hz),6.52-6.50(m, Ar**H**, 2H), 6.15 (s, N**H$_2$**, 2H), 4.04-4.00 (t, -OC**H$_2$**$CH_2$-, 2H), 2.64 (s, -C**H$_3$**, 3H), 2.40 (s, -C**H$_3$**, 3H), 1.85-1.28 (m, -C**H$_2$**-, 32H), 0.91-0.88 (t, -$CH_2$C**H$_3$**, 3H); IR ($\upsilon_{max}$, cm$^{-1}$, KBr): 3402, 3278 ($\upsilon NH_2$) 2919, 2849 ($\upsilon$ aliphatic C-H), 1610 ($\upsilon$C=N), 1564 ($\upsilon$ aromatic C=C), 1514,1462 ($\upsilon$N=N), 1170, 1144 ($\upsilon$ Ph$OCH_2$-).

**5.4 Results and discussion**

In this work, we have prepared twelve new homologues of 2-((E)-((3-amino-4-((E)-(2, 4-dimethylphenyl) diazenyl)phenyl)imino)methyl)-5-*n*-alkoxyphenol. All the synthesized compounds were characterized by FT-IR, $^{1}$H-NMR, and $^{13}$C-NMR spectroscopy, and liquid crystal properties were checked by differential scanning calorimeter (DSC) and polarizing optical microscope (POM). In the structurally similar compounds, Iftime et al. have shown based on various NMR experiments that the reaction in the amine group takes place in the para position to the azo group, such as $^{1}$H, $^{1}$H COSY (Correlation Spectroscopy), $^{1}$H,$^{13}$C HMQC (Heteronuclear Multiple Quantum Coherence), $^{1}$H,$^{13}$C HMBC (Heteronuclear Multiple Bond Coherence), $^{1}$H,$^{15}$N HMBC, and $^{1}$H,$^{1}$H NOESY [19].

In the $^{1}$H-NMR spectrum of (E)-4-((2,4-dimethylphenyl)diazenyl) benzene-1,3-diamine two singlet at δ 6.27 and 3.97 ppm attributed to two free -$NH_2$ groups in the compound. The singlet peaks at δ 2.58 and 2.38 ppm, because there are the two methyl groups in the compound. The aromatic peak appears between δ 7.7-5.9 ppm. These data are in good agreement with the structure of the synthesized compound. In the $^{1}$H-NMR spectrum of synthesized series, the ArOH of salycylaldimine was observed as a singlet at approximately δ = 13.76 ppm. The azomethine proton (-CH=N-) appeared at δ 8.58 ppm as a singlet. The aromatic protons of the phenyl ring were observed in between δ 7.90-6.50 ppm. The singlet observed at 6.15 ppm, due to the presence of a free $NH_2$ group and confirmed that the imine bond was formed within one amino group, as reported in the literature [19]. The (-$OCH_2$-) alkoxy protons appeared at δ 4.03 as a triplet. The singlet at δ 2.64 and δ 2.40 ppm are due to the protons of the two methyl groups (-$CH_3$) in the compound. The other (-$CH_2$) protons of the alkoxy chain are found in the range of δ 1.85-1.28 ppm as a multiplet. The proton of the terminal methyl group of the alkoxy chain is observed at δ 0.90 ppm as a triplet. The formation of Schiff's base was confirmed by the presence of a characteristic sharp peak

of imine hydrogen (H-C=N) at δ 8.58 ppm and the characteristic peak of benzaldehyde hydrogen (H-C=O) at δ 9.71 ppm disappears.

In the $^{13}$C-NMR spectrum of compounds, the carbon bonded with the hydroxy group of salcylaldimine appears in the range of δ 164.0 ppm. The imine (-CH=N-) carbon is observed near δ =161.7 ppm. All other aromatic carbon atoms are observed in the range of δ 150.8 to 101.5 ppm. The carbon bonded with the oxygen of the alkoxy chain appears at δ =68.0 ppm. The δ around 21.4 ppm and 18.4 ppm is designated as the carbon atom of the methyl group (-$CH_3$) of the compound. The carbon of the terminal methyl group (-$CH_3$) of the alkoxy chain appears around δ 14.2 ppm. The ESI-Mass spectra of one of the homolog **G7** $[M + H]^+$ peak obtained at m/z 459.27 confirmed the structure of the molecule.

The infrared spectra of the synthesized compounds show different vibration modes, corresponding to different functional groups in the molecule. Because the primary amino group (-$NH_2$) is present in the molecule, there are two moderately strong absorption bands near 3410 and 3280 $cm^{-1}$. In the vicinity of 2919-2859 $cm^{-1}$, the aliphatic stretching vibration of methylene (-$CH_2$-) of the alkyl chain appears**.** The stretching vibration of (-N=N-) appears as low-intensity bands around 1510 $cm^{-1}$ and 1470 $cm^{-1}$. The strong absorption band at 1610 $cm^{-1}$ is due to the imine group (-C=N-) present in the compound. The medium intensity band at approximately 1560-1570 $cm^{-1}$ is attributed to the aromatic -C=C- stretching vibration. The medium intensity band around 1170 $cm^{-1}$ and 1140 $cm^{-1}$ is corresponding to alkyl aryl ethers.

A thermogravimetric analysis was carried out on **G7** and **G14** as representative compounds to verify the thermal stability of the synthesized homologue series. TGA thermogram of **G7** and **G14** is depicted in **Figure 6.** No mass loss up to 150 $^{o}$C indicates the absence of moisture and crystallisation water. The decomposition temperature of the **G7** and **G14** is higher than 270 °C, indicating that they are stable to their clearing points.

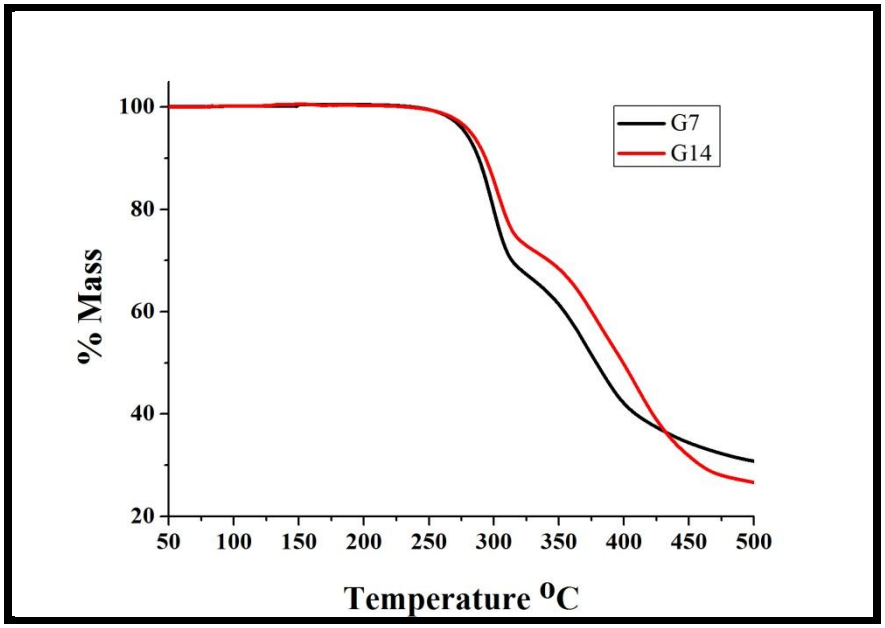


**Figure 6.** TGA thermogram of compound **G7** and **G14**

**Mesomorphic behaviour**

Differential scanning calorimetry (DSC) and polarizing optical microscopy (POM) are used to examine the phase transition temperature in $^{o}$C and the associated enthalpy change ($\Delta$H kJ mol$^{-1}$). The results are presented in **Table 1.**

All compounds of the synthetic series are mesogenic and have high thermal stability. In the homologous series, the lower derivatives from *n*-ethoxy **(G2)** to *n*-heptoxy **(G7)** have an enantiotropic nematic phase. In this phase, the constituent molecules are completely disordered with respect to each other, but the intermolecular forces of attractions are such that molecules retain their preferred orientation as they diffuse through the sample. The POM image of the *n*-heptyloxy derivative **(G7)**, as shown in **Figure 7a**, shows the nematic droplet texture formed when the isotropic liquid is cooled to 162.8°C. After further cooling, the

droplet texture of the nematic phase at 150.2 $^{o}$C becomes the thred like texture of the nematic phase, as shown in **Figure 7b**.

| Series-G | | |
|---|---|---|
| **Gn** | **Heating** | **Cooling** |
| **G2** | Cr 161.4 (30.2) N 190.1(0.5) I | I 180.4 (0.3) N 118.3 (20.2) Cr |
| **G3** | Cr 150.9 (31.6) N 169.2 (0.6) I | I 165.7 (0.2) N 130.7 (25.6) Cr |
| **G4** | Cr 161.8 (36.9) N 178.6 (0.3) I | I 171.4 (0.4) N 119.1 (19.5) Cr |
| **G5** | Cr 146.7 (43.0) N 166.2 (0.5) I | I 160.7 (0.4) N 120.1 (33.1) Cr |
| **G6** | Cr 137.3 (30.0) N 168.0 (0.4) I | I 161.7 (0.5) N 112.1 (16.3) Cr |
| **G7** | Cr 148.3 (43.3) N 162.9 (0.3) I | I 162.6 N 119.8 (23.4) Cr |
| **G8** | Cr 152.1 (39.4) SmA 156.5 (0.4) N167.0 (0.6) I | I 160.0 (0.8) N 139.1 (0.3) SmA 126.8 (34.4) Cr |
| **G10** | Cr 145.3 (41.5) SmA 158.3 (0.7) N 166.2 (0.8) I | I 159.4 (0.7) N 150.3 (0.4) SmA 103.9 (36.4) Cr |
| **G12** | Cr 133.7(28.0) SmA 165.8 (3.3) I | I 156.0 (2.8) SmA 96.1 (15.5) Cr |
| **G14** | Cr 128.4 (40.4) SmA 162.9 (4.8) I | I 151.9 (3.4) SmA 88.6 (22.3) Cr |
| **G16** | Cr 126.0 (32.3) SmA 153.0 (6.3) I | I 149.9 (2.9) SmA 82.7 (25.0) Cr |
| **G18** | Cr 125.6 (20.5) SmA 162.0 (1.7) I | I 151.8 (1.4) SmA 81.3 (11.8) Cr |

**Table1.** Phase transition temperatures in $^{o}$C and associated enthalpy change ($\Delta$H kJ mol$^{-1}$) for the homologous series.

Cr: Crystal; N: Nematic phase; SmA: Smectic A phase; I: Isotropic liquid.

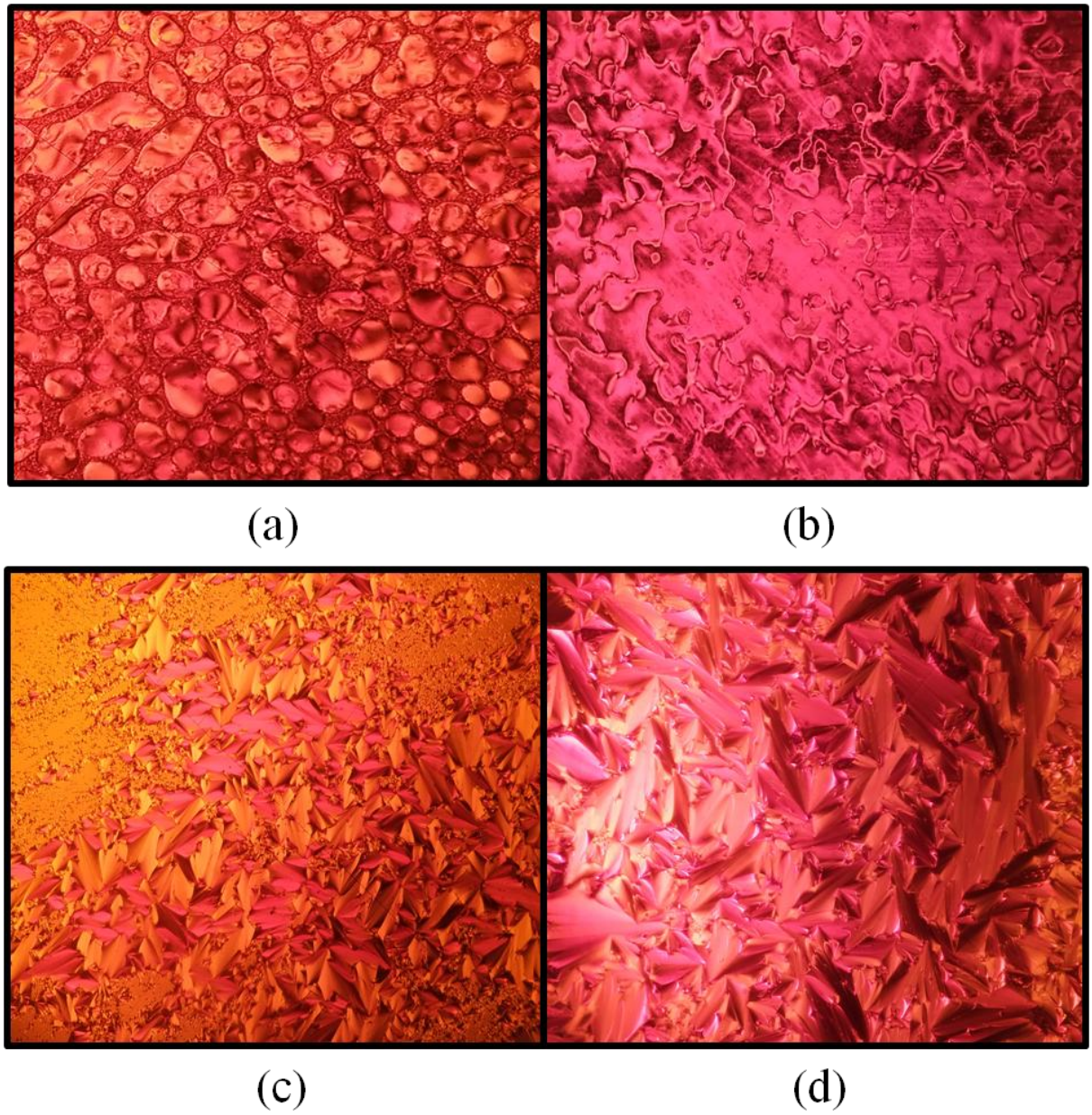


**Figure 7.** Polarising optical microscopic images (a) The droplet texture of nematic phase of **G7** on cooling at 162.2 $^{o}$C (b) The threaded texture of nematic phase of **G7** on cooling at 150.2 $^{o}$C (c) The nematic phase converted to Sm-A phase of **G10** on cooling at 150.3 $^{o}$C (d) The focal-conic fan shaped texture of Sm-A phase of **G14** on cooling at 151.9 $^{o}$C

The DSC thermograph of the n-heptyloxy **(G7)** derivative in Figure 8a shows two peaks when heated. The first peak at 148.3 $^{o}$C corresponds to the transition from the crystal to the nematic phase, and the corresponding enthalpy change is 43.3 kJ mol$^{-1}$. The second peak

at 162.9$^{o}$C is attributed to the transition from the nematic phase to an isotropic liquid, and the corresponding enthalpy change is 0.3 kJ mol$^{-1}$. The middle derivatives of the homologous series, *n*-octyloxy **(G8)** and *n*-decyloxy **(G10)** are dimorphic; in addition to the enantiotropic nematic phase, they also exhibited the smectic-A. The POM image of the *n*-decyloxy derivative **(G10)** as shown in **Figure 7c** indicates the transition from the threaded texture of a nematic phase to the focal-conic fan-shaped texture of smectic-A phase when cooled to 150.3$^{o}$C. The dimorphic behavior observed with POM is also consistent with the DSC thermogram of the *n*-decyloxy derivative **(G10).** The **G10** DSC thermogram is depicted in **Figure 8b.** There are three endothermic peaks and three exothermic peaks. The peak at 145.3 $^{o}$C with enthalpy change 41.5 kJ mol$^{-1}$corresponds to the crystal to smectic-A; the peak at 158.3 $^{o}$C with enthalpy change 0.7 kJ mol$^{-1}$ascribed to smectic-A to nematic; and the peak at 166.2 $^{o}$C, attributed nematic to isotropic liquid transitions with associated enthalpy change 0.7 kJ mol$^{-1}$. The three exothermic peaks at 159.4 $^{o}$C, 150.3 $^{o}$C, and 103.9 $^{o}$C are due to the transition from isotropic liquid to nematic, nematic to smectic-A, and smectic-A to crystal respectively. Among them, the smectic-A to crystal transition has a higher value of enthalpy change. In the higher homologous of the series from *n*-dodecyloxy **(G12)** to *n*-octadecyloxy **(G18)** nematic phase disappeared and exhibited only enantiotropic smectic-A phase. The POM image of *n*-tetradecyloxy derivative **(G14)** is depicted in **Figure 7d**, indicating a focal-conic fan-shaped texture of the smectic-A phase on cooling at 151.9 $^{o}$C. DSC thermogram of the *n*-tetradecyloxy derivative **(G14)** given in **Figure 8c**, showed two endothermic and two exothermic peaks. The two endothermic peaks correspond to the transformation of crystals into smectic-A and smectic-A into isotropic liquids. Two exothermic peaks attributed to isotropic liquid to smectic-A and smectic-A to crystal transitions. The maximum change in enthalpy (20-40 kJ mol$^{-1}$) is related to the phase transition of all compounds; it shows the presence of Cr-N / Cr-SmA phase transition during heating or N-Cr / SmA-Cr phase

transition during cooling. This is due to a significant change in molecular order during this phase transition. The minimum enthalpy change (0.2-0.8 kJ $mol^{-1}$) is associated with the phase change of any nematic phase transition; such as N-I or I-N or N-SmA or SmA-N phase transitions. This is because the nematic phase is the mesophase with the lowest degree of order and intermolecular forces are very weak. The phase transitions of SmA-I or I-SmA; accompanied by the enthalpy change in the range of 2-8 kJ $mol^{-1}$. The higher value with respect to a nematic phase transition is assigned to the SmA, which is more ordered than the nematic phase. The calculated value of the enthalpy change is consistent with typical nematic and smectic A phase transitions. [38]

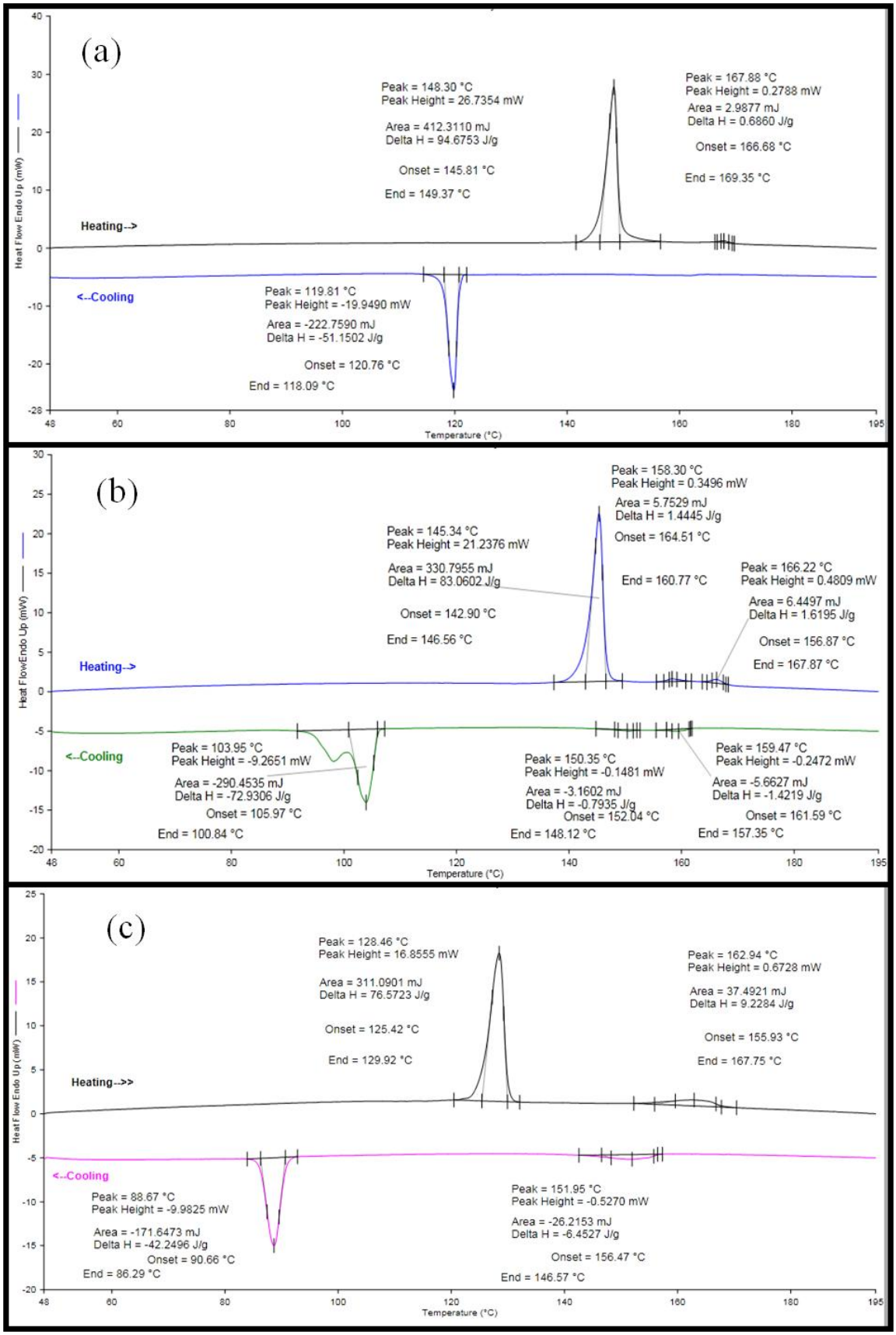


**Figure 8.** DSC traces of the: (a) G7 (b) G10 and (c) G14 on the heating and cooling, under $N_2$ atmosphere.

The influence of molecular flexibility on the transition temperature and phase sequence of the corresponding compound is illustrated in **Figure 9.** The results show that the different types of mesophases and the number of mesophases in the compound depend on the flexibility of the molecule, the number of carbon atoms in the terminal alkoxy group. The nematic phase commences from the first member of the series *n*-ethoxy derivative **(G2)** and continues to *n*-decyloxy derivative **(G10)**, while the smectic A phase starts from *n*-octyloxy derivative **(G8)** and continues to the last member of the series *n*-octadecyloxy **(G18)** derivative. The *n*-octyloxy **(G8)** and the *n*-decyloxy **(G10)** derivatives of this series show dimorphic behavior and exhibit smectic A and nematic phases. Mesophases for all homologous compounds were observed during heating and cooling, indicating the enantiotropic behavior of all compounds. It is also noted that the melting point declines significantly as the chain length increases due to increased flexibility. The temperature curve of nematic liquid to isotropic liquid follows a zigzag trajectory, with alternating rising and falling values throughout the series, and a downward trend in the series as a whole**.** The temperature at which the nematic liquid transforms into an isotropic liquid, a significant odd-even effect is observed; even-numbered alkoxy chains produce higher isotropic temperature values than odd-numbered alkoxy chains. This odd-even effect is due to the oxygen in the ether creating a steric equivalent of the $CH_2$ unit, so in odd-numbered alkoxy chains, the linear structure deviates from the more favorable all-trans chain conformation. So even the number of carbon atoms in the alkoxy chain has better order than an odd number of carbon atoms in the alkoxy chain of the terminal unit [39].As the length of the end chain increases, the effect becomes less pronounced [40].The sequential addition of methylene units promotes the flexibility of the molecule and the resulting comprehensive effect of molecular rigidity and flexibility, which varies from homolog to homolog, leading to a reversal of the trend of mesogenic behavior [41].

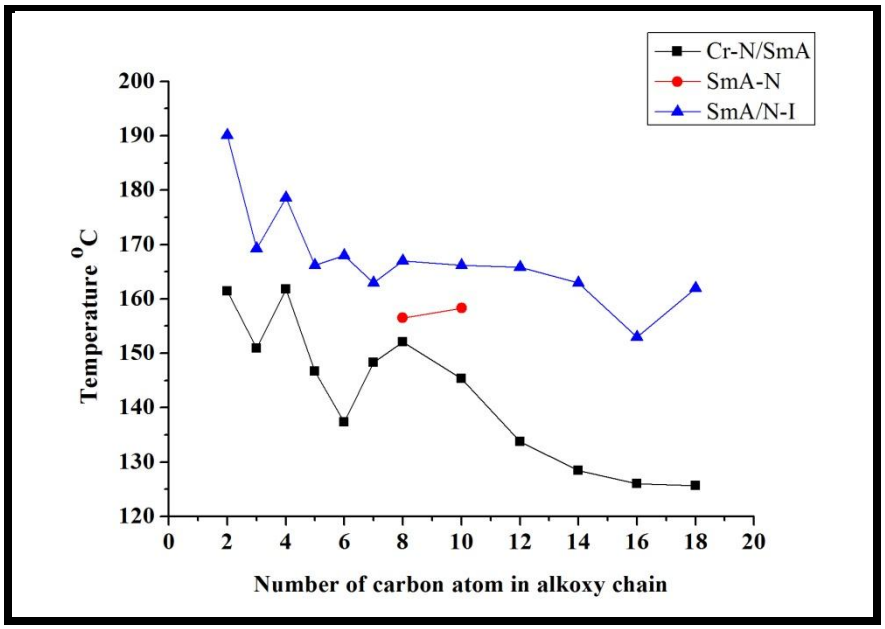


**Figure 9**. On heating phase behavior of homologous series G

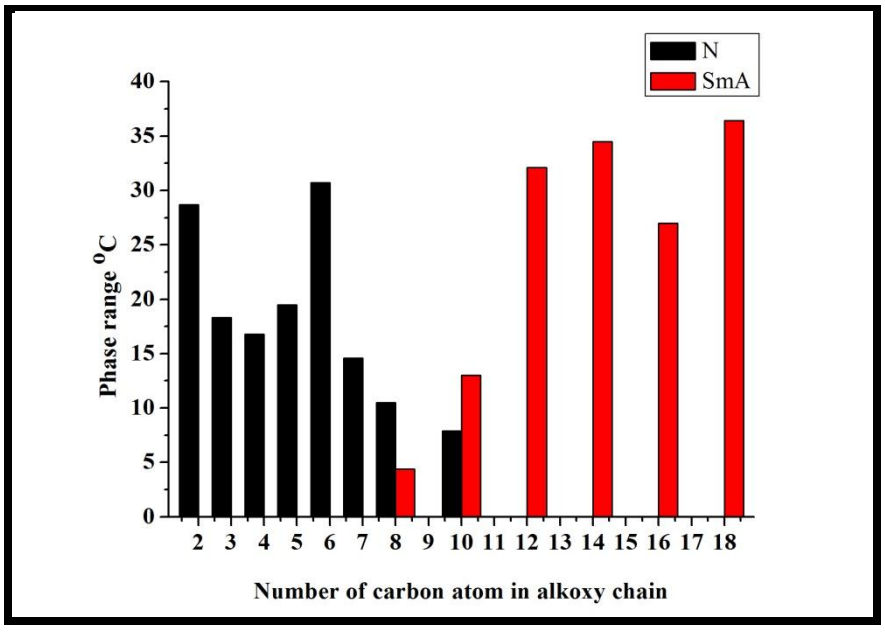


**Figure 10.** On heating smectic A and nematic phase range of series G

Refer to **Figure 10** to understand the influence of alkoxy chain length on the smectic and nematic phase ranges in the heating cycle. According to these results, the compound **(G6)** shows a wider nematic temperature range than all the mesogens of the series during the heating cycle. These results are almost consistent with the results of [42]. From the graph, it is evident that there is a significant decrease in the mesomorphic range of the nematic phase

with the increase of the alkoxy chain length and disappears after the *n*-decyloxy derivative. This is because the flexibility of the long-chain tends to destroy the molecular packing required to form the nematic phase. Although the smectic behavior increases with the length of the alkoxy chain, and the trend towards the last homologous *n*-octadecyloxy derivative continues. This is due to, the long chains attract, entangle and stabilize the layered packing required to form the smectic phase. This is consistent with previous findings [43].

**Theoretical calculation using DFT methods**

**Geometry Optimization**

DFT level calculations and full geometry optimization of all synthesized compounds have been executed using B3LYP/6-31+G (d, p) basis sets. DFT calculations have been widely used in recent years due to their ability to provide reasonably good results for large molecular structures. All calculations are performed using the Gaussian16 program [44] for calculations, and the molecular orbitals are created using Gauss View 6.0 program [45]. The structural parameters such as bond lengths and bond angles assumed for compounds theoretically were found to be consistent with the similar parameters obtained experimentally by X-ray study of closely related compounds. The geometry optimized for the minimum energy conformation of the **G2-G18** is presented in **Figure 11**. The energy of optimized geometry, HOMO-LUMO gaps, hardness (η), and global softness (S) for the synthesized compounds have summarized as follows in **Table 2.** There **Figure 12** illustrates the HOMO-LUMO energy gaps diagram of the compounds.

| | HOMO (eV) | LUMO (eV) | Energy Band gap (ΔE)(eV) | Energy (Hartree) | Hardness η=(ΔE/2) | Global softness *S*= 1/ΔE |
|---|---|---|---|---|---|---|
| **G2** | -5.5133 | -2.4664 | 3.0468 | -1260.42 | 1.5234 | 0.328213 |
| **G3** | -5.5084 | -2.4618 | 3.0465 | -1299.74 | 1.52325 | 0.328246 |
| **G4** | -5.5065 | -2.4593 | 3.0471 | -1339.06 | 1.52355 | 0.328181 |
| **G5** | -5.5048 | -2.4580 | 3.0468 | -1378.38 | 1.5234 | 0.328213 |
| **G6** | -5.5043 | -2.4574 | 3.0468 | -1417.69 | 1.5234 | 0.328213 |
| **G7** | -5.5035 | -2.4571 | 3.04631 | -1457.01 | 1.523155 | 0.328266 |
| **G8** | -5.4969 | -2.4536 | 3.0433 | -1496.33 | 1.52165 | 0.328591 |
| **G10** | -5.4961 | -2.4539 | 3.0422 | -1574.96 | 1.5211 | 0.328709 |
| **G12** | -5.5024 | -2.4563 | 3.0460 | -1653.60 | 1.523 | 0.328299 |
| **G14** | -5.5021 | -2.4563 | 3.0457 | -1732.23 | 1.52285 | 0.328332 |
| **G16** | -5.5021 | -2.4563 | 3.0457 | -1810.87 | 1.52285 | 0.328332 |
| **G18** | -5.5021 | -2.4558 | 3.0463 | -1889.50 | 1.52315 | 0.328267 |

**Table2.** Molecular orbital energies, hardness (η) and global softness (S) on compounds **G2-G18**

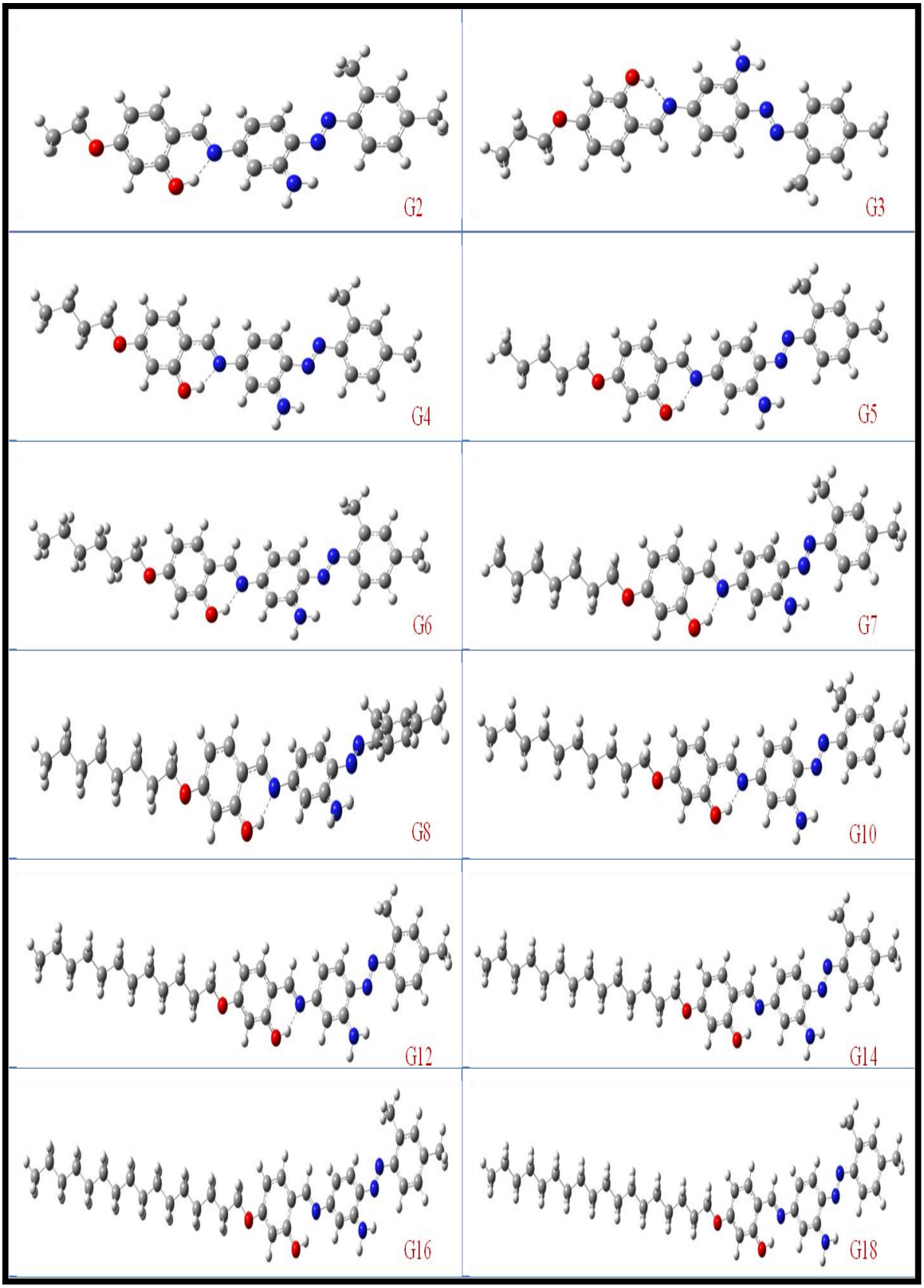


**Figure11.** An optimized geometry for the minimum energy conformation of **G2-G18**

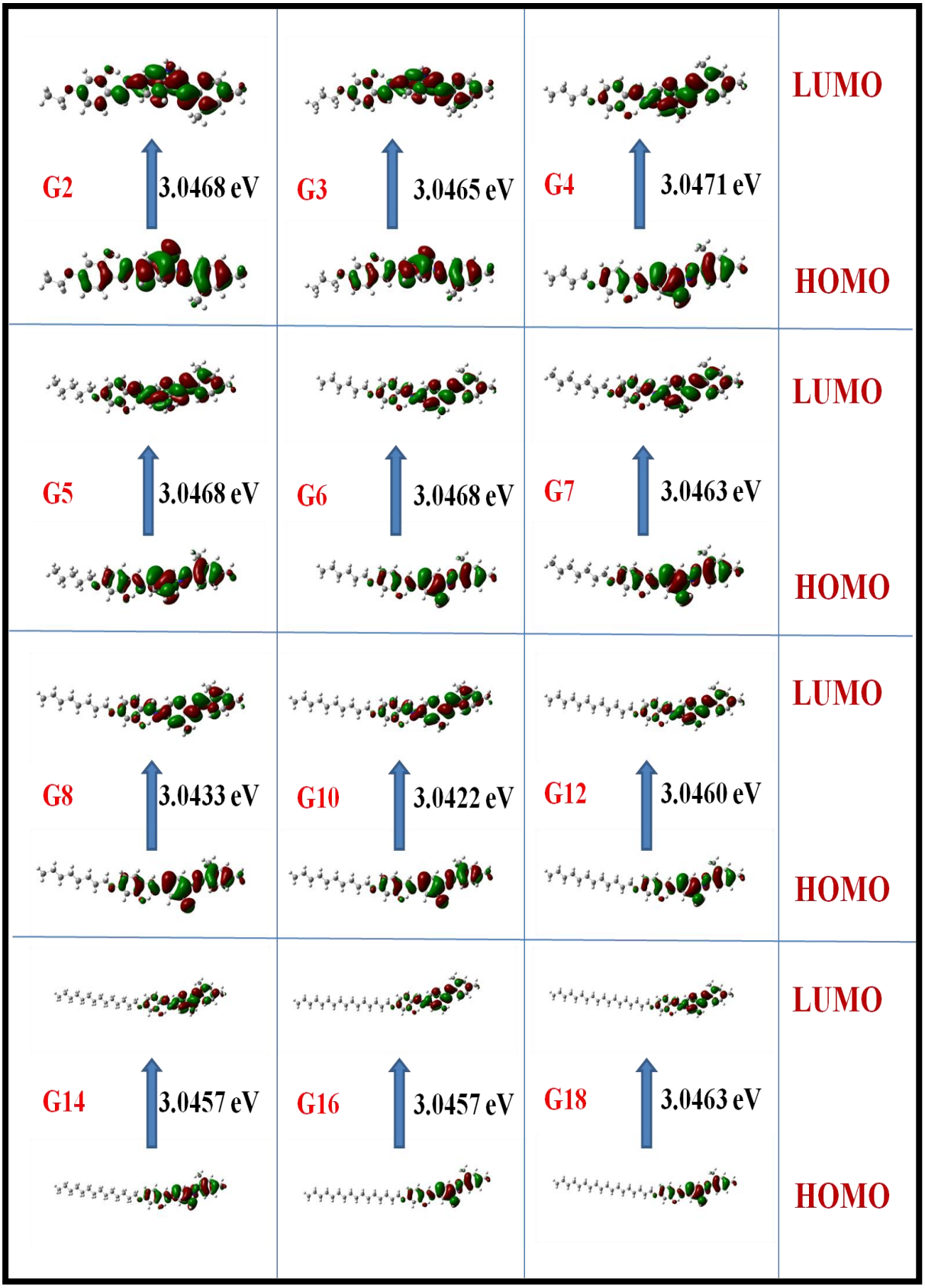


**Figure12.** The estimated plots for frontier molecular orbital of the prepared compounds

**Molecular electrostatic potential**

The charge distribution map for the synthesized compounds was calculated under the same basis sets according to molecular electrostatic potential (MESP). The MESP surfaces of compound **G2-G18** are provided in **Figure 13**. The dipole moment, molecular polarization, and many other properties depend to a large extent on the electron density on the atomic sites of the compound being studied [46]. The molecular electrostatic potential (MESP) of chemical species plays a critical role in determining the properties and potential sites associated with those properties. In the mapping of the electrostatic potential surface of compounds, the occurrence of negative potential is found to be concentrated over the oxygen whereas the positive potential is around the nitrogen.

**Effect of Dipole moment and polarizibility on mesomorphic behavior**

| **Compound** | **G2** | **G3** | **G4** | **G5** | **G6** | **G7** | **G8** | **G10** | **G12** | **G14** | **G16** | **G18** |
|---|---|---|---|---|---|---|---|---|---|---|---|---|
| $T_C$, **Smectic A** | - | - | - | - | - | - | 152.1 | 145.3 | 133.7 | 128.4 | 126.0 | 125.6 |
| $\Delta T_{SmA}$ **(Mesomorphic range)** | - | - | - | - | - | - | 4.4 | 13.0 | 32.1 | 34.5 | 27.0 | 36.4 |
| $T_C$ **(Mesomorphic stability)** | - | - | - | - | - | - | 156.5 | 158.3 | 165.8 | 162.9 | 153.0 | 162.0 |
| $T_C$, **Nematic** | 161.4 | 150.9 | 161.8 | 146.7 | 137.3 | 148.3 | 156.5 | 158.3 | - | - | - | - |
| $\Delta T_N$ **(Mesomorphic range)** | 28.7 | 18.3 | 16.8 | 19.5 | 24.4 | 14.6 | 10.5 | 7.9 | - | - | - | - |
| $T_C$ **(Mesomorphic stability)** | 190.1 | 169.2 | 178.6 | 166.2 | 161.7 | 162.9 | 167.0 | 166.2 | - | - | - | - |
| **Dipole moment, μ Total** | 2.41 | 2.44 | 2.52 | 2.49 | 2.57 | 2.52 | 3.56 | 3.57 | 2.61 | 2.61 | 2.62 | 2.62 |
| **Polarizibility (a.u)** | 443.9 | 458.0 | 472.0 | 485.4 | 498.6 | 511.5 | 525.1 | 550.5 | 575.5 | 599.6 | 613.4 | 649.2 |

**Table 3.** The dipole moment and polarizability related to the mesophase thermal stability value and the mesophase temperature range.

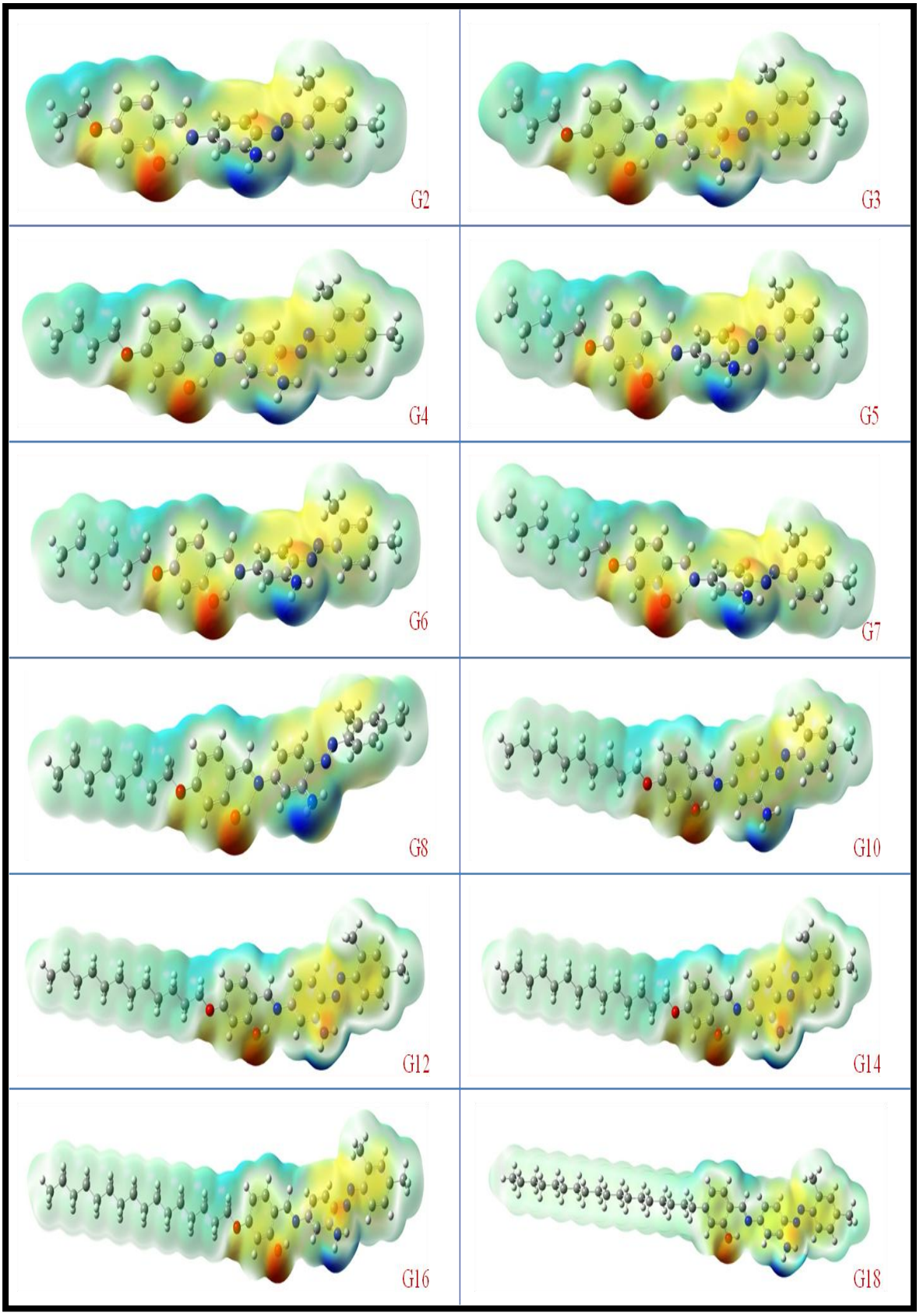


**Figure13.** Representations of electron density from total SCF density (Iso value= 0.0004; mapped with ESP)

The dipole moment and polarizability of the studied compound are related to the mesophase thermal stability value and the mesophase temperature range determined experimentally. The mesophase stability of liquid crystal compounds is dependent on intermolecular interaction, of which the attraction of dipole-dipole attraction plays a significant role [47]. As shown in **Table 3**; the estimated dipole moment and polarizability depend on the length of the alkoxy chain of the series under examination. Compared with other compounds in this series, derivatives of *n*-octyloxy (**G8)** and *n*-decyloxy (**G10)** with a higher dipole moment of almost 3.57 Debye were found to have nematic and smectic phases**.** This is explained based on the fact that an increase in the value of the dipole moment enables significant end-to-end and lateral to lateral interactions to organize the molecules into nematic or smectic phase [33]. It found that increasing the number of carbon atoms increases the polarizability of the molecule, and it will lead to a more ordered mesophase [48].It is quite evident from these data that the dipole moment and the polarizability of the molecule affect the mesophase to a large extent. Therefore, increasing the chain length of the alkoxy group will cause a more stable mesophase. In the longer chain length, the alignment of molecules in the mesophase promotes a bilayer structure [49]. In the smectic layer, the dipole moment acting through the long axis of the molecule is amplified and is important to increase the lateral attraction for maintaining order**.**

**Photoisomerization studies**

In photoisomerization studies, a 2.5 x $10^{-5}$ M solution of compound **G7** in chloroform was prepared. Initially, according to the spectrum shown by the black line in **Figure 14a**, the compound is in a trans-state. The UV spectrum of this compound shows absorption bands at 371, and 540 nm. The high-intensity band at 371nm corresponds to the π-π* transition, and the low-intensity band at 540 nm attributes to the n-π* transition. Irradiation with a

wavelength of 365nm corresponds to the band gap of transition energy π-π*, which is suitable for the conversion of trans isomers to cis isomers. Due to the irradiation, as the transform is converted to the cis form, the absorption at 371 nm decreases, and the absorption at 540 nm increases. After 25 seconds, the photo stationary state of a cis-trans mixture is achieved. The photoisomerization phenomenon in azobenzene derivatives is completely reversible. After a while, the process of thermal relaxation was observed, as shown in **Figure 14b**. In the photo stationary state, the absorption spectrum shows three isosbestic points at 260, 354, and 508 nm. Thermal relaxation after 60 minutes almost converts the entire cis form back to the transform.

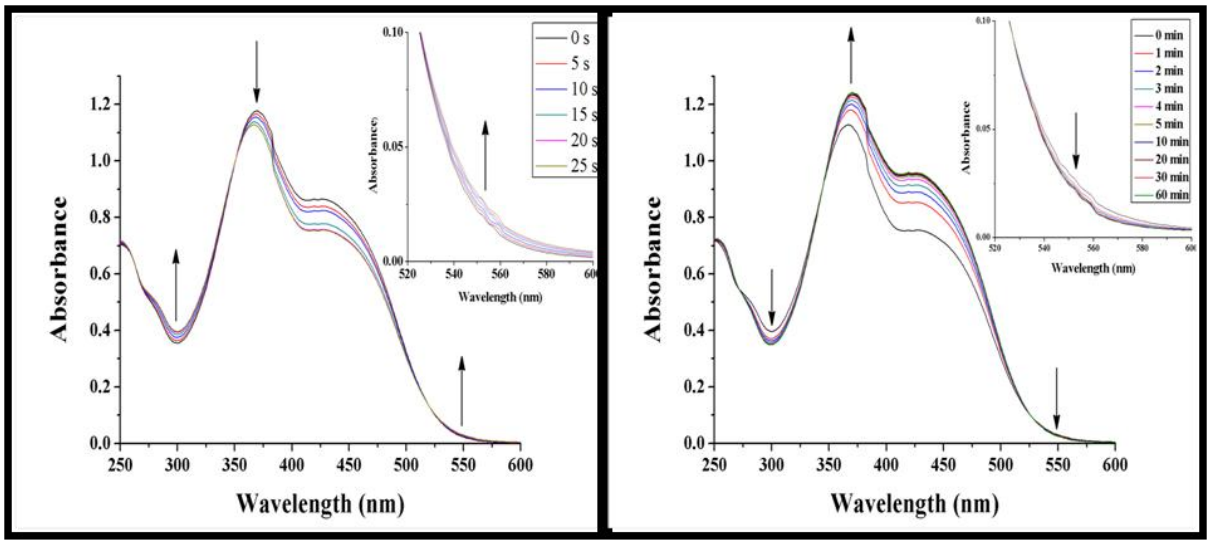


**Figure14**. (**a**) Time dependent absorption spectra during UV exposure for the compound **G7**; (**b**) Time dependent absorption spectra during the thermal back relaxation for the compound **G7.**

### 5.5 Structurally similar compounds

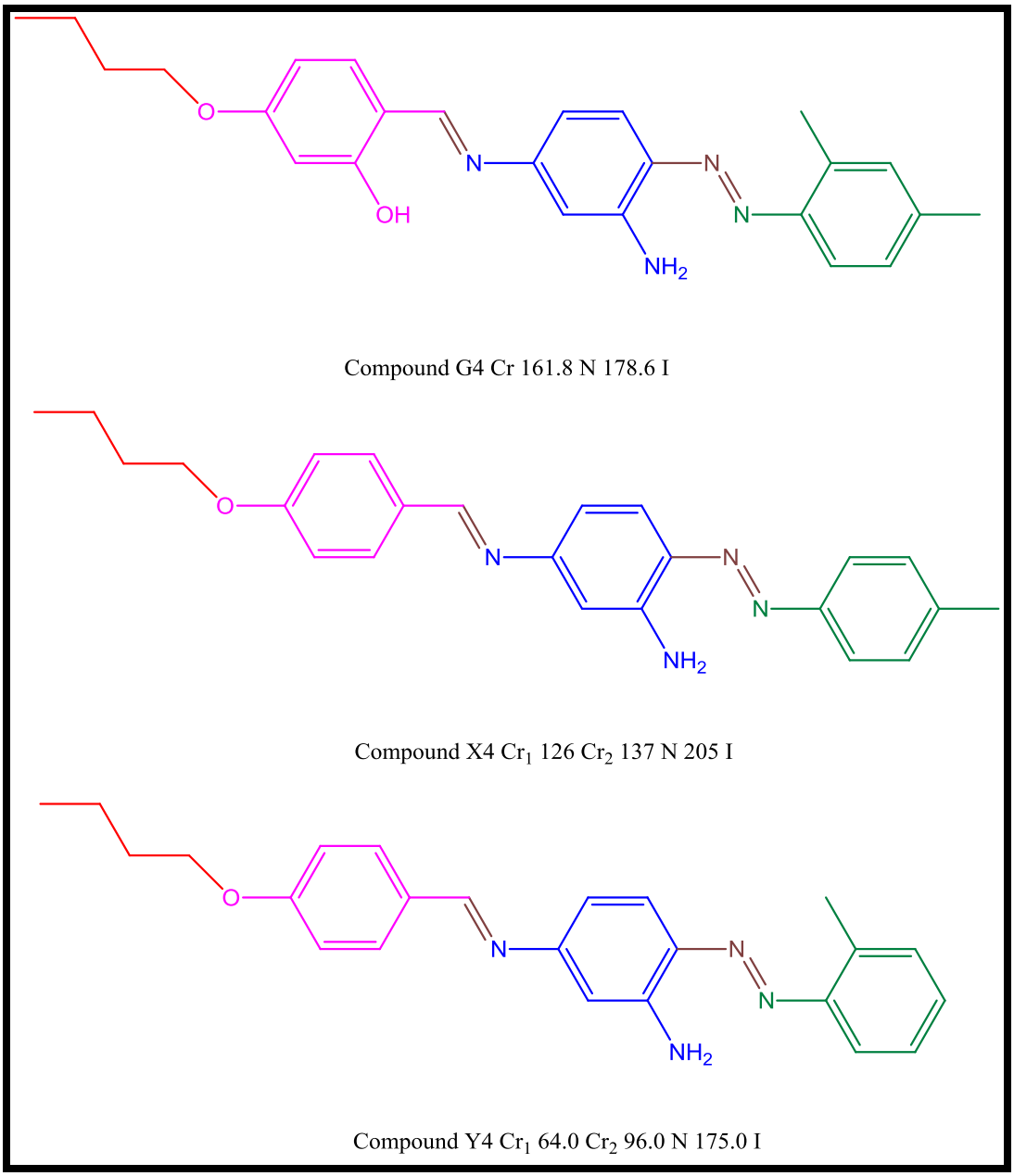


Compare the mesogenic behaviors of compound **G4** from homologous series G other known compounds X4 [19] and compound Y4 [19] with similar structures; as shown in **Figure 15.** The compound **G4,** compound X4 and compound Y4 chosen for comparison are structurally identical with respect to three phenyl rings linked through–N=N–and –C=N– central bridges as rigid core and–$OC_4H_9$ as a terminal end group that contributes to the molecular flexibility. However, they differ with respect to the molecular part –OH, –$CH_3$, as

lateral substitution which creates differences in the magnitudes of mesomorphism and the degree of mesomorphism. All three compounds exhibited nematic phase. The order of nematic phase stability is X4 > G4 > Y4 while the order of the nematic phase range is Y4 > X4 > G4.

## 5.6. Conclusion

New azo-azomethine-based homologous series have been synthesized, characterized by FT-IR, $^{1}$H-NMR, and $^{13}$C-NMR spectroscopy and mesomorphic behavior studied using Differential Scanning Calorimeter (DSC) and Polarizing Optical Microscope (POM). The synthesized homologous series of azo-azomethine is smectogenic and nematogenic. All the compounds are mesogenic and exhibited various phases depending on their molecular flexibility. The lower members are nematic; the medium members are both nematic as well as smectic, and the higher members are smectic only. It is found that as the length of the terminal alkoxy chain increases, the stability of the smectic phase increases, while the stability of the nematic phase decreases. In the present series, the obtained mesophase type is nematic/smectic or both; the phase stability of the obtained mesophase; its mesophase range depends largely on the flexibility of the molecule. The mesomorphic result indicates that the mesophase range in the cooling scan is wider than the heating scan. The results of the DFT calculation show that the calculated polarization, dipole moment, and stability increase with the increase of chain length.

**5.7 References**

[1] Benkhaya S, Souad M, Ahmed EI. Classifications , properties , recent synthesis and applications of azo dyes. Heliyon .2020;6: e03271.

[2] Hegde RS, Sunil BN, Hegde G, et al. In fl uence of alkyl and alkoxy groups on photoresponsive behaviour of bent-core azo mesogens : Synthesis , mesomorphic and photoswitching properties. J. Mol. Liq. 2020;309:113091.

[3] Madiahlagan E, B N S, Ngaini Z, et al. Synthesis, liquid crystalline properties and photo switching properties of coumarin-azo bearing aliphatic chains: Application in optical storage devices. J. Mol. Liq. 2019;292:111328.

[4] Hegde G, Kozenkov VM, Chigrinov VG, et al. Photoisomerization in photoaligned azo dyes exhibiting photostability. Mol. Cryst. Liq. Cryst. 2009;507:41–50.

[5] Niezgoda I, Jaworska J, Pociecha D, et al. The kinetics of the E-Z-E isomerisation and liquid-crystalline properties of selected azobenzene derivatives investigated by the prism of the ester group inversion. Liq. Cryst. 2015;42:1148–1158.

[6] Wang X, Li Z, Zhao H, et al. New azobenzene liquid crystal with dihydropyrazole heterocycle and photoisomerization studies: New azobenzene liquid crystal. R. Soc. Open Sci. 2020;7.

[7] Hegde G, Shanker G, Gan SM, et al. Synthesis and liquid crystalline behaviour of substituted (E)-phenyl-4-(phenyldiazenyl) benzoate derivatives and their photo switching ability. Liq. Cryst. 2016;43:1578–1588.

[8] Westphal E, Bechtold IH, Gallardo H. Synthesis and optical/thermal behavior of new Azo photoisomerizable discotic liquid crystals. Macromolecules. 2010;43:1319–1328.

[9] Rahman L, Kumar T, Sarkar SM, et al. New U-shaped liquid crystals azobenzene derived from catechol for photoswitching properties. J. Mol. Liq. 2015;202:125–133.

[10] Lin J, Ji X, Guo H, et al. Novel perylene columnar liquid crystal tuned by azo isomerization on bay-positions. J. Mol. Liq. 2019;290:111228.

[11] Pham VP, Manivannan G, Lessard RA, et al. New azo-dye-doped polymer systems as dynamic holographic recording media. 1995;242:239–242.

[12] Rahmouni A, Bougdid Y, Moujdi S, et al. Photoassisted holography in azo dye doped polymer films. J. Phys. Chem. B. 2016;120: 11317–11322.

[13] Zakerhamidi MS, Kiani S, Tajalli H, et al. Role of specific and nonspecific intermolecular interaction in electro-optical response of doped 6CHBT nematic liquid crystal with azo dyes. J. Mol. Liq. 2016;221:608–616.

[14] Natansohn A, Rochon P. Photoinduced motions in azo-containing polymers. Chem. Rev. 2002;102: 4139–4176.

[15] Mustroph H, Stollenwerk M, Bressau V. Current developments in optical data storage with organic dyes.Angew Chem. Int. Ed. Engl. 2006;45:2016-2035.

[16] Rochon P, Batalla E, Natansohn A, et al. Optically induced surface gratings on azoaromatic polymer films. Appl. Phys. Lett.1995;66:136.

[17] Gan SM, Yuvaraj AR, Lutfor MR, et al. Synthesis, liquid crystal characterization and photo-switching studies on fluorine substituted azobenzene based esters.RSC Adv. 2015;5:6279–6285.

[18] Manna AK, Mondal J, Chandra R, et al. A fluorescent colorimetric azo dye based chemosensor for detection of S2− in perfect aqueous solution and its application in real

sample analysis and building a molecular logic gate. Anal. Methods. 2018;10:2317–2326.

[19] Iftime M, Cozan V, Airinei A et al. Asymmetric azomethine amines with azobenzene moieties – liquid crystalline and optical properties. Liq. Cryst. 2019;00:1–11.

[20] Ahmed NHS, Saad GR, Ahmed HA et.al. New wide-stability four-ring azo/ester/Schiff base liquid crystals: synthesis, mesomorphic, photophysical, and DFT approaches. RSC Adv.2020;10:9643–9656.

[21] Nakum KJ, Katariya KD, Jadeja RN, et al. Schiff base of 4-n-alkoxy-2-hydroxy benzaldehyde with 4-amino acetophenone and their Cu ( II ) complexes : synthesis , characterization and mesomorphic behavior. Mol. Cryst. Liq. Cryst. 2019;690:1–13.

[22] Heng BT, Yeap GY, Mahmood WAK, et al. Alkyl chain self ordering, induction and suppression of mesophase by Cu(II) containing [1,2,3]-triazole-based bidentate salicylaldimine ligands: synthesis, characterisation and X-ray diffraction studies. Liq. Cryst. 2014;41:1897–1910.

[23] Yelamaggad C V, Tamilenthi VP. Synthesis and thermal properties of liquid crystal trimers comprising cyanobiphenyl and salicylaldimine anisometric segments. Tetrahedron 2009;65:6403–6409.

[24] Abbasi AR, Rezvani Z, Nejati K. Synthesis and properties of new liquid crystalline compounds containing an alkoxyphenylazo group. Dye. Pigment. 2006;70:71–75.

[25] Ahmed NHS, Saad GR. Effect of replacing the terminal phenyl ring with 3-pyridyl and inversion of imine linkage on the mesophase behaviour of four-ring azo/ester/Schiff base compounds. Liq. Cryst. 2020;00:1–14.

[26] Thaker BT, Kanojiya JB, Tandel RS. Effects of different terminal substituents on the mesomorphic behavior of some azo-Schiff base and azo-ester-based liquid crystals. Mol. Cryst. Liq. Cryst. 2010;528:120–137.

[27] Hamryszak L, Janeczek H, Schab-Balcerzak E. New thermotropic symmetrical and unsymmetrical azomethine with azobenzene unit and fluorinated alkyl chain: Synthesis and characterization. J. Mol. Liq. 2012;165:12–20.

[28] Iwan A, Janeczek H, Domanski M, et al. Synthesis, characterization and mesomorphic properties of new unsymmetrical azomethine-type liquid crystals derived from 4-biphenyl carboxaldehyde. J. Mol. Liq. 2010;151:30–38.

[29] Nejati K, Rezvani Z, Alizadeh E, et al. Synthesis and mesomorphic properties of symmetric tetradentate Schiff bases based on azo-containing salicylaldimines and their copper(II) complexes. J. Coord. Chem. 2011;64:1859–1870.

[30] Abid KK, Al-barody SM. Synthesis, characterisation and liquid crystalline behaviour of some lanthanides complexes containing two azobenzene Schiff base. Liq. Cryst. 2014;41:1303–1314.

[31] Zhang X bing, Tang B chen, Zhang P, et al. Synthesis and characterization of 1,3,4-oxadiazole derivatives containing alkoxy chains with different lengths. J. Mol. Struct. 2007;846:55–64.

[32] Lifka T, Zerban G, Seus P, et al. Alkoxy substituted (E,E)-3,6-bis(styryl)pyridazine-a photosensitive mesogen for liquid crystals. Tetrahedron. 2008;64:6551–6560.

[33] Gray GW. The influence of molecular structure on liquid crystalline properies. Mol. Cryst. 1966;1:333–349.

[34] Pathak SK, Nath S, De J, et al. The effect of regioisomerism on the mesomorphic and photophysical behavior of oxadiazole-based tris(N-salicylideneaniline)s: synthesis and characterization. New J. Chem. 2017;41:9908–9917.

[35] Achalkumar AS, Shankar Rao DS, Yelamaggad C V. Non-symmetric dimers comprising chalcone and cholesterol entities: An investigation on structure-property correlations. New J. Chem. 2014;38:4235–4248.

[36] Šmahel M, Poryvai A, Xiang Y, et al. Photosensitive bent-core nematic liquid crystals with various linking units in the side arms: Structure-properties relationships. J. Mol. Liq. 2020;306:112743.

[37] I. Sava, A.-M. Resmerita, G. Lisa, V. Damian, N. Hurduc, Synthesis and photochromic behavior of new polyimides containing azobenzene side groups, Polymer . 49 (2008) 1475–1482.

[38] Collings, P.J., & Hird, M. (1997). Introduction to Liquid Crystals: Chemistry and Physics (1st ed.). CRC Press, London.

[39] Jia Y-G, Luo C-C, Zhu Z-X, et al. Synthesis and properties of new (−)-menthol-derived chiral liquid crystal compounds with alkyl or alkoxy terminal groups. Liq. Cryst. 2017;44:526–537.

[40] Luo C-C, Jia Y-G, Sun B-F, et al. The effect of chain length in terminal groups on the mesomorphic behavior of novel (−)-menthol-based chiral liquid crystal compounds with a blue phase. New J. Chem. 2017;41:3677–3686.

[41] Marathe RB, Doshi A V. Study of relation between liquid crystal properties and molecular structure of halogenated benzyl alcohol ester derivative. Mol. Cryst. Liq.

Cryst. 2017;648:14–21.

[42] Ali GQ, Tomi IHR. Synthesis and characterization of new mesogenic esters derived from 1,2,4-oxadiazole and study the effect of alkoxy chain length in their liquid crystalline properties. Liq. Cryst. 2018;45:421–430.

[43] Ahmed HA, Naoum MM, Saad GR. Effect of alkoxy-chain length proportionation on the mesophase behaviour of terminally di-substituted phenylazo phenyl benzoates. Liq. Cryst. 2013;40:914–921.

[44] M.J. Frisch, G.W. Trucks, H.B. Schlegel, G.E. Scuseria, M. a. Robb, J.R. Cheeseman, G. Scalmani, V. Barone, G. a. Petersson, H. Nakatsuji, G16_C01, (2016) Gaussian 16, Revision C.01, Gaussian, Inc., Wallin.

[45] GaussView, Version 6.1, Roy Dennington, Todd A. Keith, and John M. Millam, Semichem Inc., Shawnee Mission, KS, 2016.

[46] Ahmed HA, Hagar M, El-Sayed TH, et al. Schiff base/ester liquid crystals with different lateral substituents: mesophase behaviour and DFT calculations. Liq. Cryst. 2019;46:1–11.

[47] Saad GR, Nessim RI. Effect of molecular structure on the phase behaviour of some liquid crystalline compounds and their binary mixtures VI[1]. The effect of molecular length. Liq. Cryst. 1999;26:629–636.

[48] Hagar M, Ahmed HA, El-Sayed TH, et al. Mesophase behavior and DFT conformational analysis of new symmetrical diester chalcone liquid crystals. J. Mol. Liq. 2019;285:96–105.

[49] Roushdy M. Effect of substituents and alkoxy chain length on the phase behaviour and

optical properties of 4-substituted-phenyl 4-alkoxybenzoates. Liq. Cryst. 2004;31:371–375.

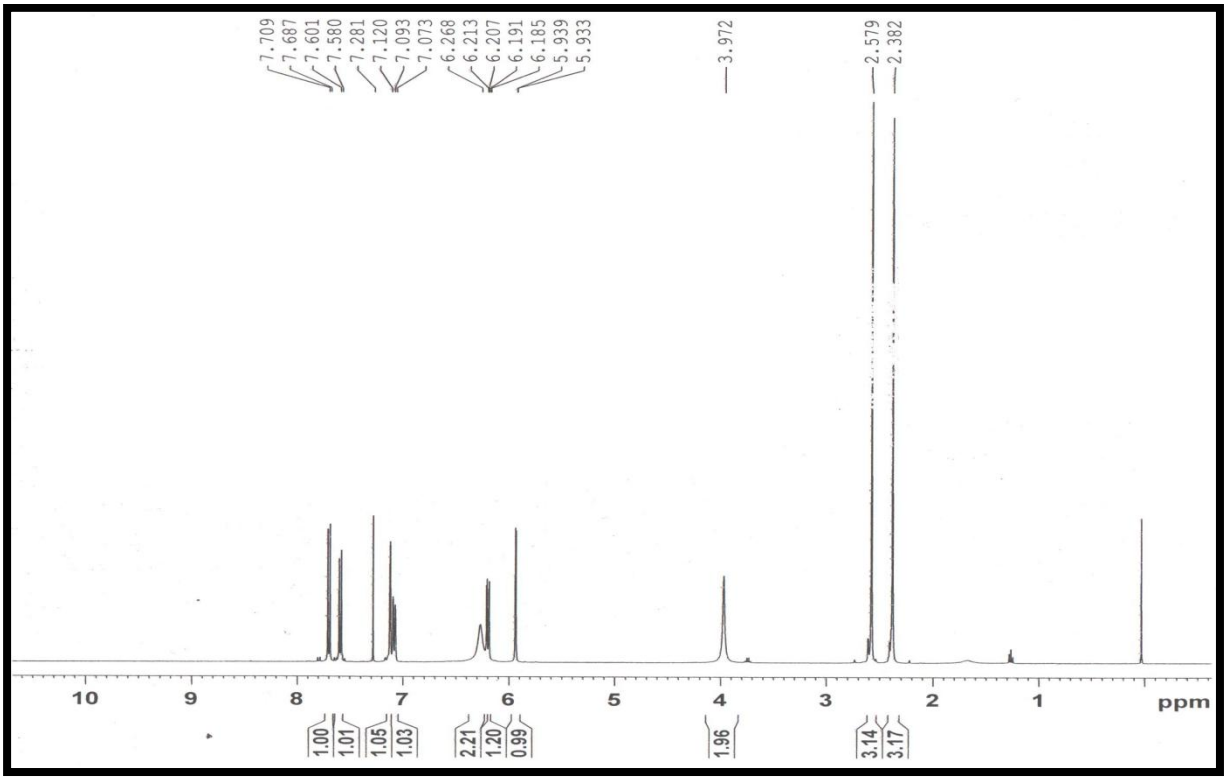


$^{1}$H NMR of (E)-4-((2,4-dimethylphenyl)diazenyl) benzene-1,3-diamine.

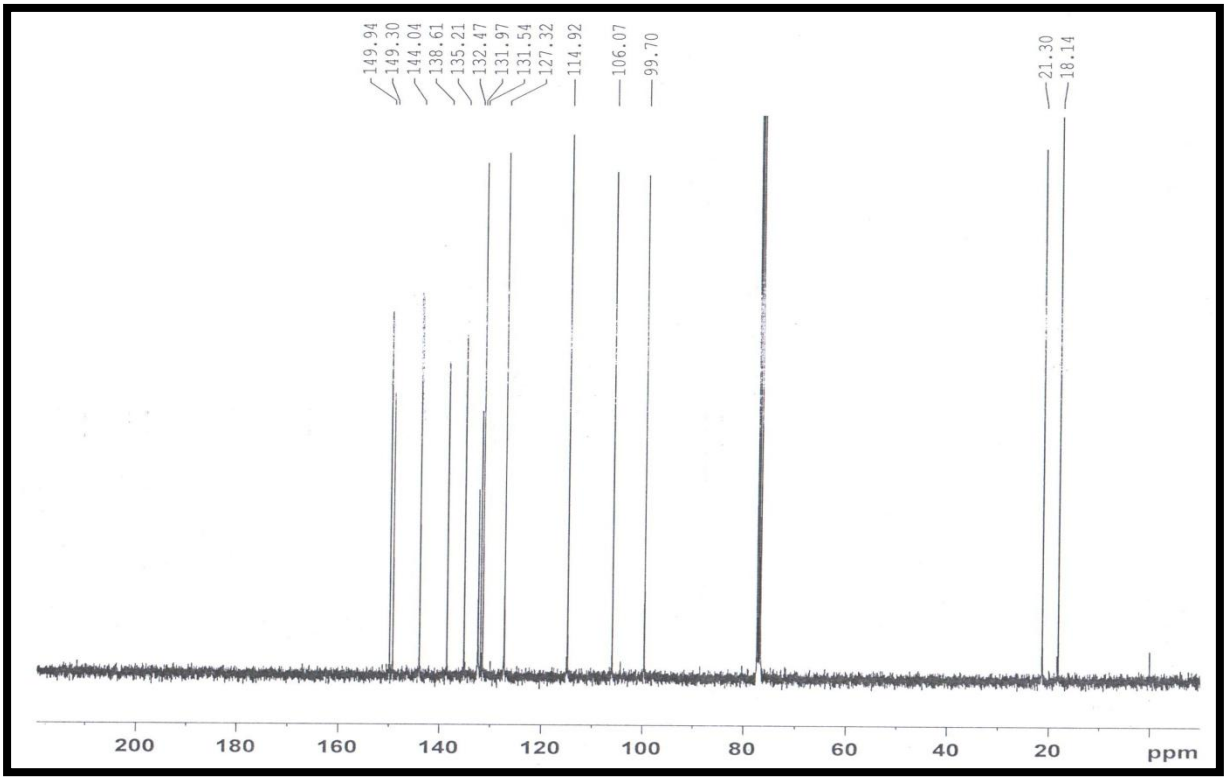


$^{13}$C NMR of (E)-4-((2,4-dimethylphenyl)diazenyl) benzene-1,3-diamine.

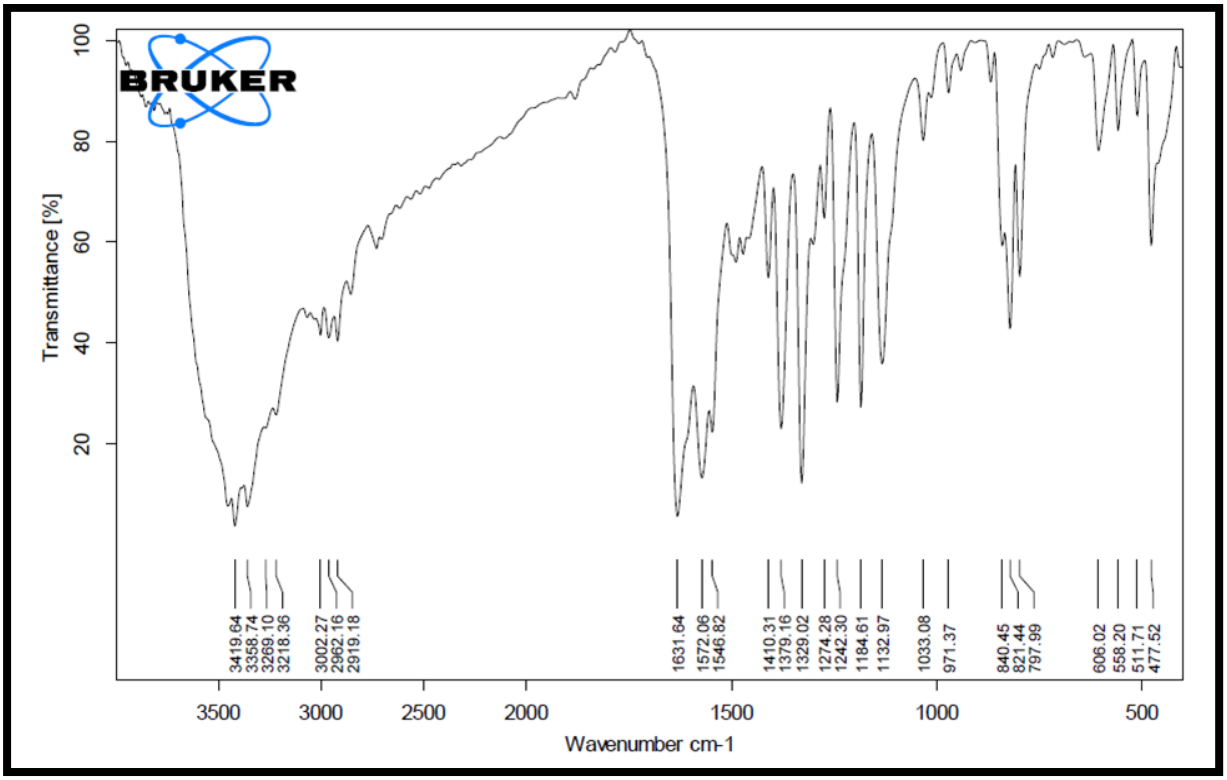


IR Spectra of (E)-4-((2,4-dimethylphenyl)diazenyl) benzene-1,3-diamine.

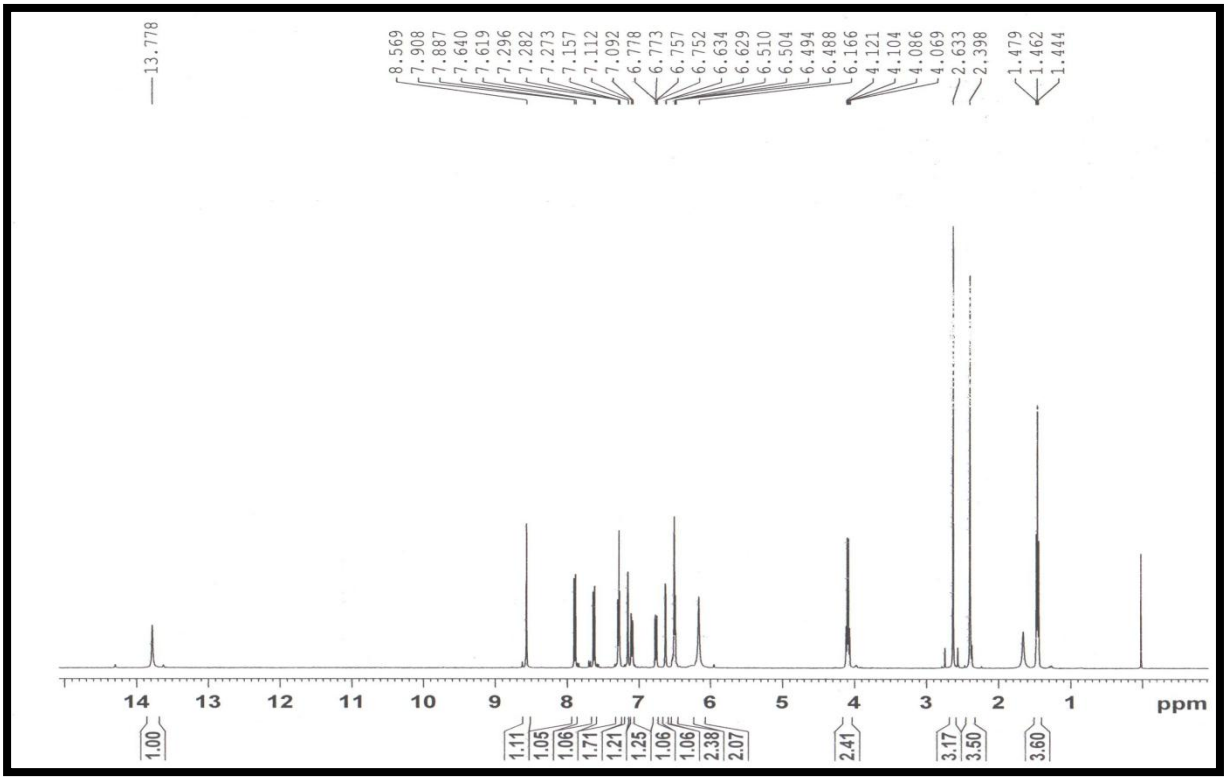


$^{1}$H NMR of G2

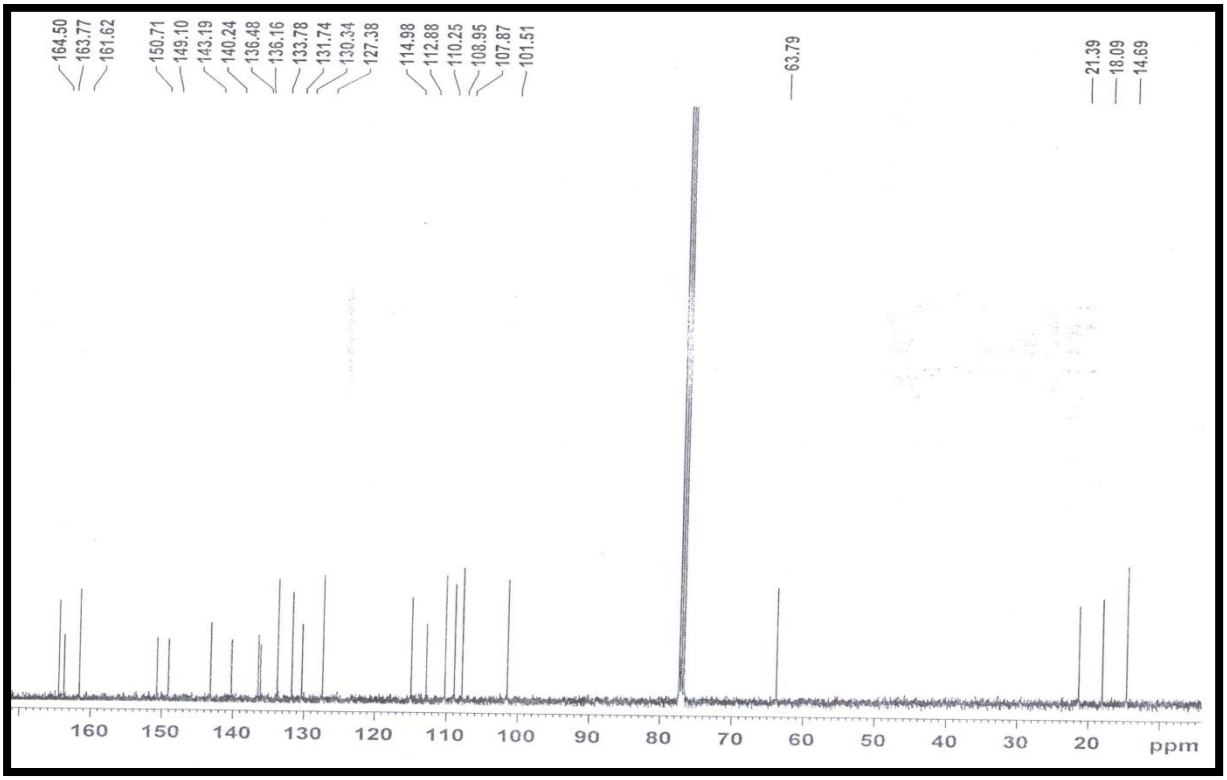


$^{13}$C NMR of G2

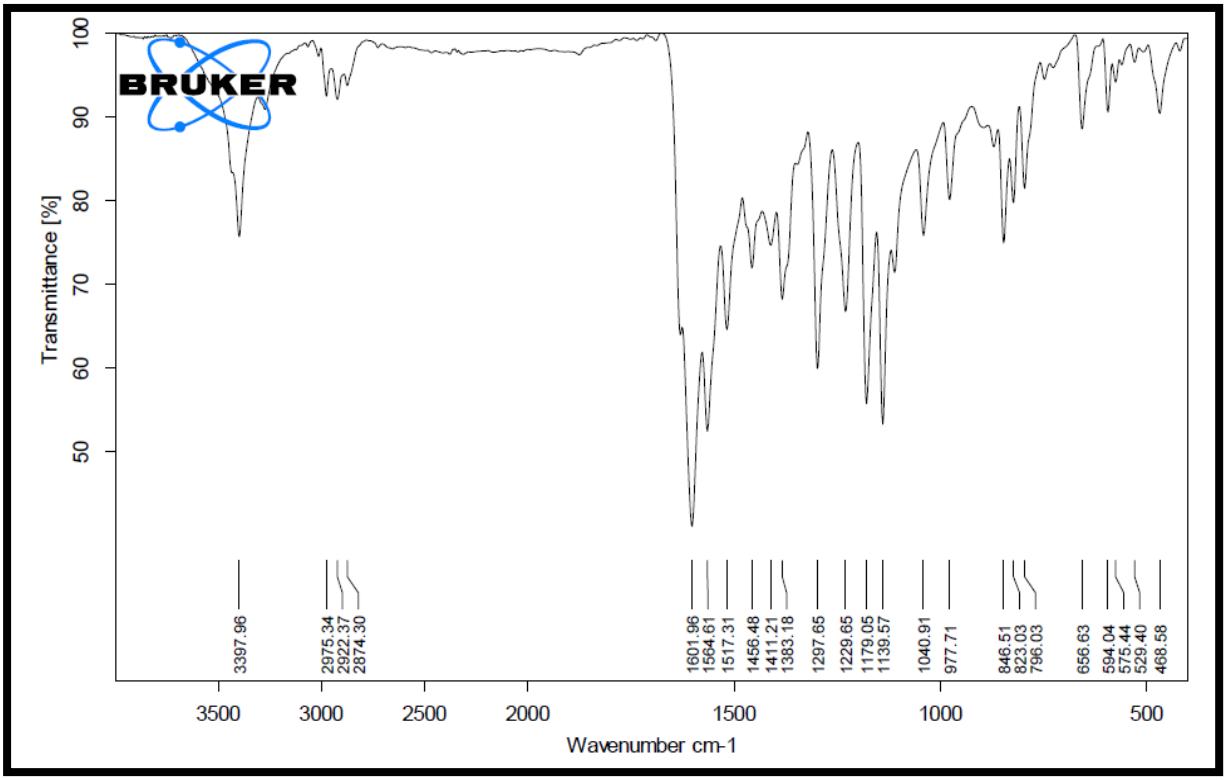


IR Spectra of G2

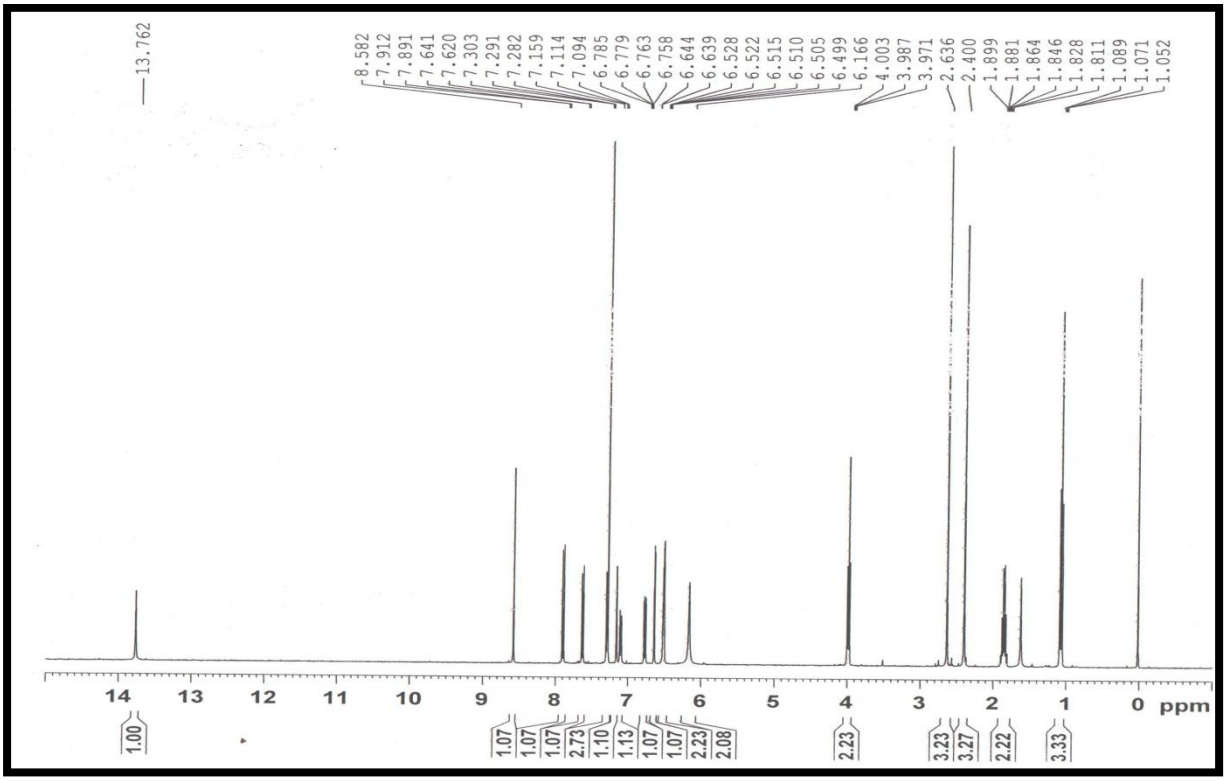


$^{1}$H NMR of G3

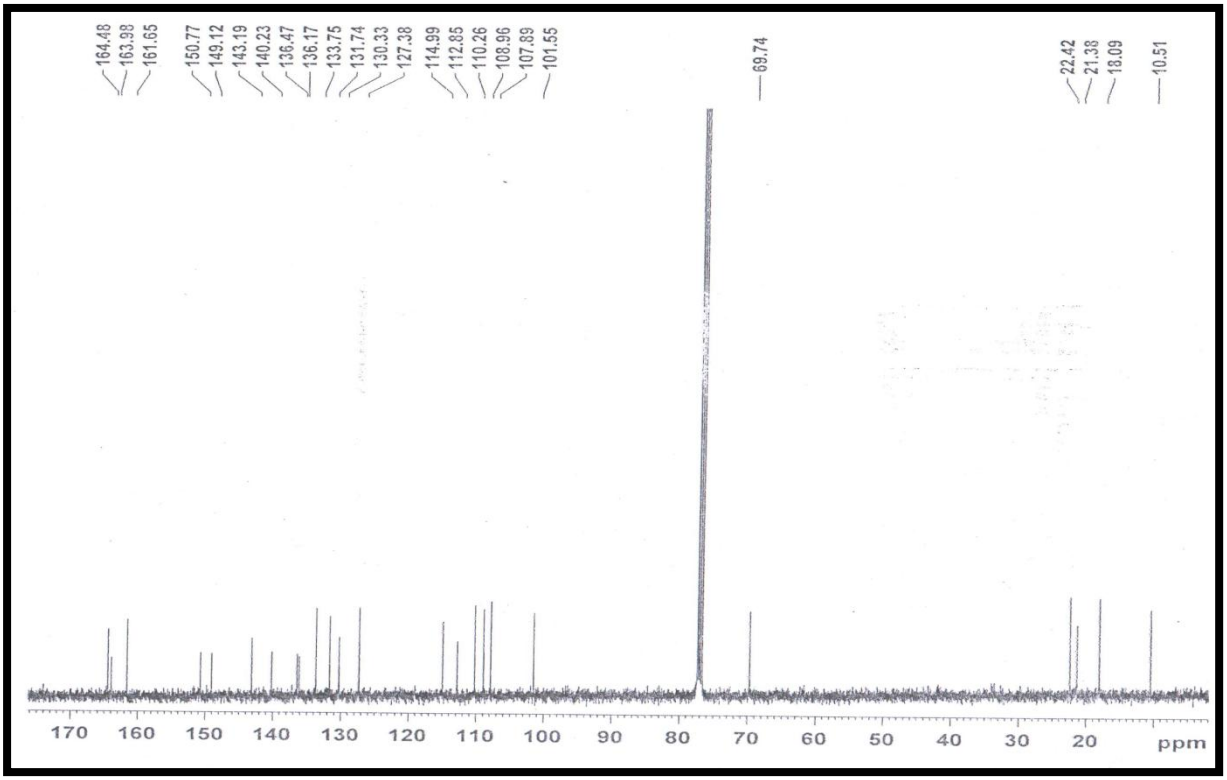


$^{13}$C NMR of G3

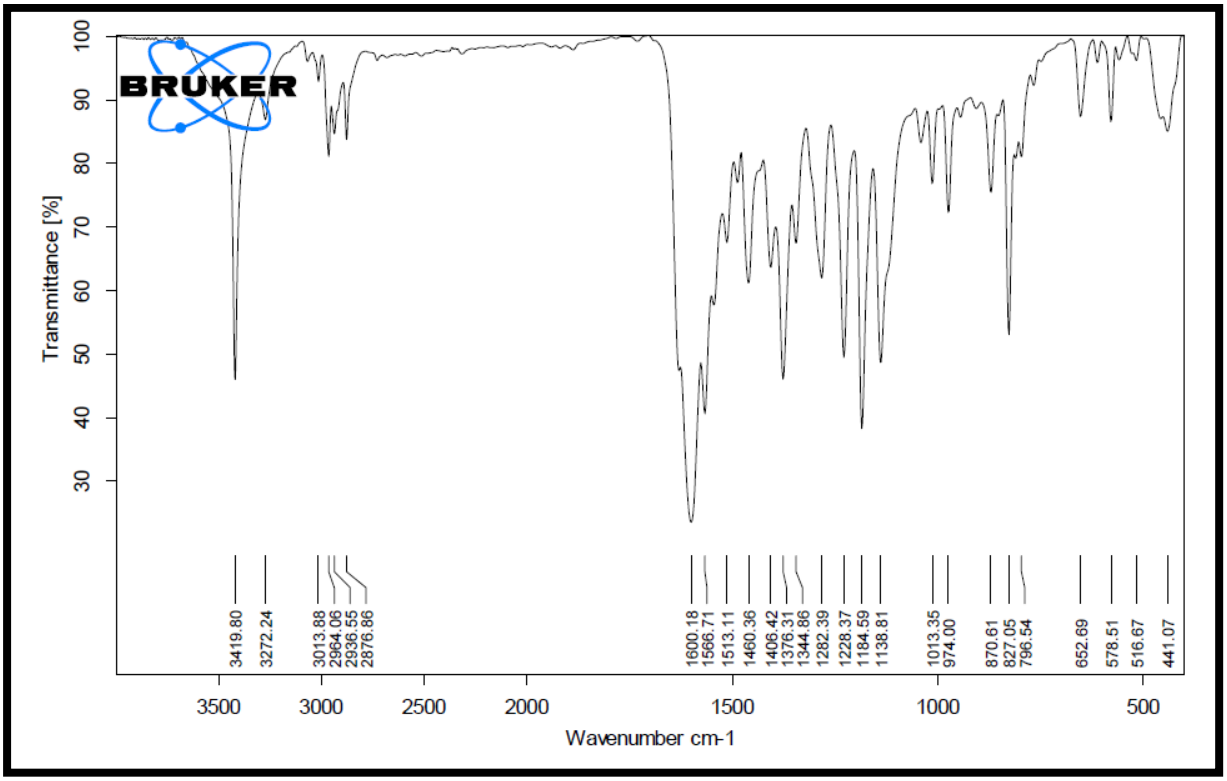


IR Spectra of G3

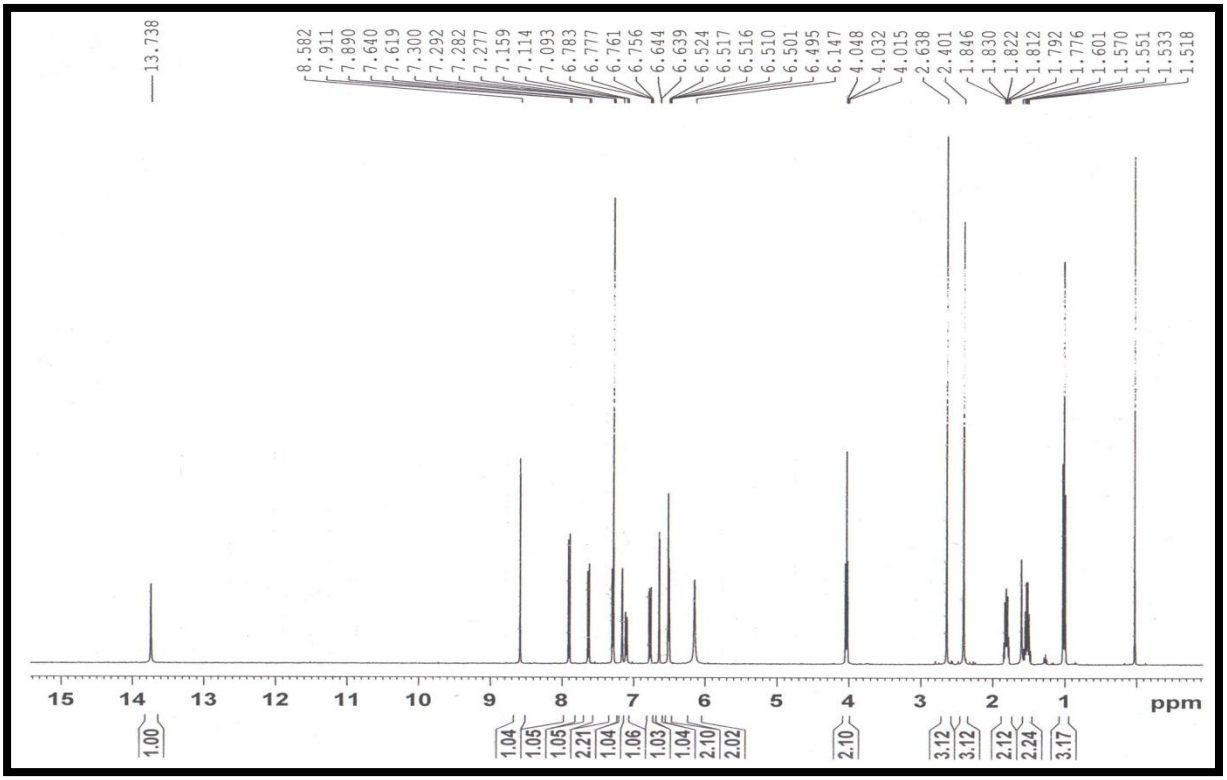


$^{1}$H NMR of G4

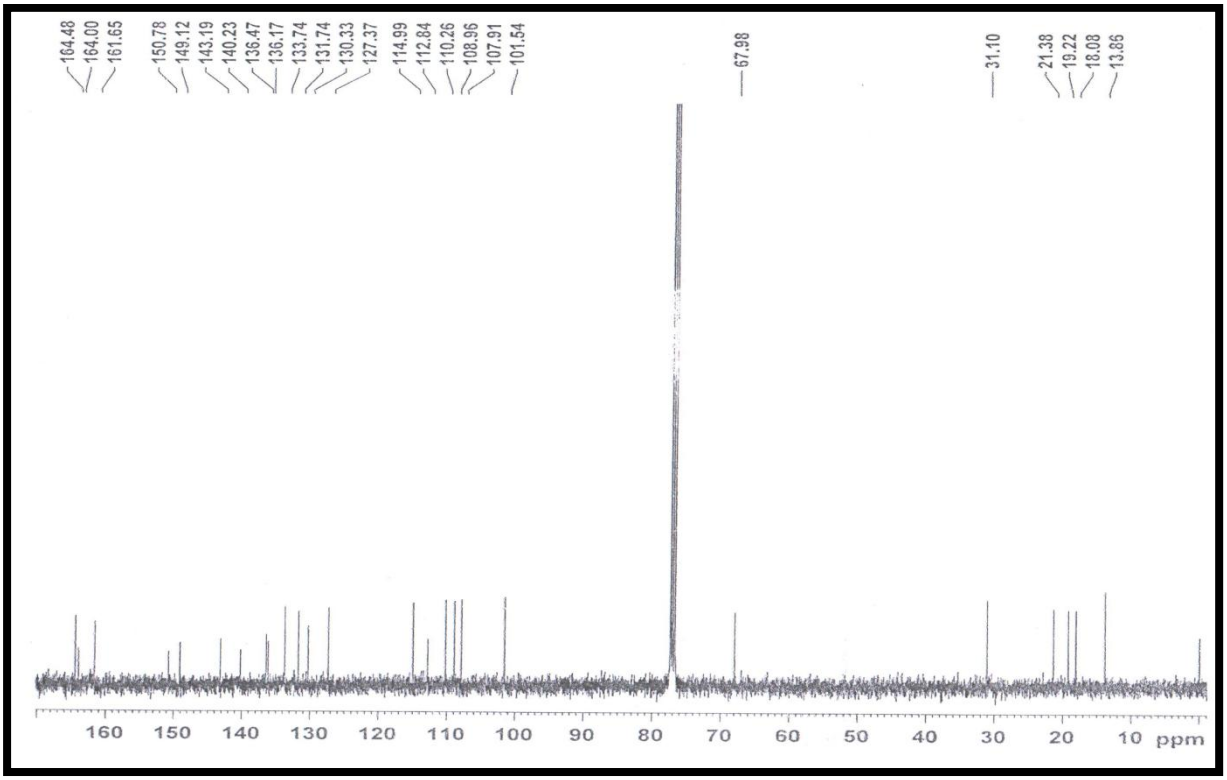


$^{13}$C NMR of G4

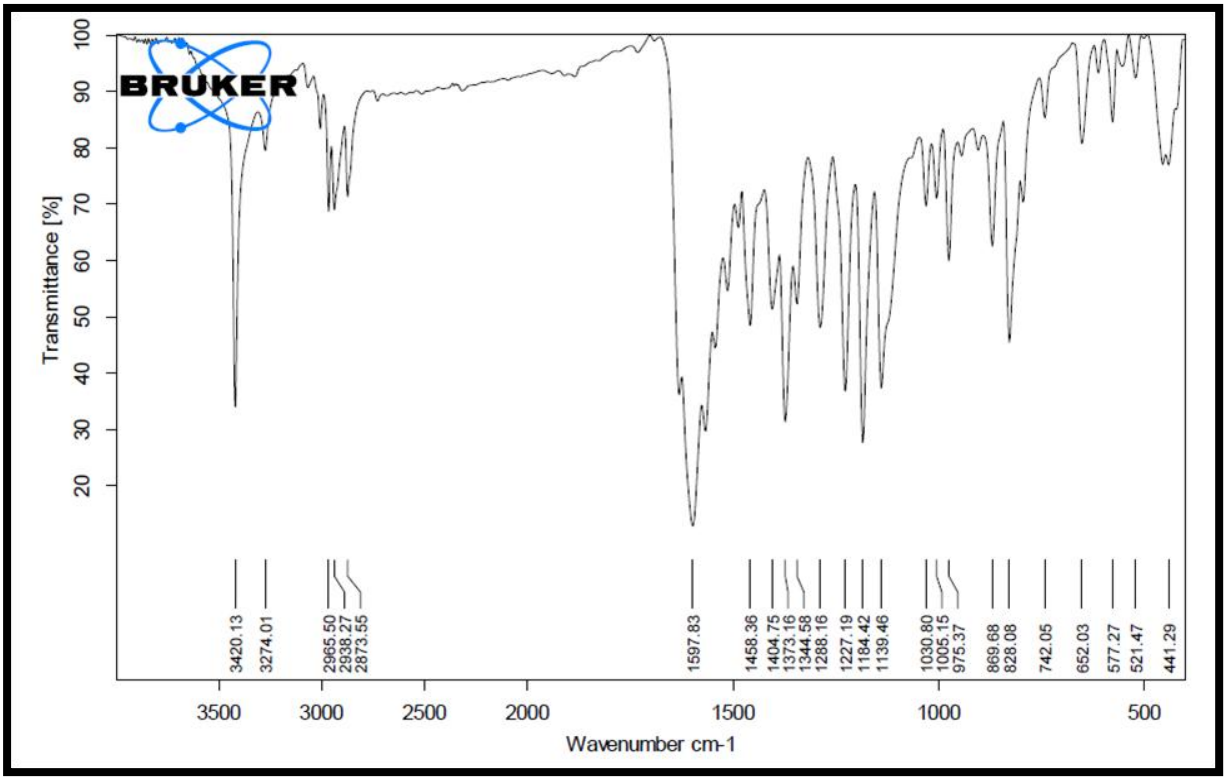


IR Spectra of G4

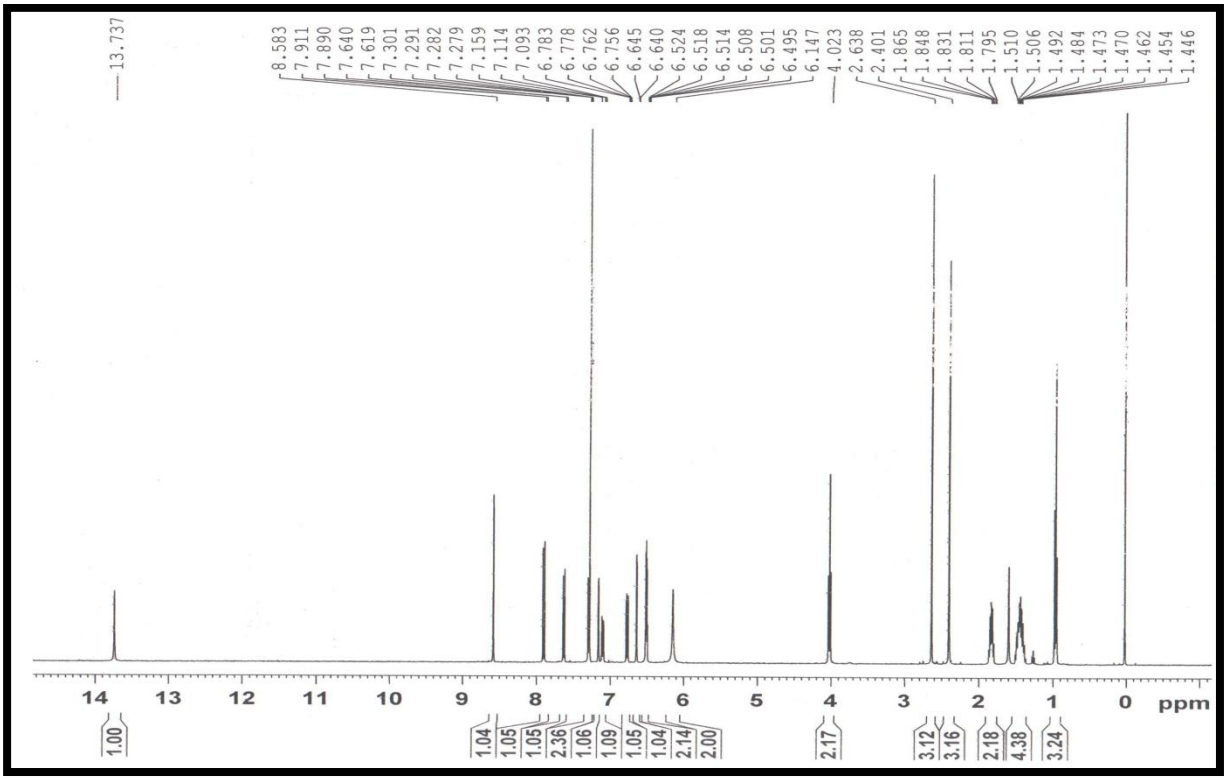


$^{1}$H NMR of G5

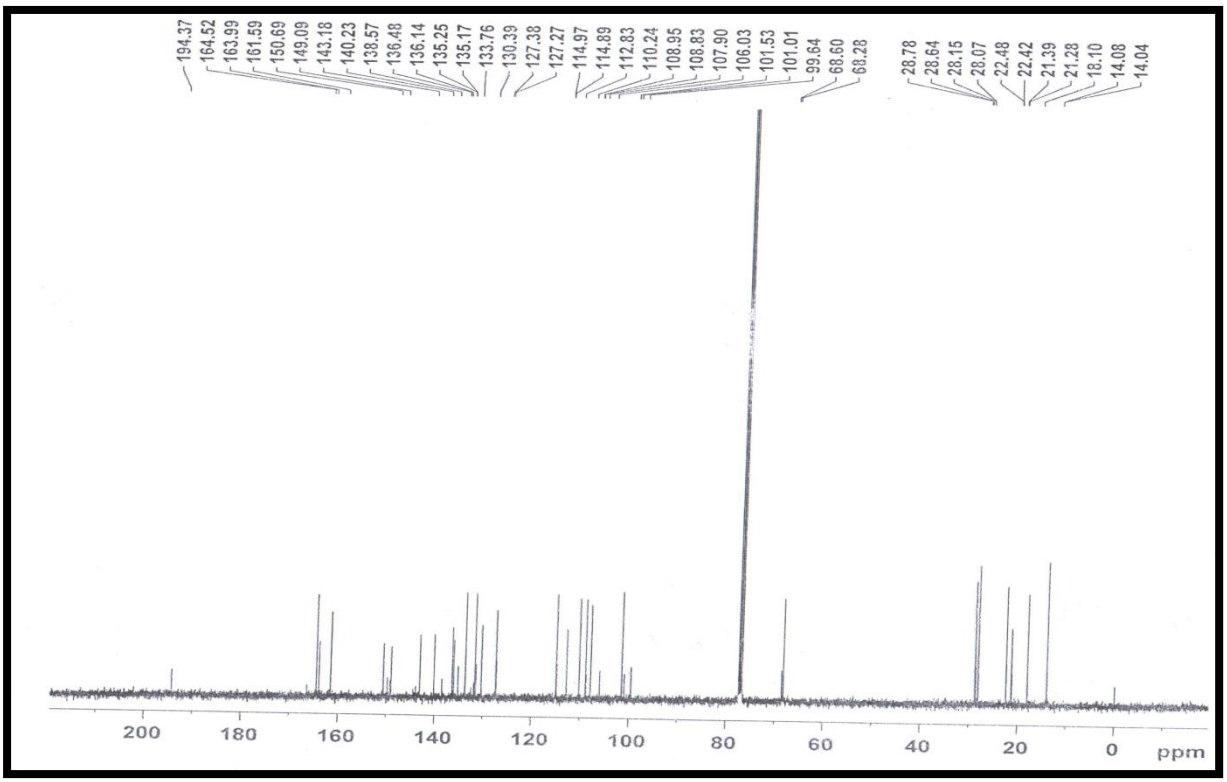


$^{13}$C NMR of G5

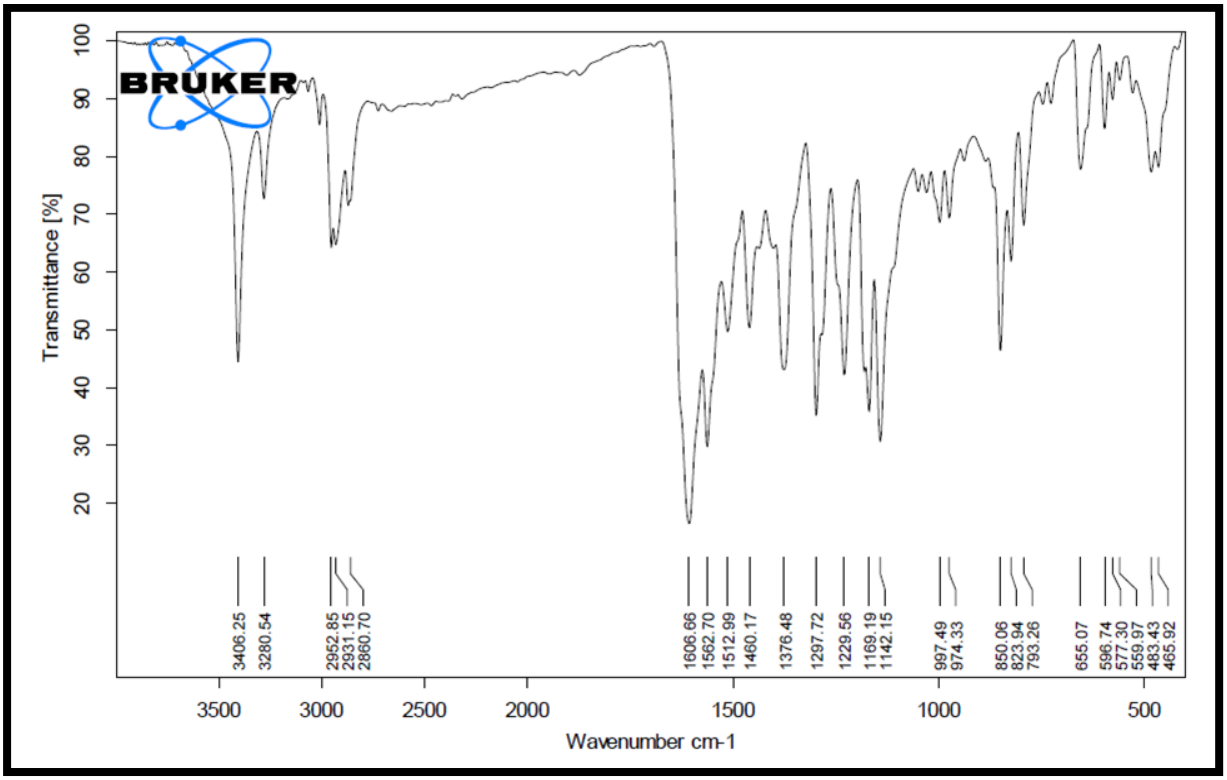


IR Spectra of G5

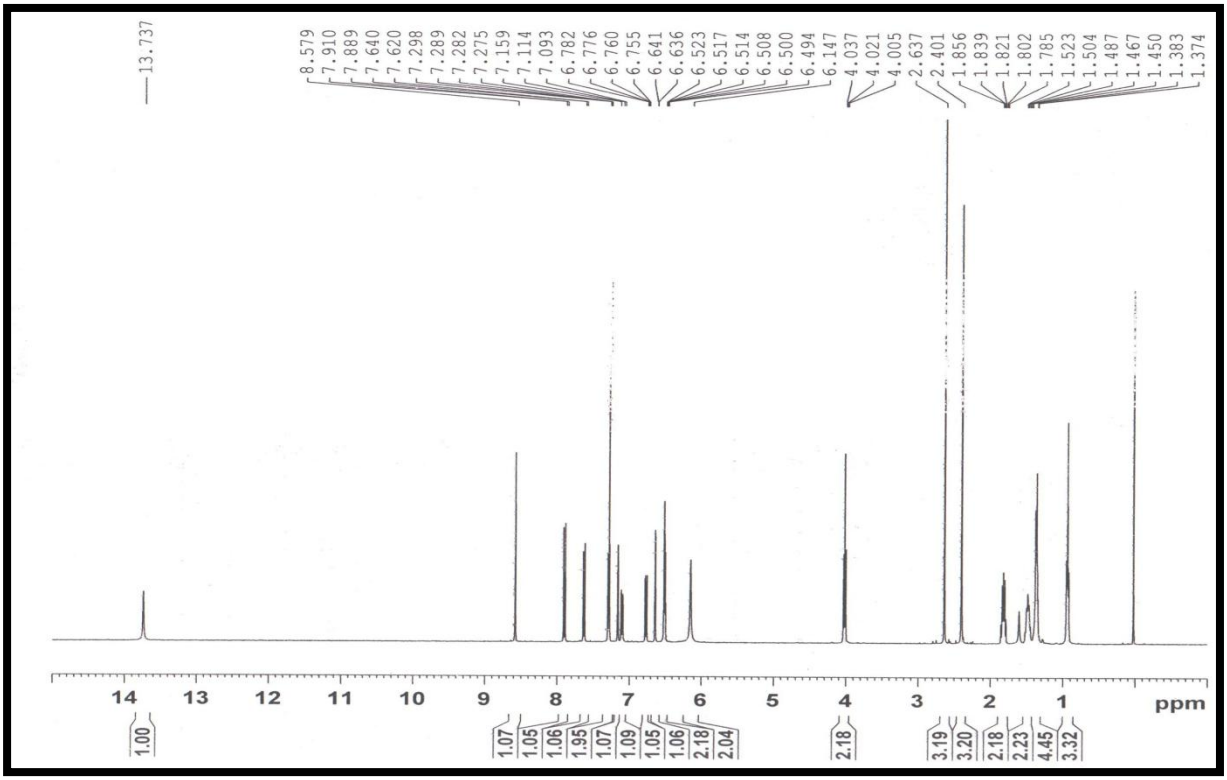


$^{1}$H NMR of G6

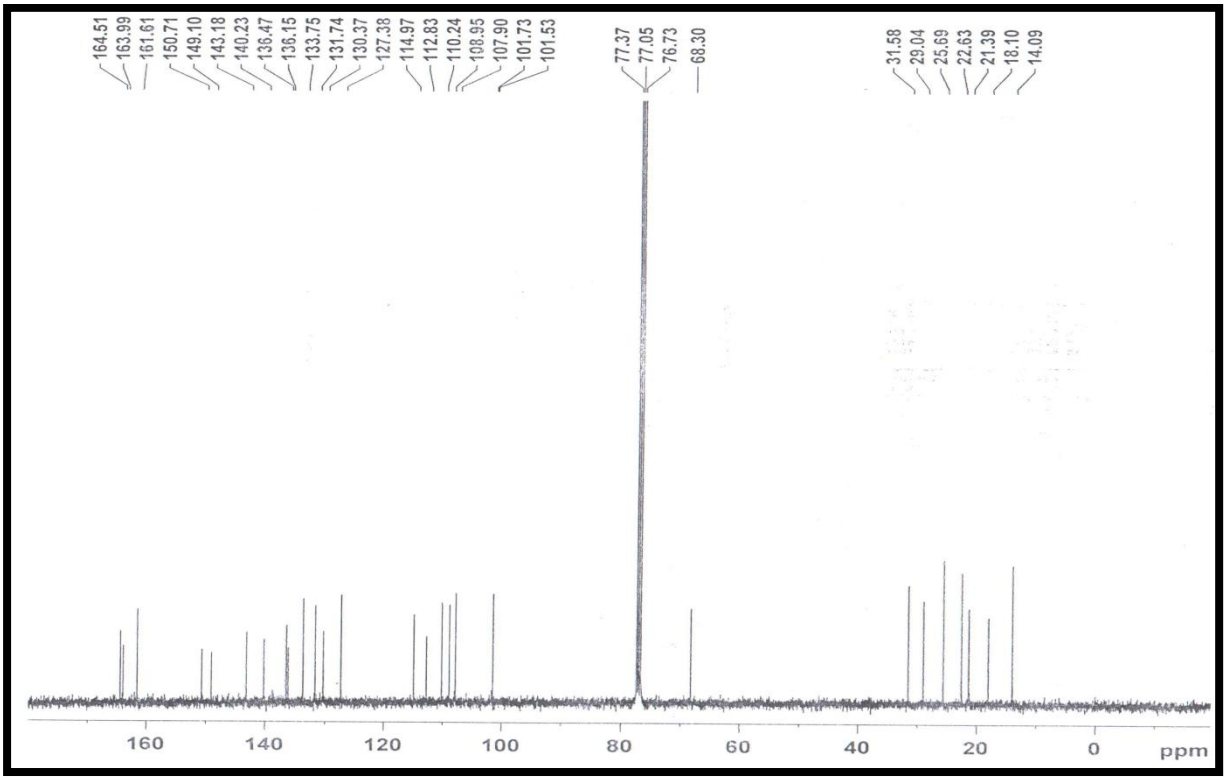


$^{13}$C NMR of G6

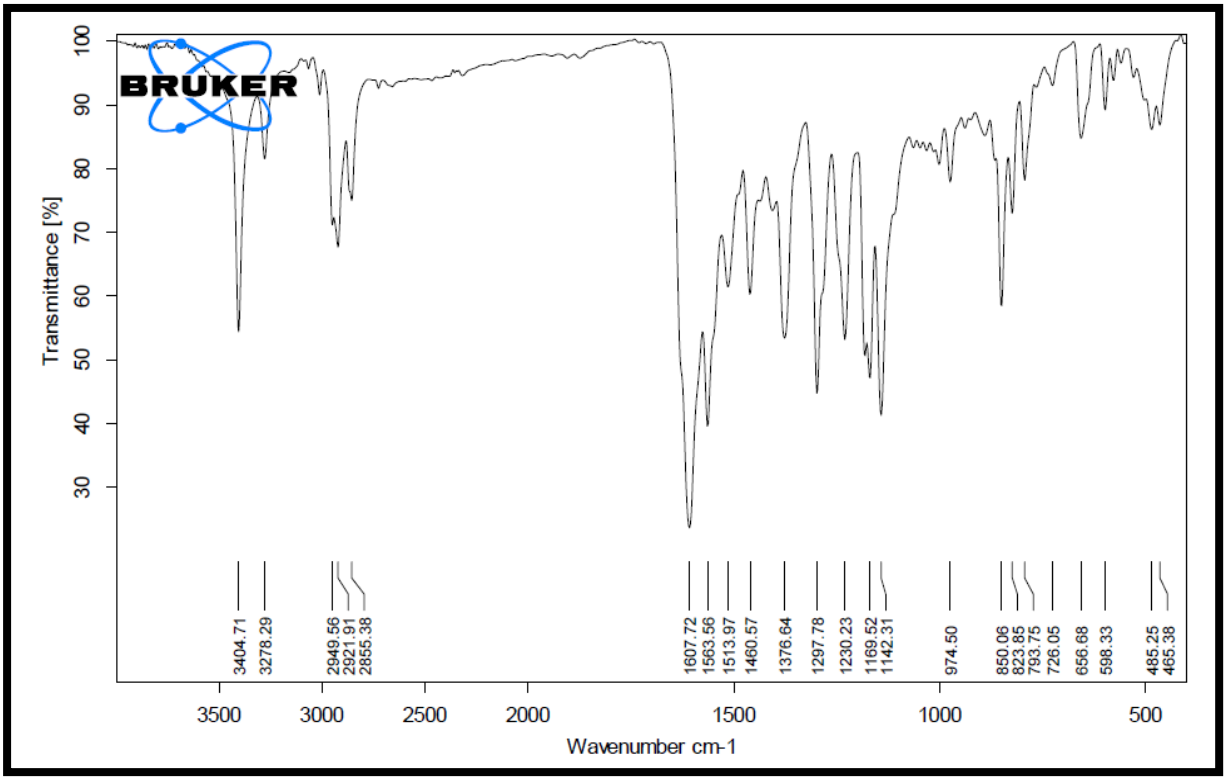


IR Spectra of G6

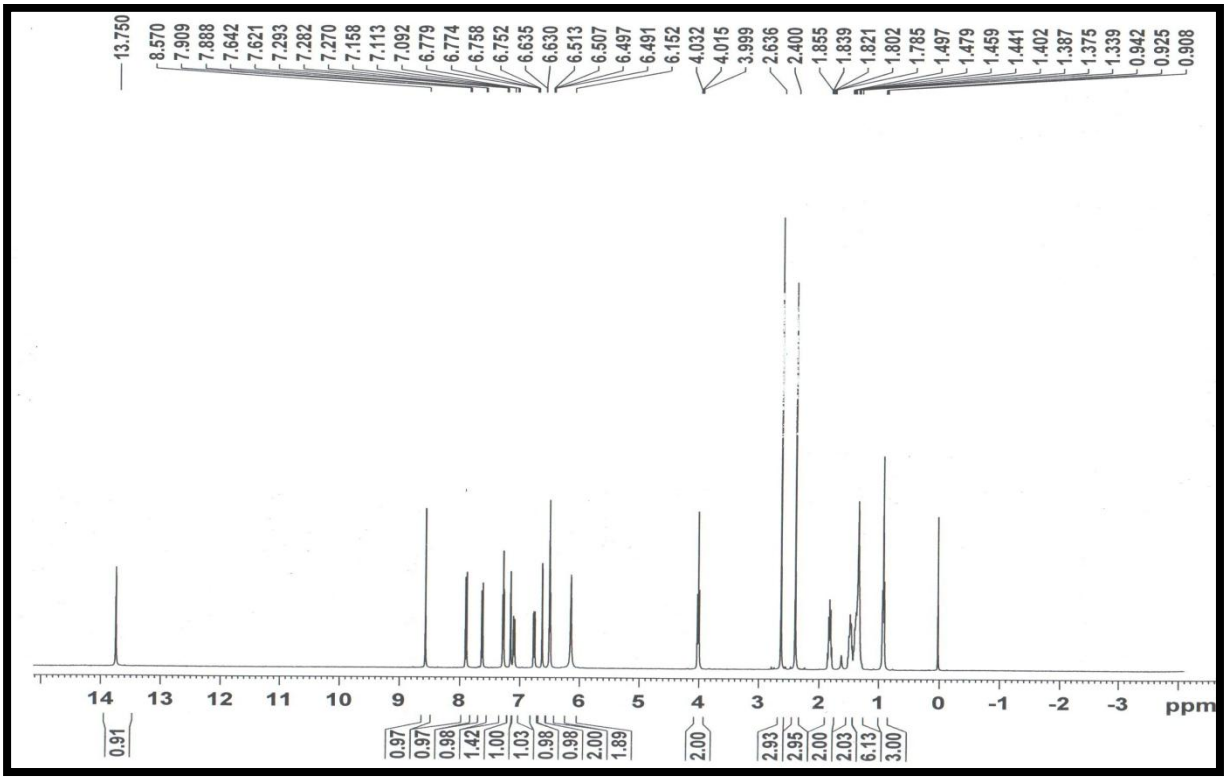


$^{1}$H NMR of G7

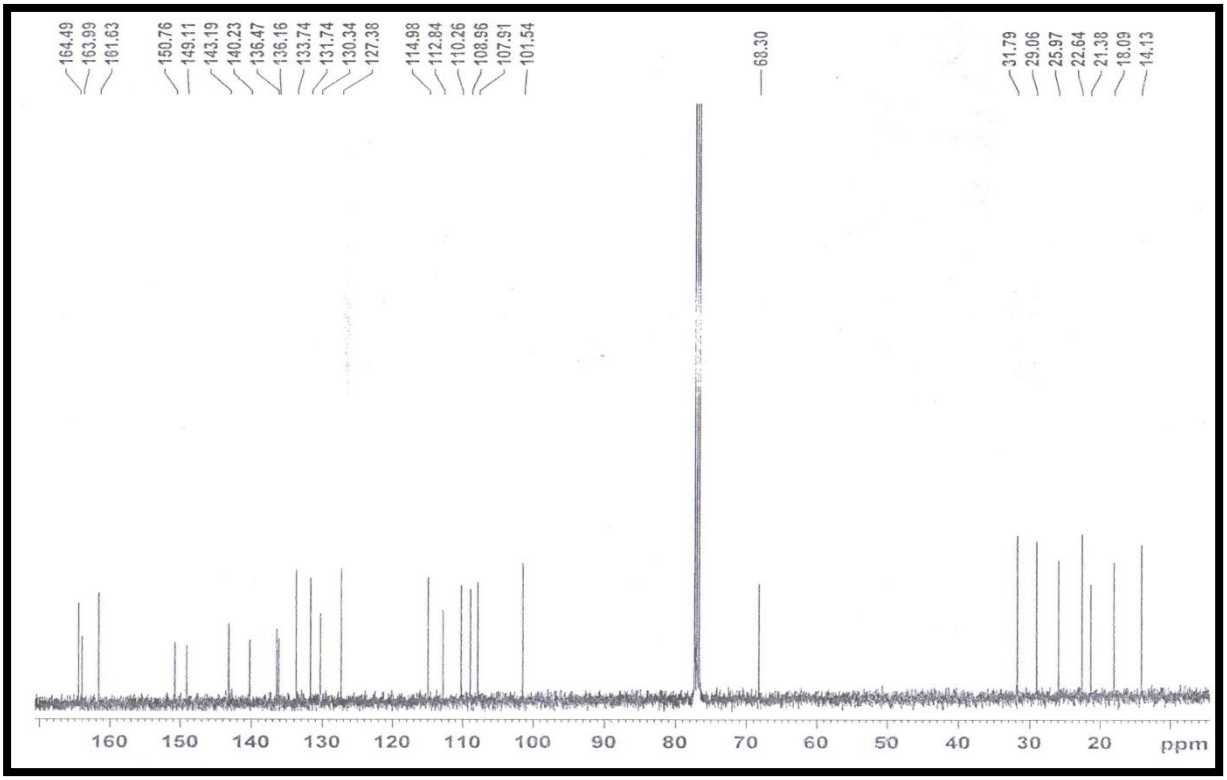


$^{13}$C NMR of G7

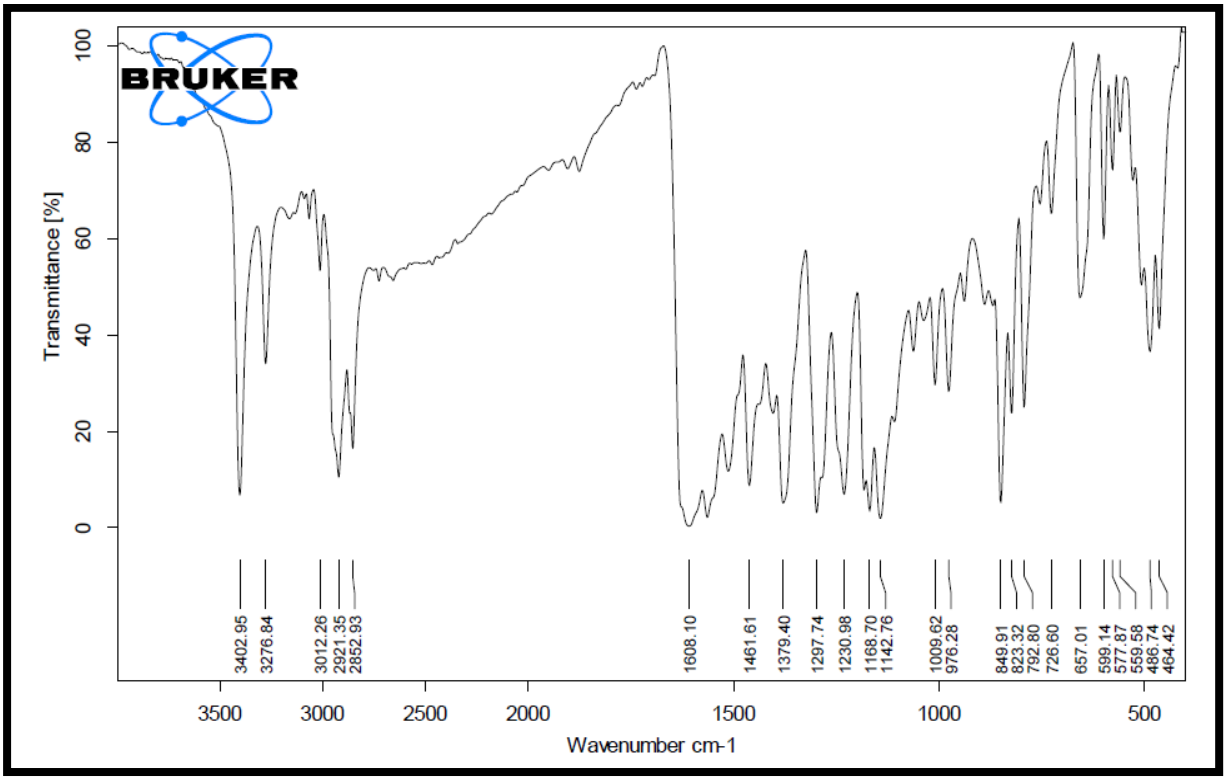


IR Spectra of G7

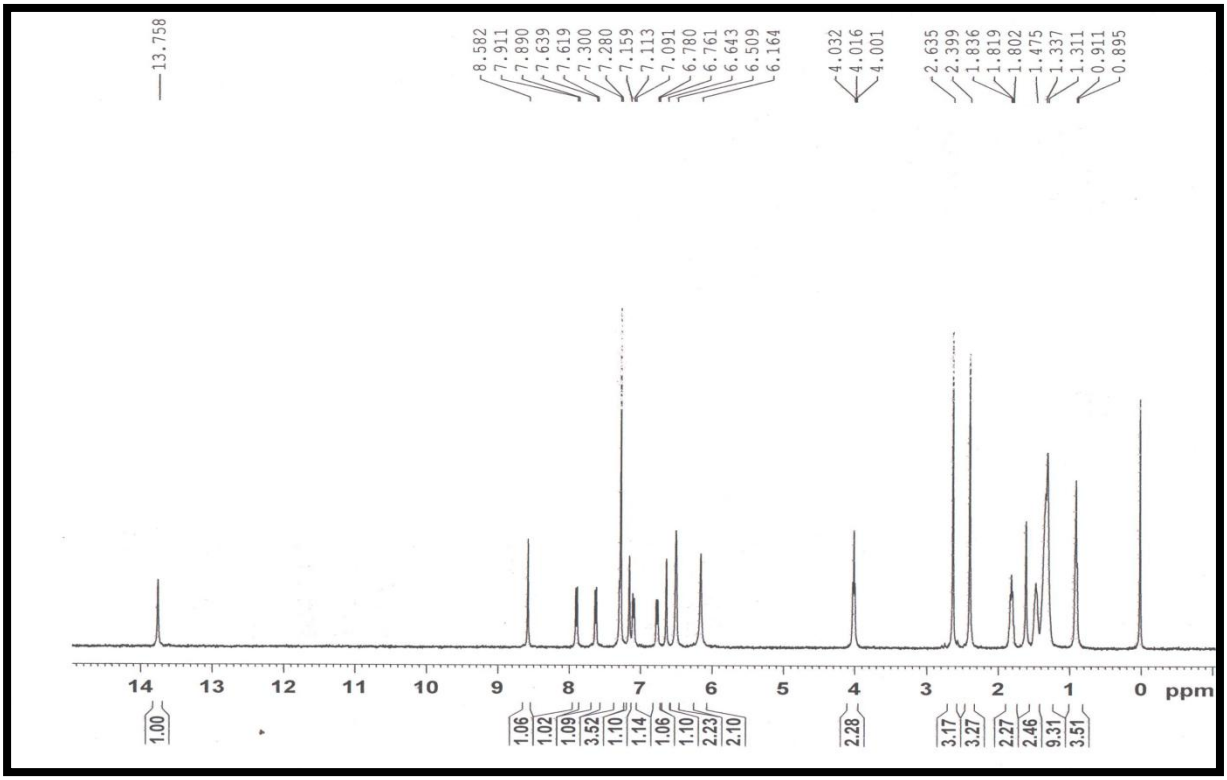


$^{1}$H NMR of G8

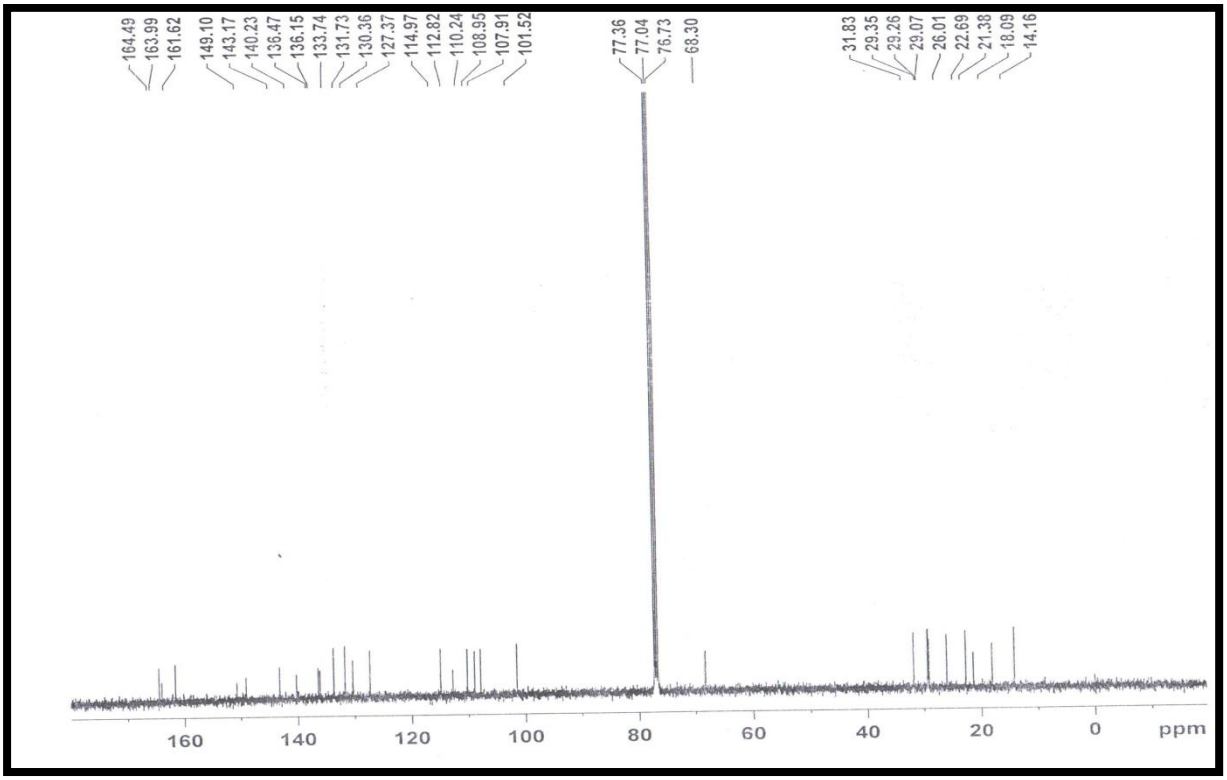


$^{13}$C NMR of G8

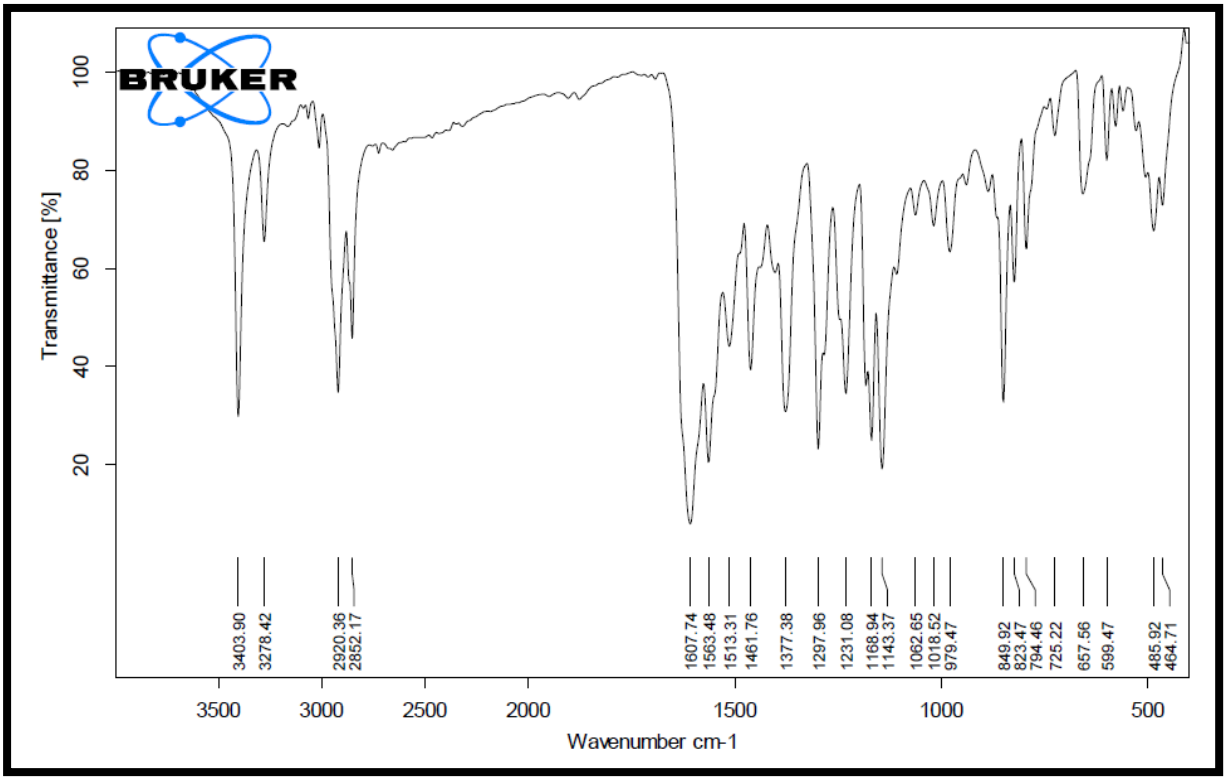


IR Spectra of G8

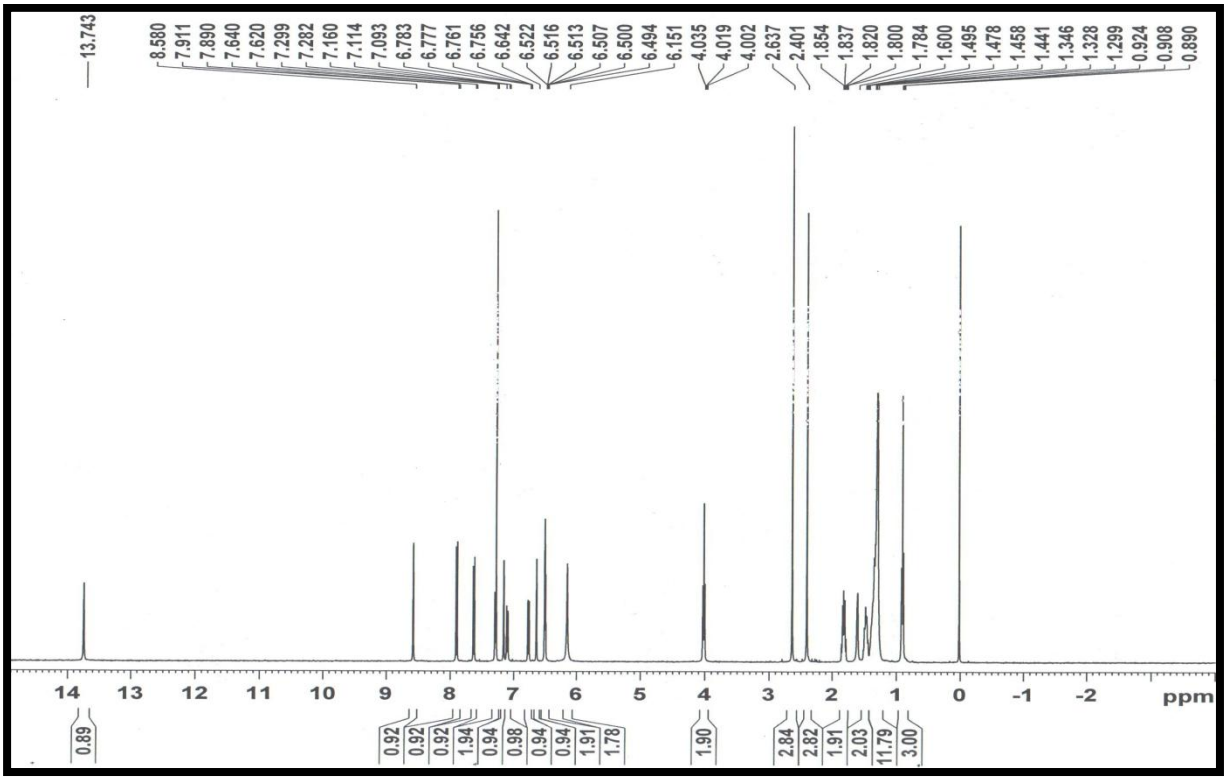


$^{1}$H NMR of G10

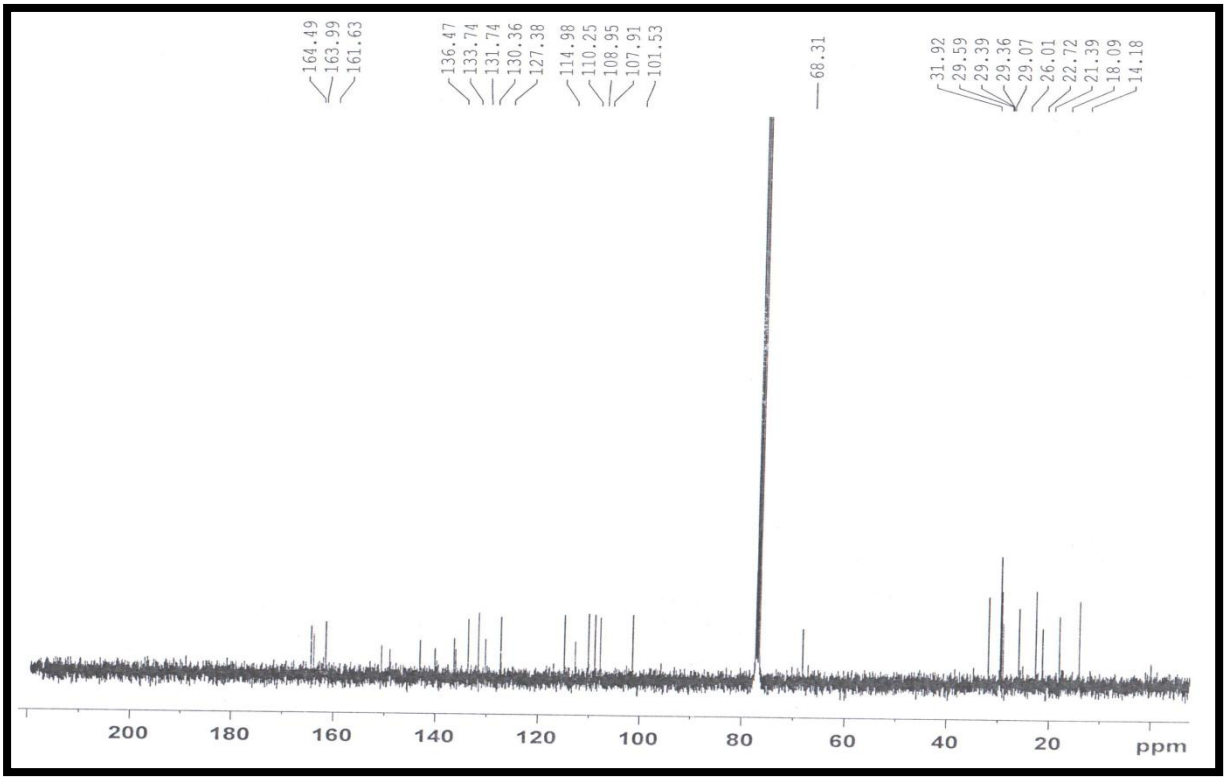


$^{13}$C NMR of G10

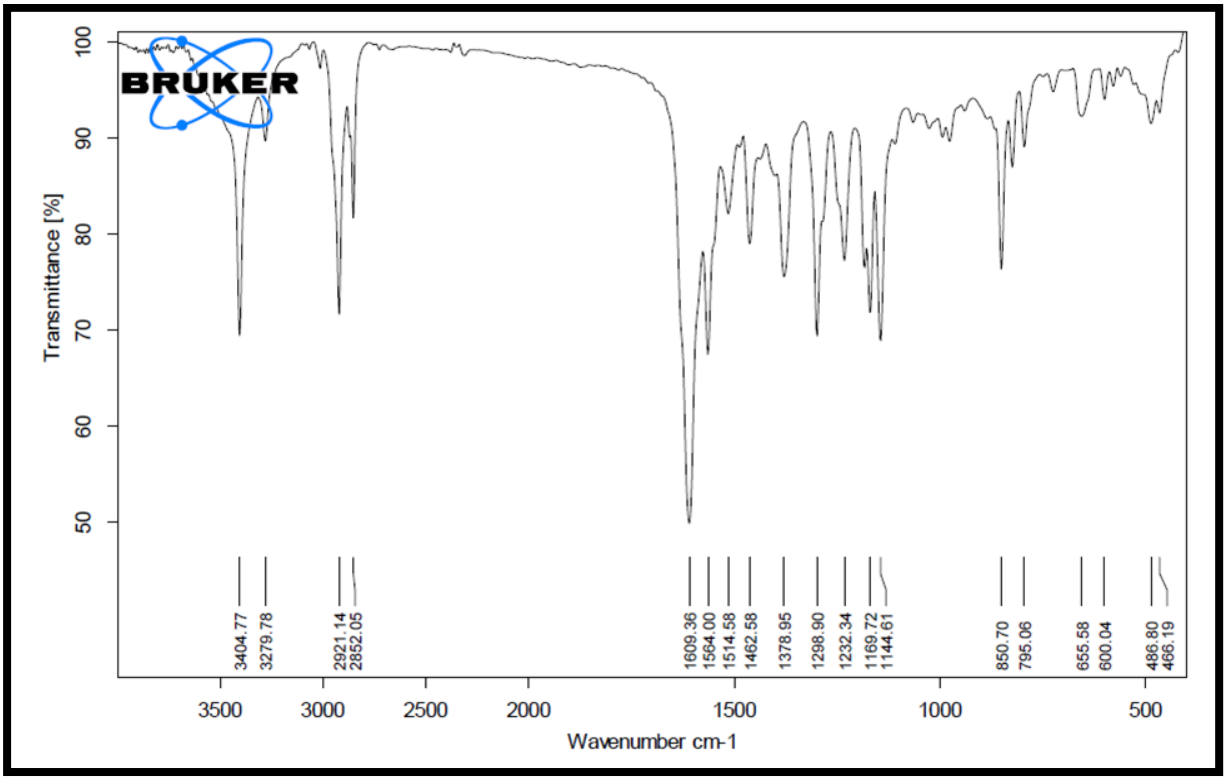


IR Spectra of G10

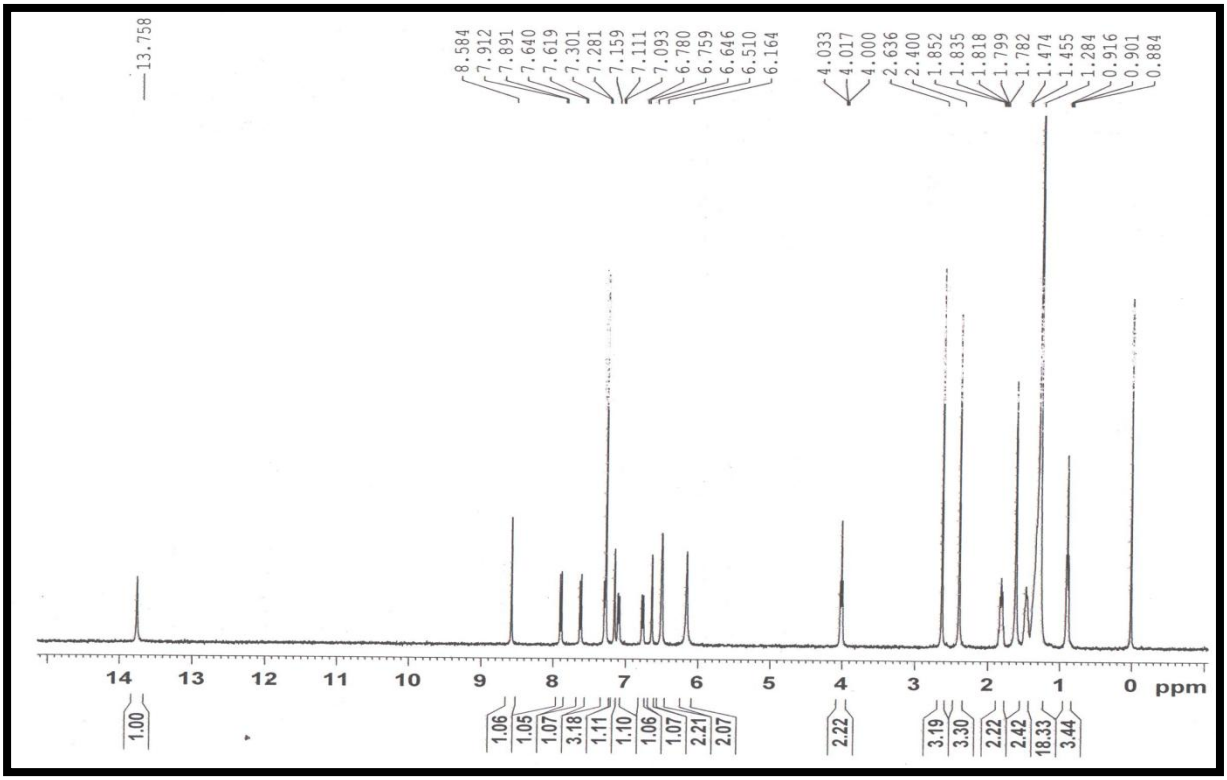


$^{1}$H NMR of G12

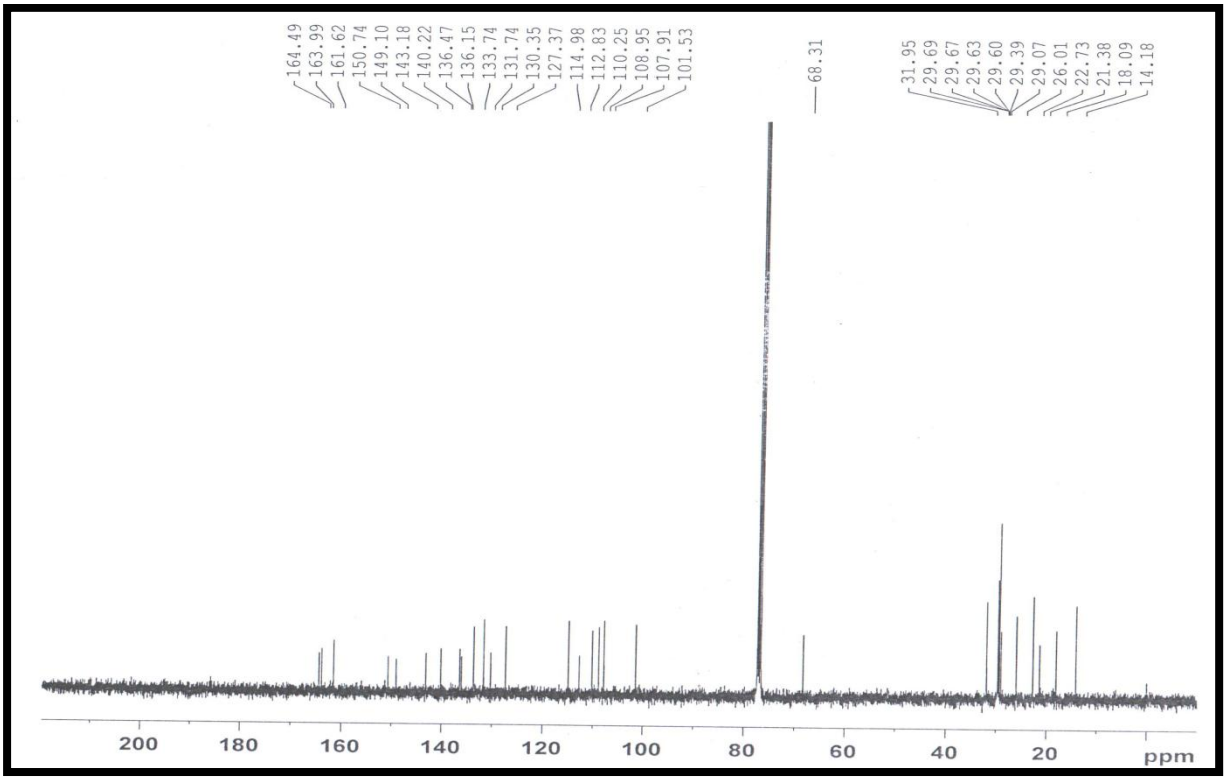


$^{13}$C NMR of G12

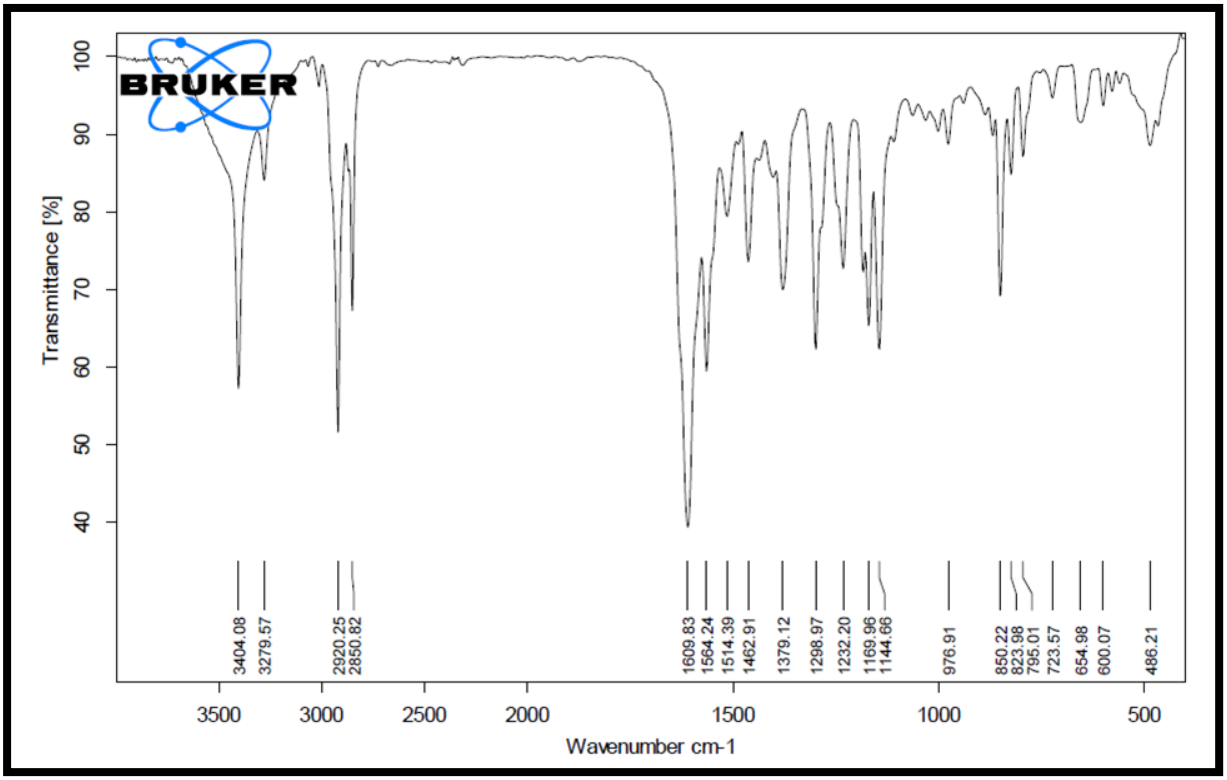


IR Spectra of G12

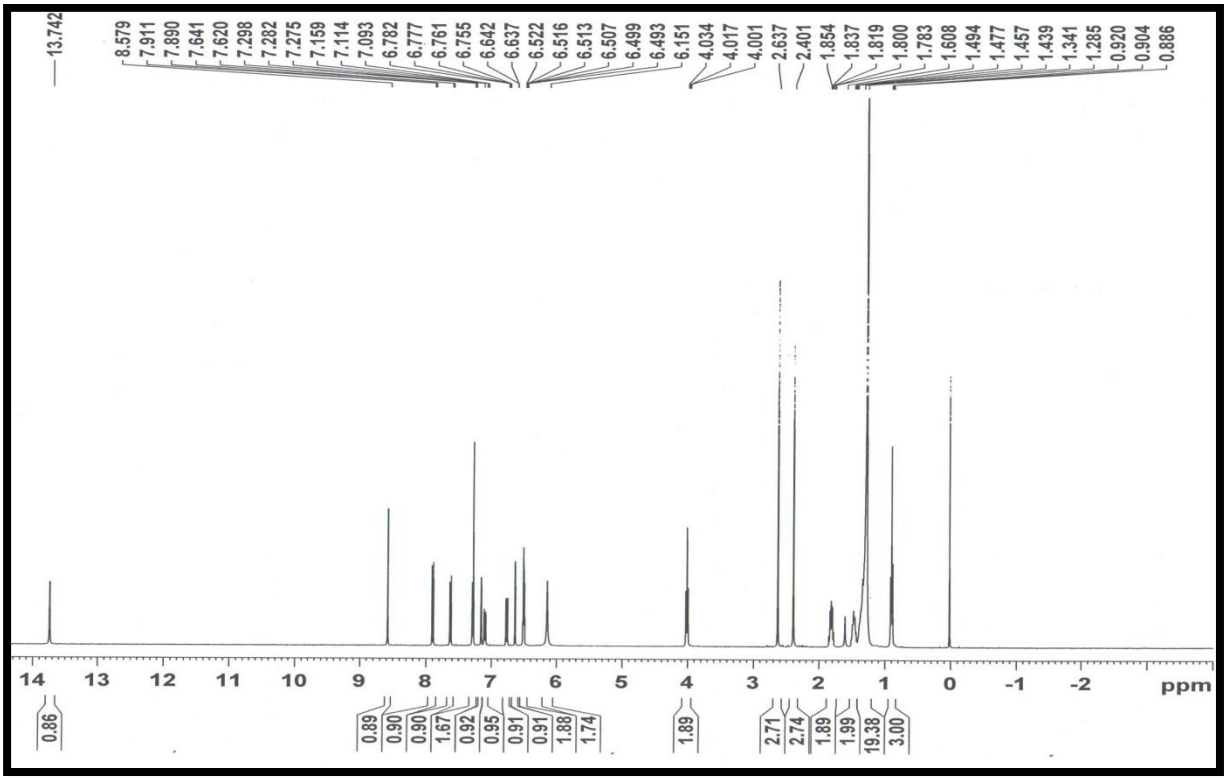


$^{1}$H NMR of G14

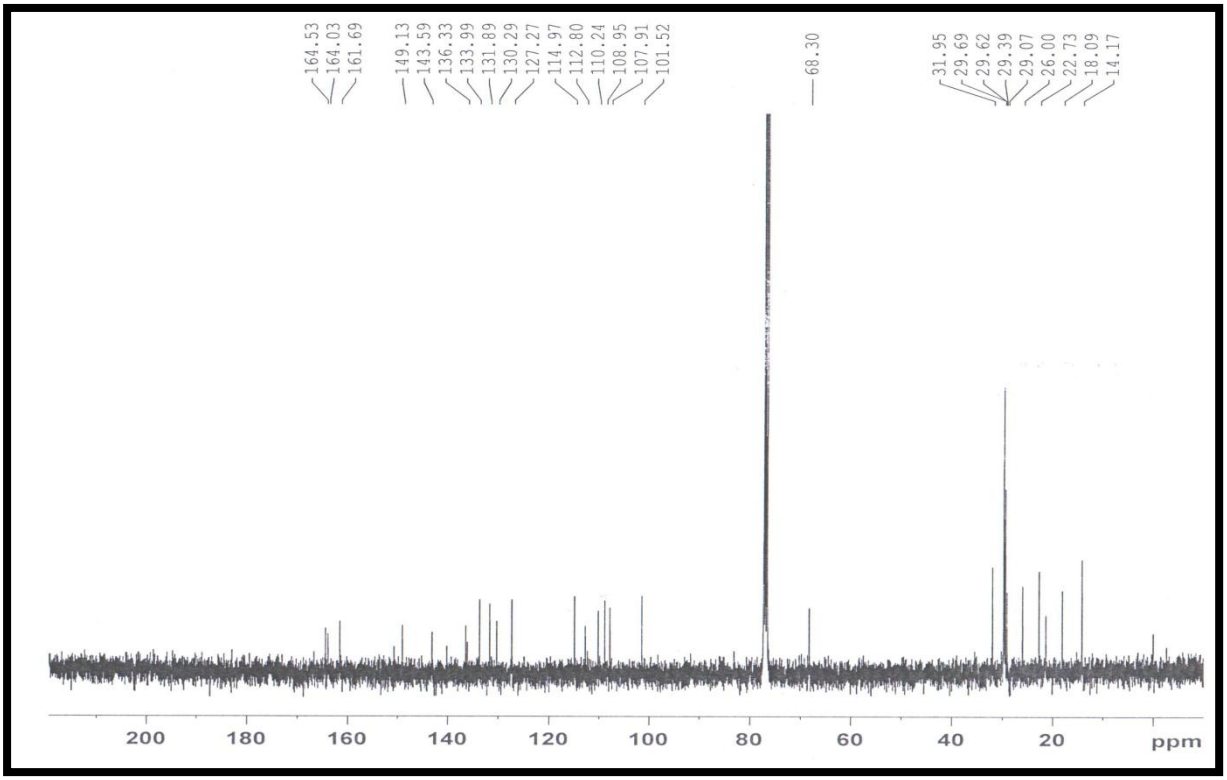


$^{13}$C NMR of G14

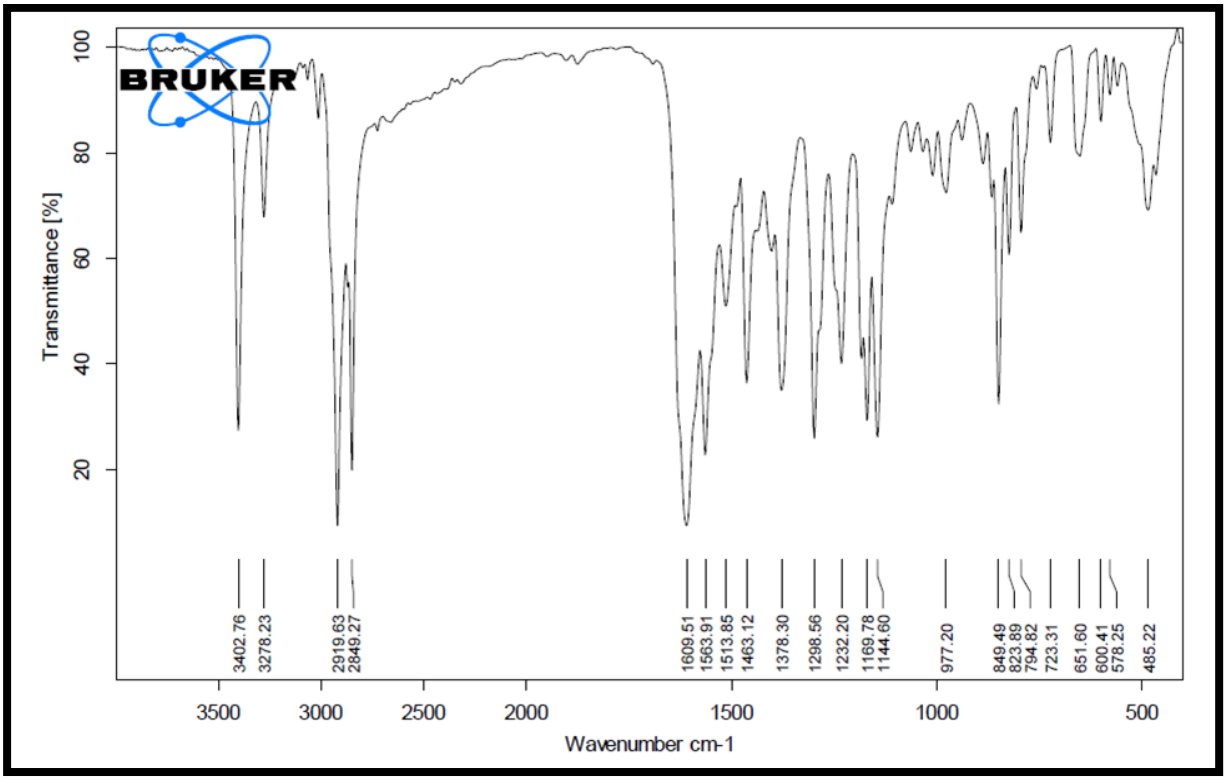


IR Spectra of G14

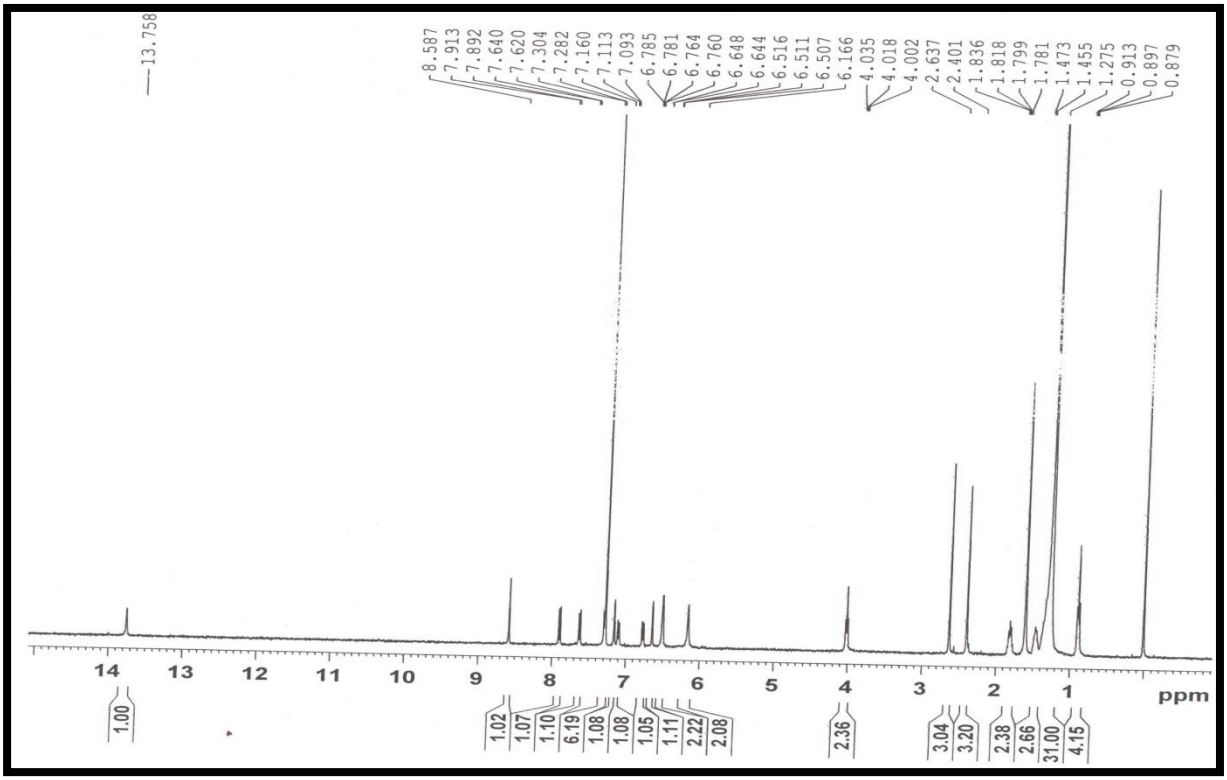


$^{1}$H NMR of G16

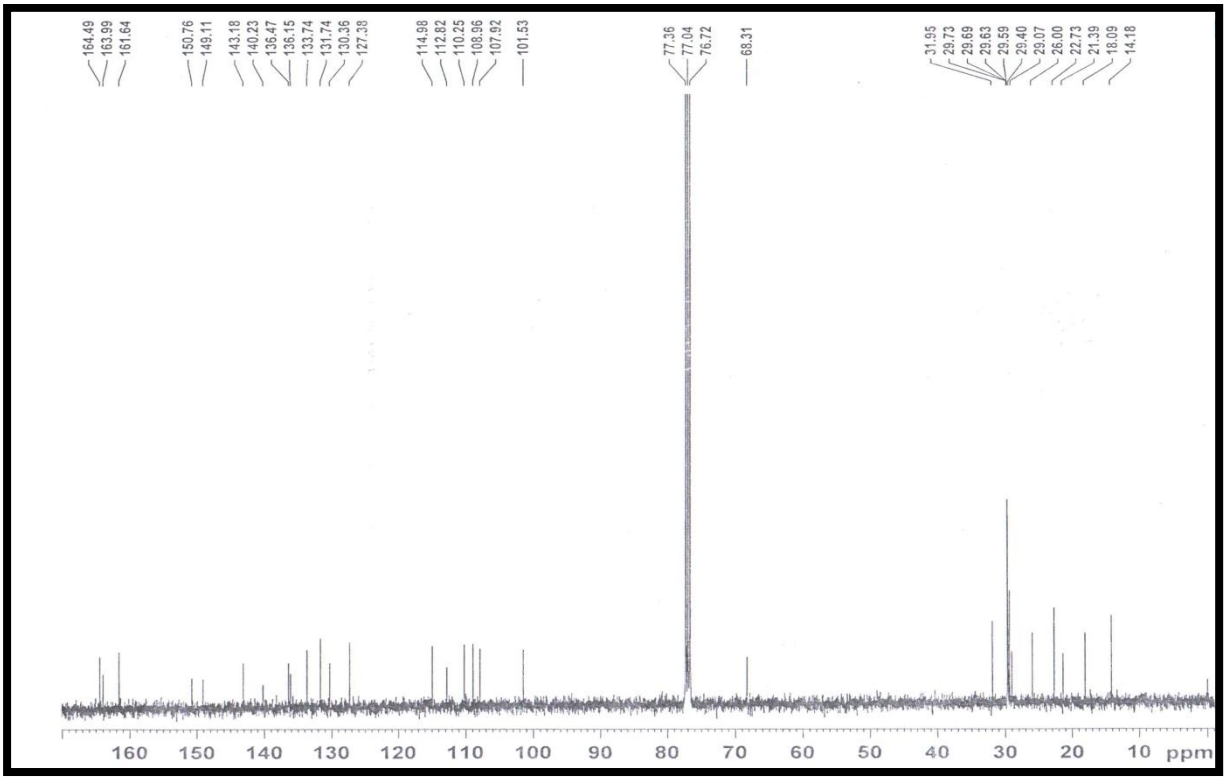


$^{13}$C NMR of G16

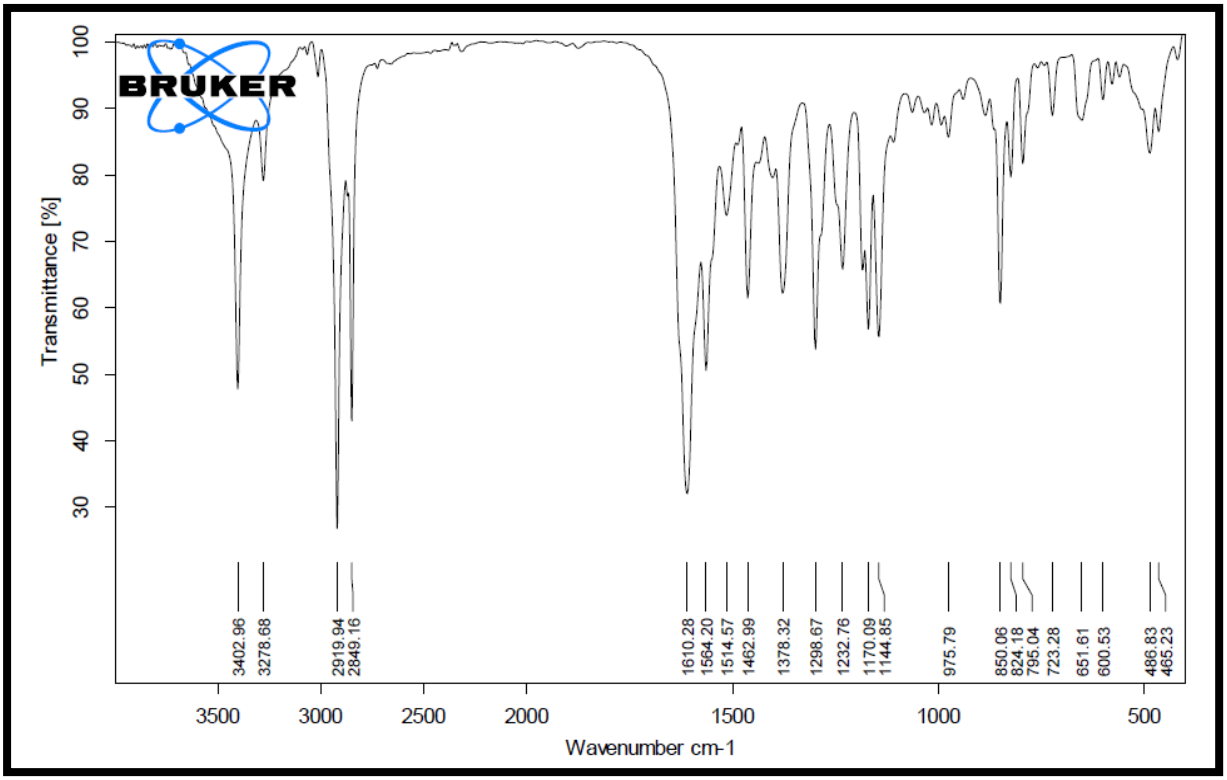


IR Spectra of G16

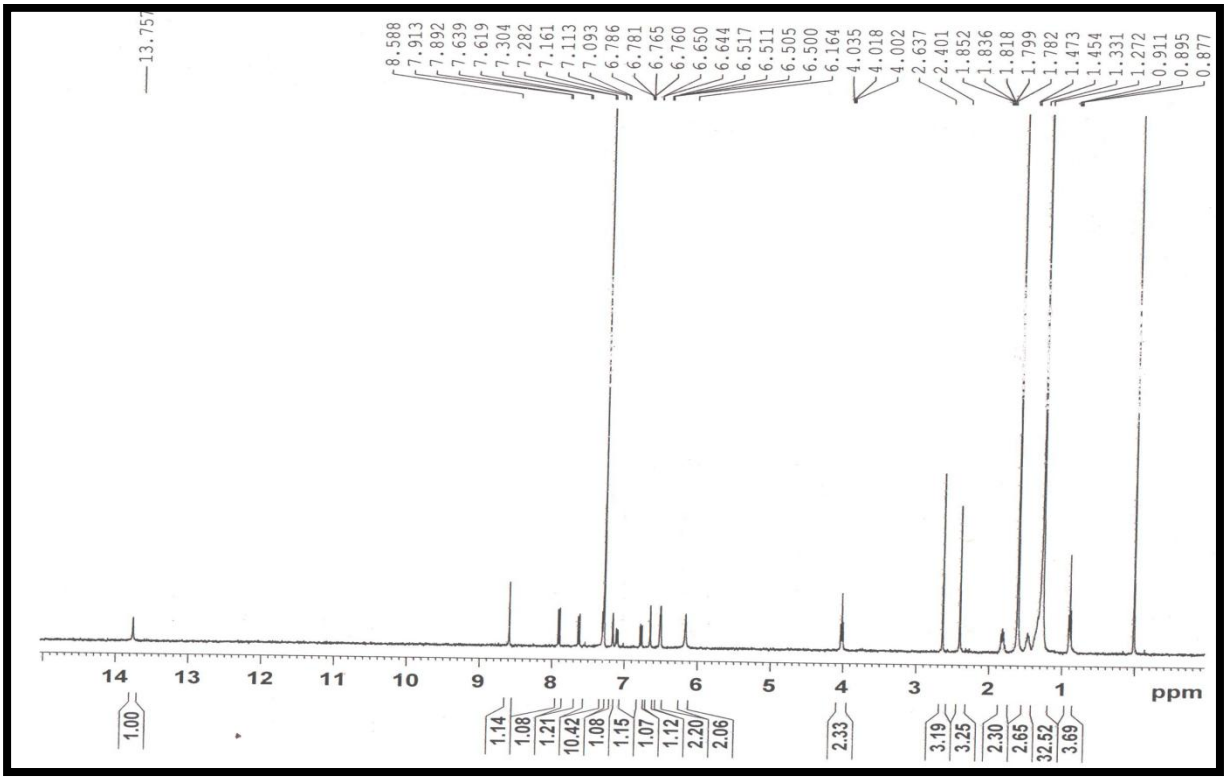


$^{1}$H NMR of G18

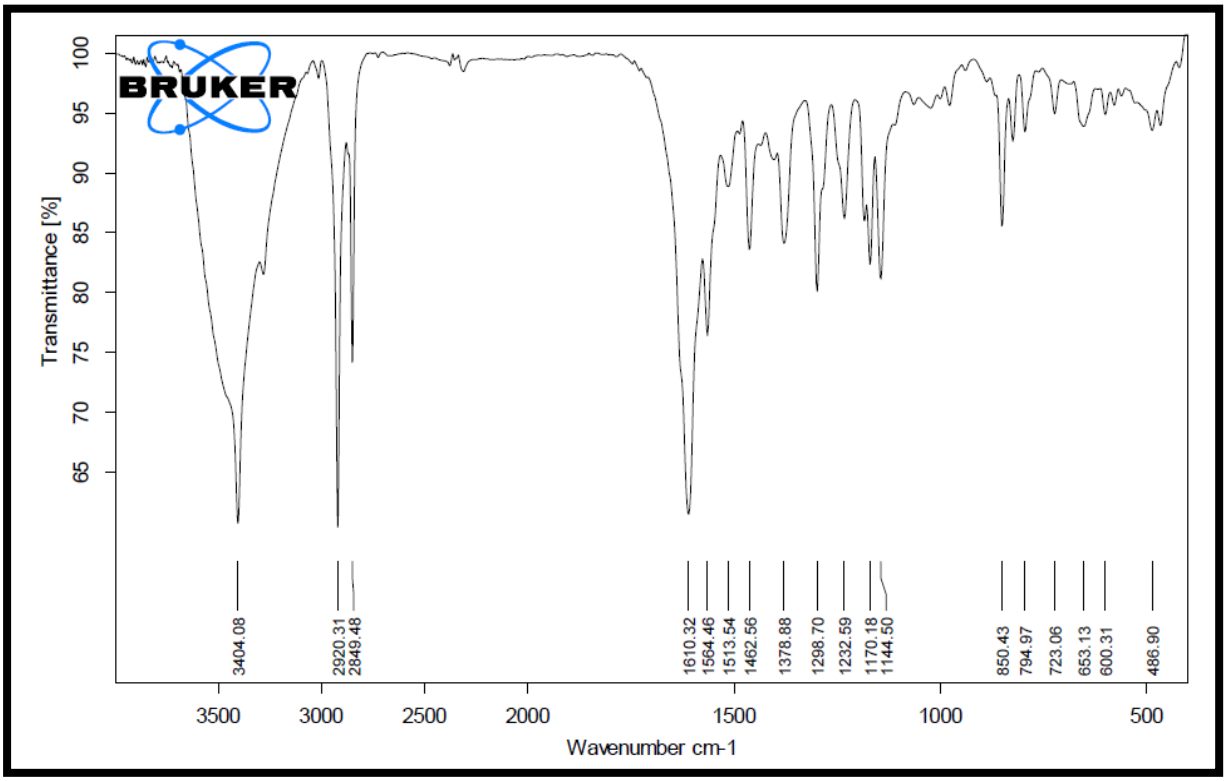


IR Spectra of G18